INVESTIGATION OF ERK INHIBITION AND HEDGEHOG SIGNALING IN MYOGENESIS AND CANCER-ASSOCIATED MUSCLE WASTING

Ernie Dennis Au

Submitted to the faculty of the University Graduate School

in partial fulfillment of the requirements

for the degree

Doctor of Philosophy

In the Department of Biochemistry & Molecular Biology,

Indiana University

May 2018

Accepted by the Graduate Faculty of Indiana University, in partial fulfillment of the requirements for the degree of Doctor of Philosophy.

Doctoral Committee

Teresa A. Zimmers, Ph.D., Chair

David B. Burr, Ph.D.

Maureen A. Harrington, Ph.D.

Jingwu Xie, Ph.D.

December 18, 2017

Dedication

To my mother and father, for supporting and encouraging me in anything and everything I do. I am truly lucky to have you both as parents.

Acknowledgements

I would like to thank my Ph.D. mentor, Dr. Teresa Zimmers. I am grateful that you welcomed me into your lab, and for the guidance and mentorship that you have given me throughout the course of my graduate career. I am forever indebted to you for the knowledge and experiences I have gained during my time there.

I would also like to express my sincere gratitude to my committee members, Drs. David Burr, Maureen Harrington, and Jingwu Xie. You guys have always taken time out of your busy schedules for our meetings and provided excellent insight and feedback regarding my work.

Lastly, I would like to extend my appreciation to past and current members of the Zimmers laboratory, especially Dr. Andrea Bonetto. Being able to learn from and discuss ideas with them has been invaluable.

Ernie Dennis Au

INVESTIGATION OF ERK INHIBITION AND HEDGEHOG SIGNALING IN MYOGENESIS AND CANCER-ASSOCIATED MUSCLE WASTING

The ability to preserve, protect, or grow skeletal muscle would greatly benefit patients in health and disease. Understanding the molecular pathways that regulate muscle size is necessary to develop interventions. The extracellular signal-related kinase (ERK) and Hedgehog signaling pathways each play necessary roles in skeletal muscle development. The ERK pathway has been shown to both stimulate and inhibit muscle development at different stages, while Hedgehog signaling is vital for embryonic muscle development. Thus, these pathways represent prime targets for manipulation in diseases associated with muscle loss.

In prior studies, cancer patients treated with the ERK inhibitor, Selumetinib, experienced significant gains in lean body mass. To study the mechanisms responsible, we tested the potential of Selumetinib to protect against muscle wasting in muscle cell cultures and in mice with experimental lung cancer. Selumetinib was able to induce hypertrophy of cultured muscle cells. In mice, we observed a reduction in tumor mass and in circulating mediators of muscle wasting including inflammatory cytokines. However, Selumetinib treatment did not prevent cancer-induced muscle loss. Together, these data suggest a diversity in the underlying molecular mechanisms and the

need for careful consideration when extrapolating results across different disease states, clinical trials, and model systems.

In separate studies, we found that the Hedgehog pathway was increased in mice and patients with cancer-associated muscle wasting and inflammation. In a series of studies in muscle cell cultures, in genetically modified mice, and in mice bearing tumors, we found that inflammatory cytokines activated Hedgehog expression in muscle. Hedgehog signaling promoted the replication of muscle stem cells but reduced the expression of genes that specify mature muscle. Inhibiting Hedgehog signaling promoted muscle growth, while activating it caused muscle wasting. Furthermore, we identified unique properties of two proteins activated by Hedgehog, Gli1 and Gli2, where Gli1 appears to promote muscle stem cell proliferation and Gli2 mature muscle gene expression. These data implicate the Hedgehog pathway, GLI1 and GLI2 as targets for treatment of muscle wasting diseases.

Teresa A. Zimmers, Ph.D., Chair

Table of Contents

Chapter 1

Introduction

Skeletal muscle

Skeletal muscle is one of the most highly plastic tissues in the human body. It comprises approximately 40% of total body mass, making it the most abundant tissue of the body [1]. Skeletal muscle is the main organ system for locomotion. Mechanically, it functions to provide movement, generate force, and in the performance of daily activities. Metabolically, it provides amino acids and other substrates to other vital organs upon demand. The maintenance of skeletal muscle mass is critical for respiration, locomotion, metabolism, and hinges on a homeostatic balance between protein synthesis and degradation. I would argue that it is of utmost importance to have sufficient skeletal muscle to meet the metabolic requirements of healing or recovering, because muscle is where the body stores its reserves. In disease, the wasting of that muscle, which is normally necessary physiologically, becomes pathological because there is no healing of the wound or because the muscle has become epigenetically stuck in the wasting mode. This occurs during disease states such as acquired immunodeficiency syndrome, cardiac failure, and cancer [2-6]. Moreover, it is essential to maintain skeletal muscle mass in order to preserve vitality and quality of life [7-10].

Skeletal muscle development and myogenesis

During embryogenesis, skeletal muscle develops from the somites in the paraxial mesoderm [11]. Several factors play critical regulatory roles during this process and are indispensable for muscle formation. Two of the major regulatory genes for muscle progenitors cells are *Pax3* and *Pax7* [12]. These transcription factors are necessary for the survival, specification, and progression into myogenesis of progenitor cells [13]. Other key components are the muscle specific genes myogenic regulatory factor 4 (MRF4), myogenic factor 5 (Myf5), and myogenic differentiation 1 (MyoD) (Figure 1-1). Upregulation of these factors allows for muscle cell differentiation, and are required for skeletal muscle formation [14-17]. Two other important proteins responsible for the activation of muscle specific genes are myogenin and myocyte enhancer factor 2 (MEF2) [18-20]. Along with several signaling molecules, these factors coordinate a complex network that determines when and where skeletal muscles will form and develop.

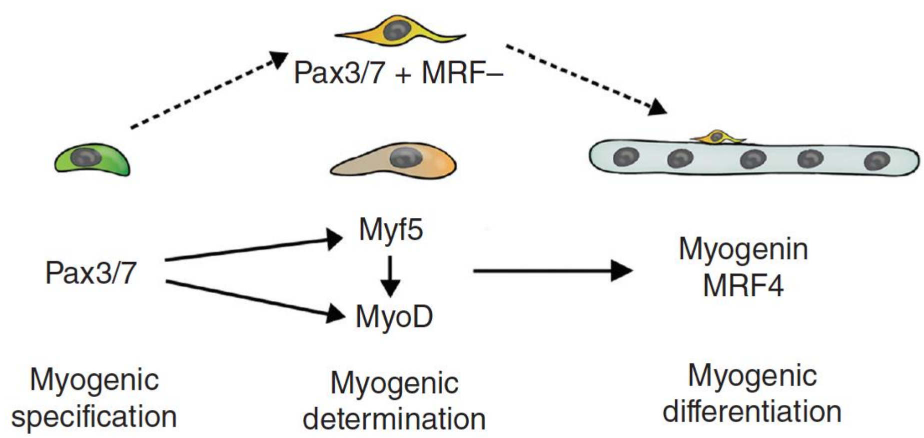

Figure 1-1. Myogenic differentiation. The Pax3 and Pax7 transcription factors control the myogenic specification of progenitor cells. They directly target and induce expression of Myf5 and MyoD for myogenic determination. This is followed by an upregulation of myogenin and MRF4 and induction of myogenic differentiation. Pax3/7 positive cells that do not express myogenic regulatory factors remain as muscle satellite cells, which can undergo myogenesis as a result of future stimuli. Figure is taken from Dumont et al., 2015 [21].

Skeletal muscle in health and disease

The importance of skeletal muscle is undisputable, and its loss extremely debilitating. Muscle wasting reduces quality of life, decreases response/tolerance to therapy, and increases morbidity and mortality. The loss of skeletal muscle can occur during acute trauma, systemic disease, or chronic illness. Trauma, such as volumetric muscle loss, can lead to prolonged or permanent functional deficits [22,23]. With systemic disease such as cancer-induced cachexia, preventing the loss of muscle mass has been shown to prolong life in animal models [24,25]. In chronic diseases that can often be incurable, preventing muscle loss may improve patient's quality of life. It has been shown that in chronic obstructive pulmonary disease, muscle mass and strength correlate directly with mortality [26,27]. As such, it is imperative to investigate new targets for therapeutic intervention of muscle wasting diseases.

Current therapies

Treatment options to preserve muscle mass or prevent wasting are limited, and some are not feasible with certain patients. Exercise is a validated form of therapy and has shown efficacy in animal models of muscle atrophy, but its use excludes patients who are bed-ridden or critically ill [28,29]. Increasing nutrient uptake has also been explored as a potential avenue of treatment. In cancer cachexia, clinical trials using various appetite stimulants have shown some efficacy with regards to muscle mass and improving quality of life [30-33]. One of the main features of cachexia is a chronic state of systemic inflammation. As such, other strategies aim to inhibit the inflammatory cytokines that are known to cause wasting. Antagonists to Activin and Myostatin have been shown to protect against atrophy and increase muscle and body mass [25,34-36]. Hormones such as ghrelin and insulin-like growth factor 1 have also been investigated for the treatment of muscle wasting in various systemic and chronic disease states [37-40]. In patients, ghrelin administration has been shown to have positive effects on body weight [41,42]. However, these therapeutic strategies are controversial as they increase the levels of various growth hormones, and may inadvertently increase the risk or growth of cancer or neoplasias [43,44].

There is unlikely to be one universal treatment for muscle wasting in any disease state, and multimodal approaches are likely needed. Thus, it is necessary to explore other molecular pathways that play a role in the regulation of skeletal muscle mass in the hopes of exploiting their therapeutic potential.

Extracellular signal-regulated kinase in skeletal muscle

The activity of extracellular signal-regulated kinase (ERK) can be stimulated by a variety of growth factors and mitogens [45,46]. These factors activate receptors, in conjunction with other adaptors, to initiate a signaling cascade through small GTP-binding proteins. These binding proteins activate the main components of the pathway which is composed of Raf, MEK1/2 and ERK. Once activated, ERK can phosphorylate a variety of transcription factors and results in a modulation of target gene expression (Figure 1-2).

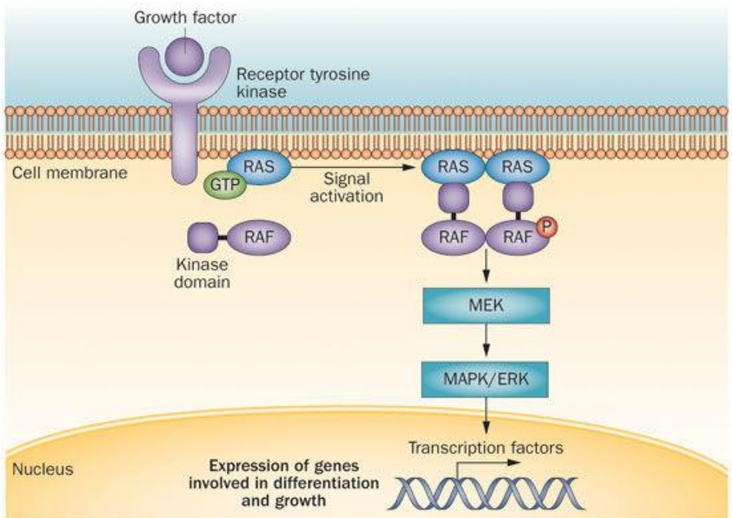

Figure 1-2. ERK signaling pathway. Signaling is initiated by the binding of factors to receptors. This results in the activation of a downstream signal transduction. Figure is taken from Gibney et al., 2013 [47].

In skeletal muscle myoblasts, ERK has been shown to play stage-dependent roles. ERK activation in satellite cells has been shown to promote their proliferation while suppressing differentiation, by preventing withdrawal from the cell cycle [48-51]. This activity can be induced by a variety of factors including fibroblast growth factor and insulin-like growth factor [52-55]. As it promotes proliferation, ERK activity is decreased during the initial phases of myogenic differentiation. However, as differentiation proceeds, ERK is again activated [56-58], with the ERK2 isoform shown to be essential for formation and fusion of murine myoblasts [59,60]. While the exact mechanisms by which ERK exerts both inhibitory and stimulatory roles during differentiation remain unclear, it has been suggested that its function is dependent on its cellular localization [61].

Hedgehog signaling in skeletal muscle

The Sonic hedgehog (Shh) signaling cascade has been studied extensively for its role in development. The pathway consists of ligands, the

Patched (Ptch) receptor, and the Smoothened (Smo) receptor. The effectors of this signaling pathway are the downstream Gli family of transcriptions factors, which regulate target gene expression (Figure 1-3). Hedgehog is another pathway that plays an important role in skeletal muscle. During development, Shh is instrumental in skeletal muscle patterning and fiber distribution [62]. In addition, Shh has been shown to directly initiate the myogenic program in muscle progenitor cells in the developing limb bud. This is accomplished through a Gli mediated activation of Myf5 [63]. Moreover, Shh signaling is also responsible for regulating the migration of progenitor cells that will give rise to various skeletal muscles [64]. While the pathways role in muscle development has been well described, its role in adult skeletal muscle remains unclear.

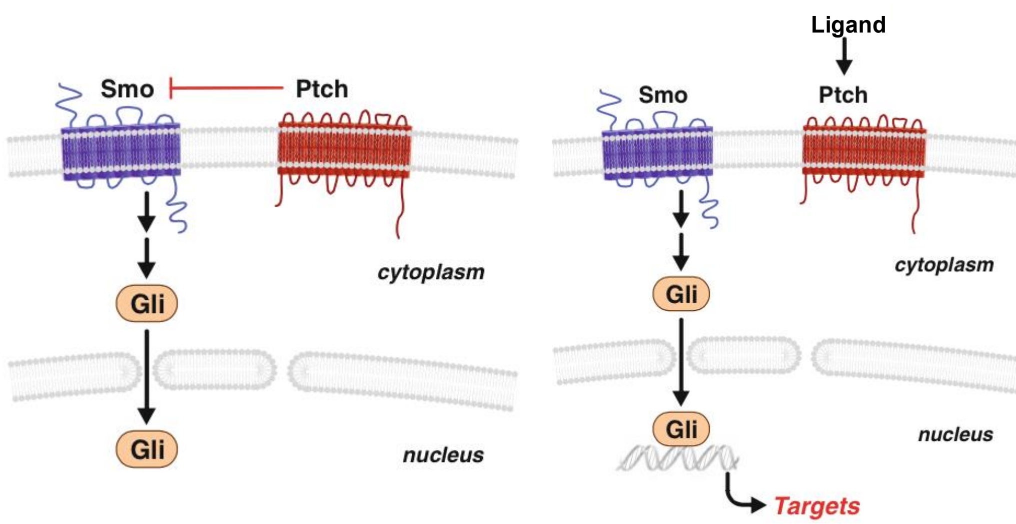

Figure 1-3. Hedgehog signaling pathway. In the absence of a ligand, the activity of Smo is repressed by Ptch (left). Binding of a ligand to the Ptch receptor relieves its repression on Smo, thus allowing for activation of the downstream Gli transcription factors (right). Figure is taken from Martin et al., 2010 [65].

Summary

The ability to preserve, protect, or grow skeletal muscle would greatly benefit patients across several disease states. Muscle-preserving therapies could improve quality of life, prolong life, and increase tolerance to treatments [66-68]. Given their roles in the development of skeletal muscle and myogenesis, the ERK and Shh pathways represent prime candidates for further investigation as potential therapeutic targets for diseases associated with muscle wasting.

Chapter 2

Investigating MEK inhibition as a treatment for cancer-induced cachexia

Introduction

It is estimated that roughly 50% of patients who die of cancer, die with cachexia, and some 30% die as a result of the cachexia [69]. This uncontrolled loss cannot be fully reversed with nutritional support, leading to progressive impairment of motor function and immobility [4,70]. Muscle wasting reduces quality of life, decreases response to therapy, and contributes directly to mortality. Low muscle mass also increases chemotherapy toxicity, while chemotherapy can cause muscle wasting and contribute to cachexia directly [71-74]. Currently there are no approved therapies for cancer cachexia, although treatment approaches include promoting appetite and absorption of food, anti-inflammatory drugs, and pro-anabolic approaches [75,76]. As such, it is imperative to explore additional means to combat this devastating syndrome.

Several underlying mechanisms have been implicated in directly contributing to cachexia. Cachexia has been referred to as an energy imbalance disease, where intake is decreased and expenditure is increased. However, even with a measured energy intake, the imbalance remains [77]. The loss of muscle mass is largely due to abnormalities in protein metabolism, with a constant cycle in which degradation outweighs synthesis. This was shown to be caused partly by increased activity of the ubiquitin-proteasome pathway or autophagy [78,79]. Degradation of myofibrillar proteins results directly in muscle weakness, fatigue, and atrophy. Signaling pathways responsible for the turnover of skeletal muscle proteins can be induced by a multitude of inflammatory cytokines, both tumor- and host-derived. Cachectic mediators include tumor necrosis factor alpha (TNFα), Myostatin, Activin, members of the transforming growth factor beta (TGF-β) superfamily of ligands, and Interleukin-6 (IL-6) [80-84]. IL-6 binds IL-6 receptor and GP130 to activate signal transduction cascades of the downstream ERK, Akt, and STAT3 pathways [85]. It has been shown by others, as well as in our lab, that IL-6 alone is sufficient to induce muscle wasting both *in vitro* and *in vivo* [86-88]. This is largely through activation of STAT3 [88] downstream of GP130 and JAK. Inhibition of IL-6, IL-6 receptor, or STAT3 have all been shown to reduce cachexia in experimental systems [89-92]. Moreover, therapies targeted at inhibiting IL-6 have shown promise in human lung cancer cachexia [93].

In addition to IL-6, a variety of mitogenic and inflammatory stimuli can activate the Mitogen activated protein kinase (MAPK)/ERK pathway. These include various cytokines and growth factors which signal through tyrosine kinase receptors [94]. MEK1/2 activation of ERK influences survival, growth, proliferation, and inflammatory processes [95,96]. The MEK pathway can also be activated by oncogenic Ras. As such, the pathway has been a target of interest for potential anti-cancer therapies [97]. The selective small molecule MEK1/2 inhibitor, Selumetinib, decreases phosphorylation and activation of ERK1/2 [98] and shows efficacy in various cancer models of the lung, skin, ovary and liver [99-102].

A phase II clinical trial of Selumetinib showed weight gain in patients with biliary cancer, a condition that is typically associated with severe wasting [103].

Retrospective re-analysis of those data showed that patients receiving Selumetinib experienced significant gains in skeletal muscle, while those on standard therapy experienced muscle loss [103,104]. In skeletal muscle, inhibition of the ERK pathway, via a dominant negative form of Raf or a pharmacological inhibitor, resulted in robust myotube hypertrophy [105]. ERK inhibition has also been shown to derepress myogenic differentiation caused by cardiotrophin-1, a member of the IL-6 family of cytokines [106]. During early stage skeletal muscle cell differentiation, myogenin expression becomes upregulated. This increase in myogenin mRNA levels is accompanied by a concomitant decrease in ERK1/2 phosphorylation, and pharmacological inhibition of ERK1/2 significantly increases myogenin mRNA [107]. Moreover, in a C26 colon carcinoma mouse model of cancer cachexia, ERK inhibition was shown to be protective against muscle wasting [108,109].

Given the encouraging results of Selumetinib in patients and of ERK inhibition in animal models, we sought to investigate the effect of Selumetinib in a Lewis lung carcinoma (LLC) model of cancer-induced cachexia [110]. Based on the results of the retrospective analysis, and the published literature on the effects of ERK inhibition on skeletal muscle, we hypothesized, given its reported hypertrophic effects, that inhibition of ERK would protect against cachexia. We found that MEK inhibition lead to *in vitro* hypertrophy, *in vivo* tumor killing and inhibition of IL-6 in mice, but showed no evidence of anti-cachexia effects [111].

Materials and methods

Cell cultures

LLC cells were maintained at low confluency at 37°C in a humidified atmosphere of 5% CO_2. The cells were grown in culture medium consisting of Dulbecco's Modified Eagle Medium (DMEM), 10 % fetal bovine serum (FBS), 100 u/mL penicillin, and 100 mg/mL streptomycin. In preparation for injection, cells were trypsinized, counted, and resuspended in phosphate buffered saline (PBS).

Murine C2C12 myoblasts (ATCC) were maintained at low confluency in a humidified atmosphere of 5% CO_2. Culture medium consisted of DMEM with 10% FBS, 100 u/mL penicillin, and 100 mg/mL streptomycin. To induce differentiation, confluent cells were switched to differentiation medium consisting of DMEM with 2% horse serum, 100 u/mL penicillin, and 100 mg/mL streptomycin. Myoblasts were differentiated for four days into mature myotubes. At this time, either 10 nM Selumetinib or vehicle was added to the media and the myotubes cultured for an additional two days.

In the experiment using plasma from LLC tumor bearing mice, C2C12 cells were again differentiated for four days. The media was then replaced with media consisting of DMEM with 2% plasma from control or LLC tumor bearing mice, 100 u/mL penicillin, and 100 mg/mL streptomycin. These groups were further divided into groups either receiving vehicle or 10 nM Selumetinib. The myotubes were then cultured for an additional two days prior to downstream analyses.

Animals

All experimental animal protocols were approved by and used in compliance with the Indiana University School of Medicine Institutional Animal Care and Use Committee. Eight week old male C57BL/6J mice were obtained from The Jackson Laboratory and allowed to acclimate for one week prior to the start of the experiment. Mice were maintained on a regular light-dark cycle and allowed free access to food and water throughout the duration of the experiment. The following experimental groups were used for this study: Control + vehicle (n=6), LLC + Vehicle (n=8), and LLC + Selumetinib (n=8). Mice designated in the tumor bearing groups were subcutaneously injected with $1x10^6$ LLC cells into the interscapular region on day 0, with treatments beginning 24 hours later. Selumetinib (Selleck Chemical) was solubilized in a vehicle of 0.5% methylcellulose and 0.2% Tween 80. Vehicle or 25 mg/kg of Selumetinib was administered twice daily by gavage to the designated groups [112-114]. Body weights of all mice were recorded daily. The study concluded on day 17 when some mice reached the criteria for a humane endpoint, at which point all mice were euthanized under isoflurane general anesthesia. Skeletal muscles, tumors, and organs were dissected free and weighed. Tissues were snap frozen in liquid nitrogen while some were preserved using alternative methods based on the downstream analysis (described later), and stored at -80°C. The weights of individual tissues are expressed as a percentage of the animal's initial body weight (IBW) in order to normalize for small difference in starting body size.

Immunofluorescence and immunohistochemistry

C2C12 myotube cultures were fixed and permeabilized in an ice cold solution of acetone:methanol (1:1) at -20°C for 20 minutes. Following fixation, the cells were rehydrated in PBS for 10 minutes at room temperature. Cells were then blocked in an 8% bovine serum albumin (BSA) solution for one hour before being incubated with a primary antibody against myosin heavy chain (MyHC) (MF 20, Developmental Studies Hybridoma Bank), at a dilution of 1:200 in PBS, overnight at 4°C with gentle agitation. The following day, cells were washed with PBS and incubated with an AlexaFluor 488-labeled anti-mouse IgG (R37120, Life Technologies) secondary antibody, at a dilution of 1:1,000 in PBS, for one hour at room temperature and protected from light. Nuclei were stained with DAPI and images were captured on an Axio Observer.Z1 (Zeiss). Myotube diameters were measured using ImageJ analysis software (Wayne Rasband, U.S. National Institutes of Health). Only fully formed myotubes with the majority in the field of view were measured.

Skeletal muscle fiber cross-sectional area (CSA) was measured using the tibialis anterior muscle. Following necropsy, tibialis anterior muscles were mounted on cork discs with Tissue-Plus Optimal Cutting Temperature (Fisher Scientific) and frozen in 2-methlybutane cooled in liquid nitrogen before being stored at -80°C. Frozen sections were cut using a Leica CM1860 cryostat (Leica Microsystems Inc.). Slides of muscle sections were fixed in ice cold 100% acetone at -20°C for 10 minutes, and rehydrated in PBS for 10 minutes. Sections were then blocked in an 8% BSA solution for one hour at room temperature before being incubated with a primary antibody against dystrophin (VP-D508, Vector Laboratories), at a dilution of 1:60 in PBS, overnight at 4°C. The following day, sections were washed with PBS and incubated with an AlexaFluor 594-labeled anti-mouse IgG (R37121, Life Technologies) secondary antibody, at a dilution of 1:1,000 in PBS, for one hour at room temperature. Images were captured with an Axio Observer.Z1 and muscle fiber cross-sectional area was measured using an ImageJ macro developed by Dr. Richard Lieber [115].

For immunohistochemical analysis, tumor tissue was fixed in formal and embedded in paraffin before sectioning. Sections were first deparaffinized in xylene and ethanol. Antigen retrieval was accomplished by boiling slides in a 10mM sodium citrate buffer at pH 6.0 for 10 minutes. The sections were then cooled at room temperature for 30 minutes before being blocked in an 8% BSA solution for 1 hour. A primary antibody against IL-6 (ab6672, Abcam), at a dilution of 1:1,000 in PBS, or normal rabbit IgG (Santa Cruz Biotechnology) was then incubated on the sections overnight at 4°C. Antibody detection was done using the ImmPRESS HFP Anti-Rabbit IgG (Peroxidase) Polymer Detection kit and ImmPACT DAB Peroxidase (HRP) Substrate as per manufacturer's instructions (Vector Laboratories).

Western blotting

Skeletal muscle and tumor tissue were homogenized on ice in lysis buffer consisting of 25 nM TrisHCl pH 7.6, 150 mM NaCl, 1% NP-40, 1% sodium deoxycholate, 0.1% sodium dodecyl sulfate (SDS), protease and phosphatase inhibitor cocktail tablets (Roche). Tissue homogenates were then separated by centrifuging at 14,000 rpm for 15 minutes at 4°C. Following centrifugation, the supernatant was collected and stored at -80°C. Protein concentration of the supernatant was measured using the Pierce BCA Protein Assay Kit (Thermo Fisher Scientific) as per the manufacturer's instructions. Equal amounts of protein extracts (30 μg) were denatured at 95°C for 5 minutes in sample loading buffer consisting of 125 mM Tris pH 6.8, 4% SDS, 20% glycerol, 1% bromphenol blue, and 200 mM dithiothreitol (DTT). Samples were resolved on Tris-Glycine gels before being transferred to nitrocellulose membranes (Bio-Rad Laboratories). Membranes were blocked in SEA BLOCK (Thermo Fisher Scientific) blocking buffer for one hour at room temperature and then incubated at 4°C overnight with gentle agitation with primary antibodies against: IL-6 (AB1839, EMD Millipore), α-Tubulin (12G10, Developmental Studies Hybridoma Bank), Phospho-p44/42 MAPK (ERK1/2) , p44/42 MAPK (ERK1/2), and GAPDH (4370, 4695, 5174, Cell Signaling Technology). All primary antibodies were used at a dilution of 1:1,000 in SEA BLOCK. Following primary antibody incubation, membranes were washed in a solution of PBS and 0.2% Tween 20. Anti-mouse IgG DyLight 680 and anti-rabbit IgG DyLight 800 secondary antibodies (5470, 5151, Cell Signaling Technology)., at a dilution of 1:10,000 in SEA BLOCK, were incubated on the membranes for one hour at room temperature with gentle agitation. Following a final wash, membranes were imaged and quantified using an ODYSSEY CLx Infrared Imaging System and software (LI-COR).

IL-6 immunoassay

Whole blood was collected from all mice during euthanasia, via cardiac puncture, into BD Vacutainer Plastic Blood Collection Tubes with K_2EDTA (Fisher Scientific) and kept on ice. Plasma was separated by centrifugation at 3,500 rpm for 15 minutes at 4°C and stored at -80°C. IL-6 was detected by a mouse magnetic 1-plex custom kit as per the manufacturer's instructions (Life Technologies). All samples were run in duplicate and detected using the MAGPIX (Luminex) platform.

Data analysis

Statistical significance was determined by an unpaired t test for experiments containing only two groups. In experiments that contained three or more groups, statistical significance was determined by one-way analysis of variance (ANOVA) followed by Tukey's multiple comparisons test. A p-value greater than 0.05 was considered to be statistically significant.

Results

Selumetinib induced hypertrophy in C2C12 myotubes

We first looked to see what the *in vitro* effects of Selumetinib would be on myotubes. C2C12 myoblasts proliferate as mononuclear cells when maintained at low confluency. These cells can be induced to differentiate, when switched to a low serum medium, and form multinucleated myotubes. This system has previously been used in our lab to assess either hypertrophic or atrophic effects of conditioned medium, plasma, recombinant proteins, or small molecules [86,87]. In this experiment, C2C12 myoblasts were differentiated into myotubes for four days. The cultures were then incubated with either vehicle or 10 nM Selumetinib for an additional 2 days, with a media change after the initial 24 hours (Figure 2-1).

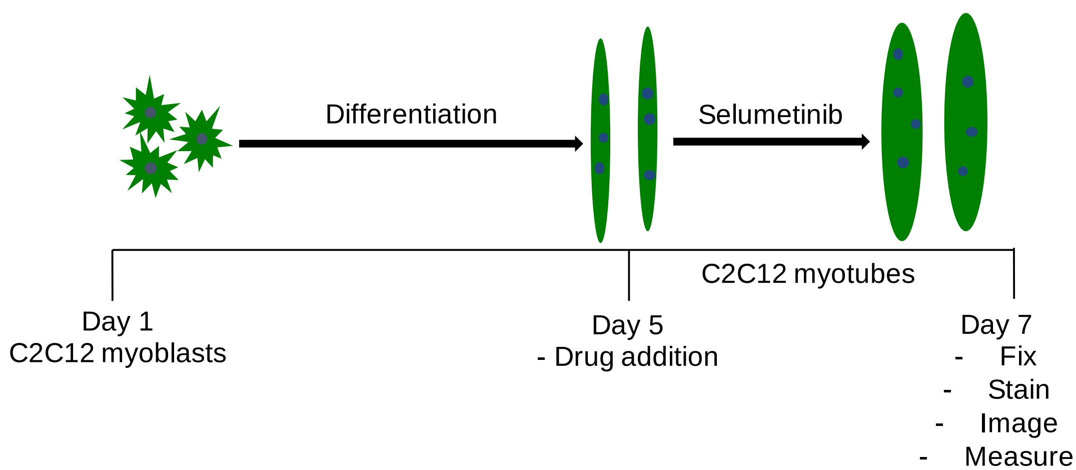

Figure 2-1. *In vitro* C2C12 model of Selumetinib treatment. Graphical representation of experimental design with C2C12 cells. Myoblasts were differentiated into myotubes for four days before receiving the indicated treatment for an additional two days.

Western blotting analysis showed that Selumetinib significantly reduced phosphorylation of ERK1/2 at both 1 and 10 nM (Figure 2-2A). Accompanying the reduced ERK1/2 activation, was a significant increase in myotube diameter

(+15.24%) compared to control (Figure 2-2B). This effect was seen with 10 nM Selumetinib treatment, but not at the 1 nM concentration. Higher doses were tested and found to be toxic (data not shown). These data suggest that inhibition of ERK1/2 phosphorylation induces C2C12 myotube hypertrophy.

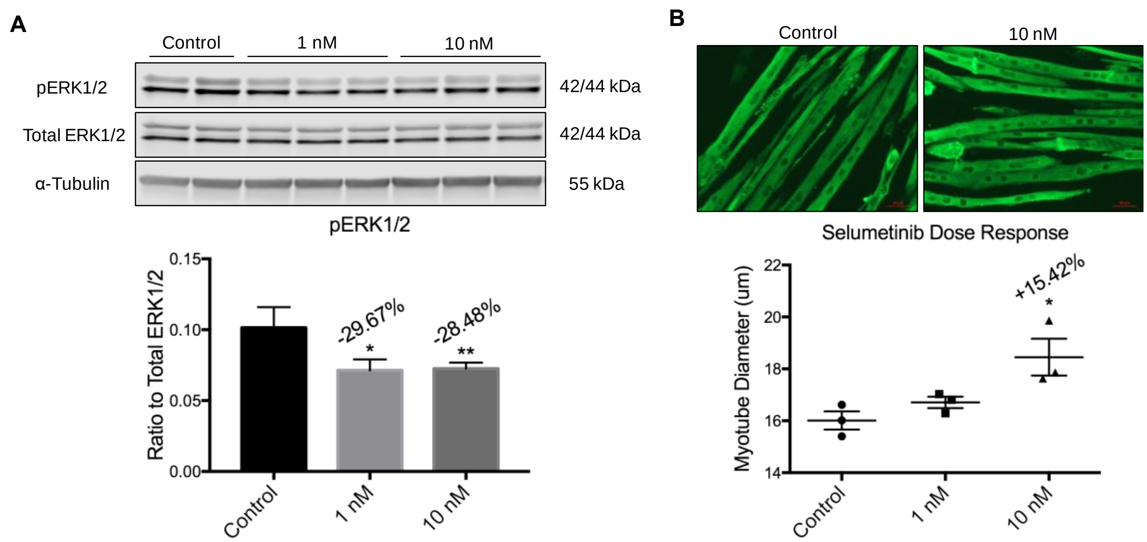

Figure 2-2. Treatment of myotubes with Selumetinib results in hypertrophy. C2C12 myoblasts were differentiated into myotubes before treatment with varying concentrations of Selumetinib. **A**: Western blotting analysis of C2C12 myotubes shows that 1 and 10 nM of Selumetinib reduced phosphorylated ERK1/2 (normalized to total ERK1/2). Data are expressed as the means ± standard deviation (SD). Statistical significance was determined by one-way ANOVA. *p<0.05, **p<0.01 versus Control. **B:** Representative images of myotubes treated with 10 nM Selumetinib or vehicle. Myotube Cultures were stained for MyHC. Treatment with 10 nM Selumetinib induced myotube hypertrophy (+15.24%). All conditions were performed in triplicate and the data are expressed as the means ± standard error of the means (SEM). Statistical significance was determined by one-way ANOVA. *p<0.05 versus Control.

Selumetinib inhibited phosphorylation of ERK1/2 in skeletal muscle

With hypertrophic effects on myotubes observed *in vitro*, we next sought to investigate the *in vivo* effect of Selumetinib on skeletal muscle in the context of cancer-induced cachexia. To test this, we injected C57BL/6J mice with LLC cells, a validated and traditional model of experimental cancer cachexia, while control mice received a PBS injection. Treatment with 25 mg/kg Selumetinib or vehicle control was given twice daily by gavage and began 24 hours after tumor cell inoculation. Body weights were recorded at baseline and daily throughout the course of the experiment. No changes in body weight or body composition were observed amongst the groups (data not shown). On day 17 of the experiment, tumor bearing mice receiving vehicle treatment began to meet the criteria for euthanasia due to humane reasons. At this point, mice in all groups were euthanized and necropsies performed to harvest various skeletal muscles and organs. In order to determine if there was an on-target effect of Selumetinib on skeletal muscle, western blotting analysis for phospho-ERK1/2 was performed on lysates from quadriceps muscles. We found that systemic administration of Selumetinib was able to inhibit phosphorylation of ERK1/2 in the skeletal muscle (Figure 2-3A). Compared to vehicle treated controls and LLC tumor bearing mice, Selumetinib treatment in tumor bearing mice reduced phospho-ERK1/2 73.31% and 74.03% respectively (Figure 2-3B). Levels of total ERK1/2 protein were not statistically different between any group. This data suggested that Selumetinib had an on-target effect in skeletal muscle.

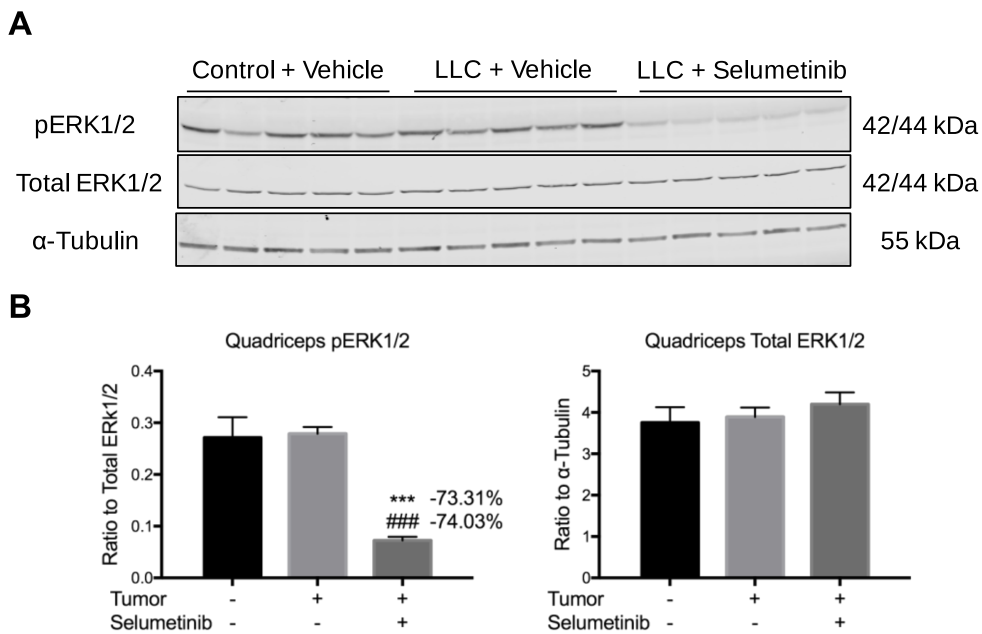

Figure 2-3. *In vivo* inhibition of ERK1/2 phosphorylation in skeletal muscle. LLC cells were injected subcutaneously into C57BL/6J mice. Tumor bearing mice received either vehicle or 25mg/kg Selumetinib. **A:** Western blotting images show that Selumetinib treatment in LLC tumor bearing mice inhibited phosphorylation of ERK1/2 (normalized to total ERK1/2) in the skeletal muscle, while levels of total ERK1/2 were unchanged. **B:** Quantification of western blotting images. Data are expressed as the means ± SD. Statistical significance was determined by one-way ANOVA. ***p<0.001 versus Control + Vehicle, ###p<0.001 versus LLC + Vehicle.

IL-6 expression was reduced in the blood and tumor tissue, but not muscle

IL-6 is an inflammatory cytokine that has been extensively studied as a causal factor in cancer-induced cachexia. It has been reported that Selumetinib blocks the production of IL-6 [116]. Based on this we next looked at whether Selumetinib could inhibit IL-6 production in this model. We first looked at IL-6 levels in the skeletal muscle. Western blotting analysis of quadriceps muscles showed no differences among any of the groups (Figure 2-4).

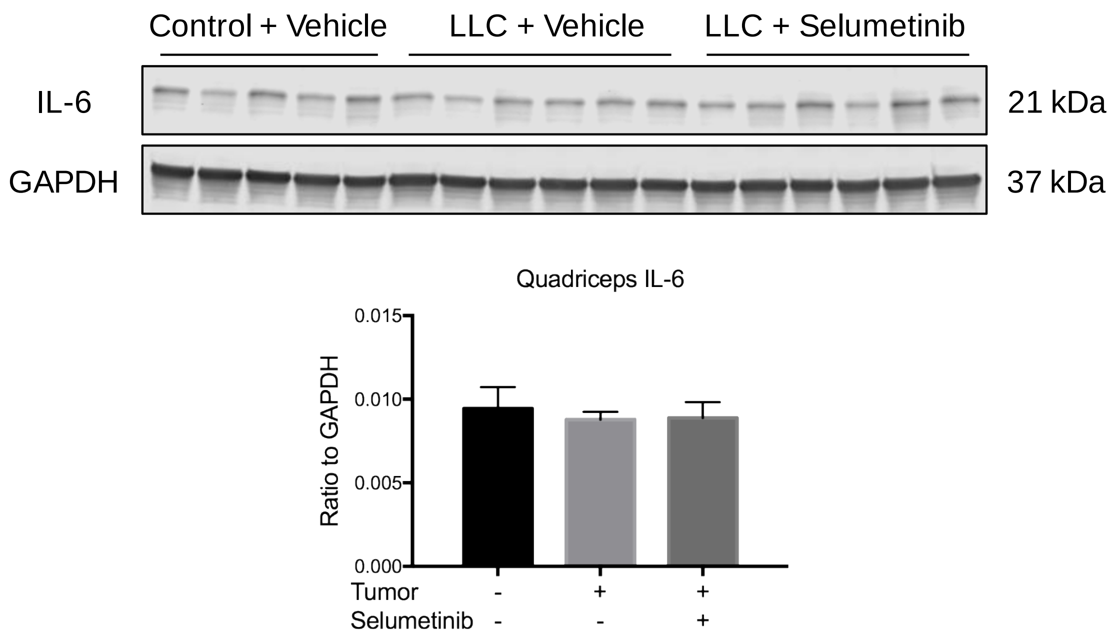

Figure 2-4. Selumetinib did not reduce IL-6 levels in muscle. Western blotting analysis shows that quadriceps IL-6 levels were not changed in cachexia or with Selumetinib treatment. Data are expressed as the means ± SD.

We next looked at levels in the tumor tissue. With western blotting analysis, we found that in tumor bearing mice treated with Selumetinib, IL-6 was significantly decreased as compared to the vehicle treated group (Figure 2-5A). This finding was further supported by immunohistochemical staining for IL-6 in sections of tumor tissue (Figure 2-5B).

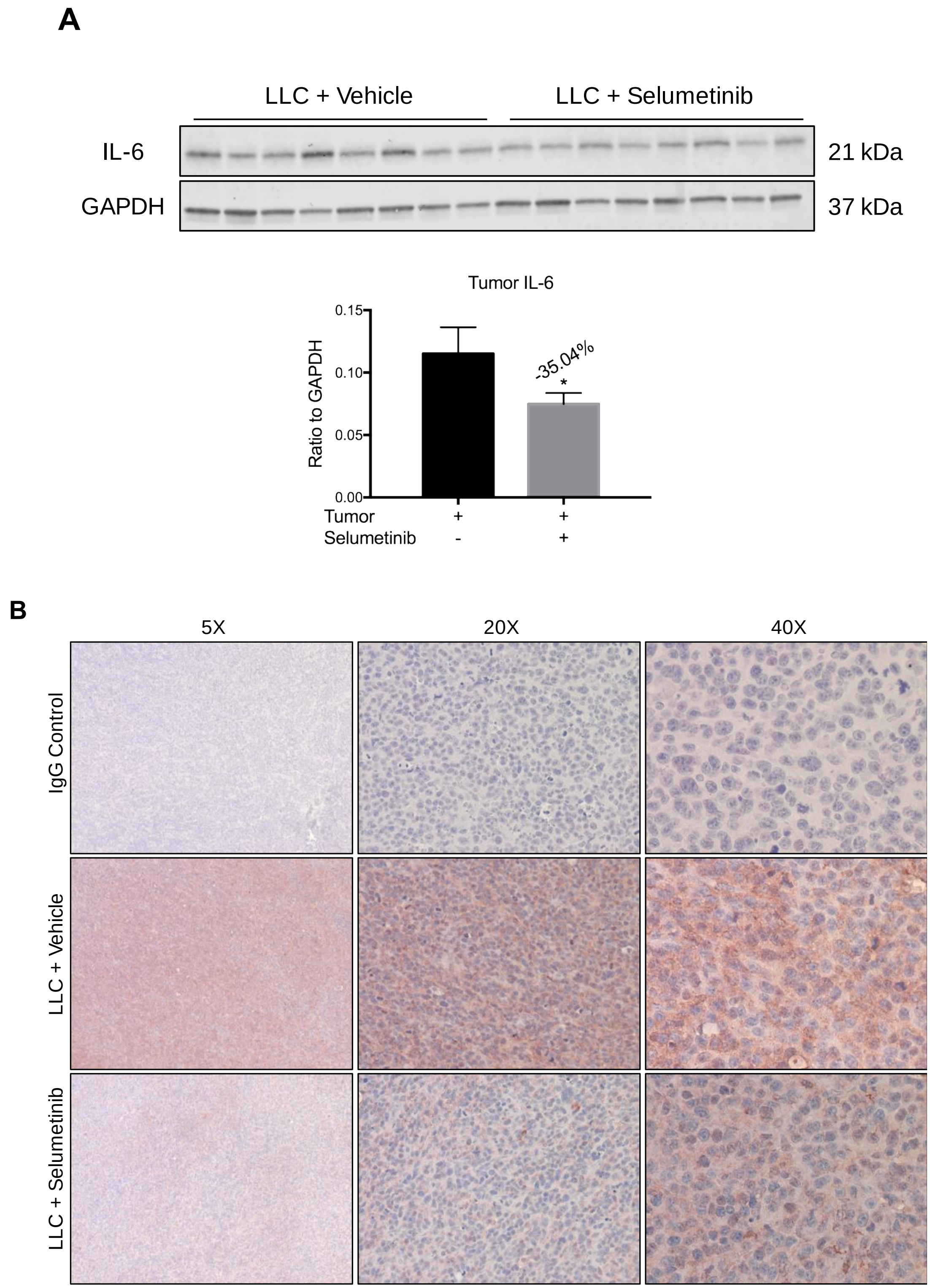

Figure 2-5. Selumetinib reduced IL-6 in the tumor. Tumor bearing mice receiving Selumetinib exhibited a significant reduction of tumor IL-6 compared to vehicle treated tumor bearers. **A:** Western blotting analysis of tumor lysates show that Selumetinib blocked the production of IL-6. Data are expressed as the means ± SD. Statistical significance was determined by unpaired t test. *p<0.05 versus LLC + Vehicle. **B:** Representative images of immunohistochemistry staining for IL-6 in tumor sections.

Lastly, we looked at circulating levels of IL-6. At the time of necropsy, whole blood was collected from all mice and the plasma extracted. Tumor bearing mice treated with vehicle showed a significant increase in the levels of IL-6 compared to vehicle treated control mice. Selumetinib treatment resulted in a drastic decrease of IL-6 levels compared to vehicle treated tumor bearers (Figure 2-6). Furthermore, the levels in the Selumetinib treated tumor bearers were not significantly different from non-tumor bearing controls. Taken together, these data show that treatment with Selumetinib reduced both tumor and circulating levels of IL-6, but not those in the skeletal muscle.

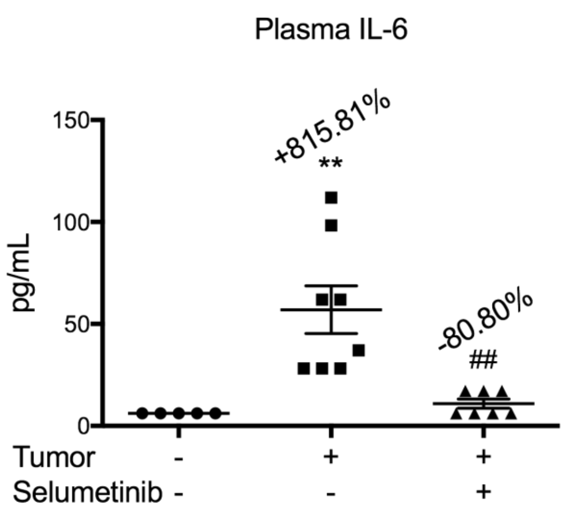

Figure 2-6. Selumetinib reduced circulating IL-6. Plasma extracted from the mice was used for an IL-6 immunoassay. Tumor bearing mice treated with vehicle had a significant increase in IL-6 compared to control mice. Selumetinib greatly reduced IL-6 in tumor bearing mice. Data are expressed as the means ± SD. Statistical significance was determined by one-way ANOVA. **p<0.01 versus Control + Vehicle, ##p<0.01 versus LLC + Vehicle.

Selumetinib reduced tumor size but did not protect against muscle wasting or fat loss

We next looked to determine if Selumetinib was able to prevent muscle and fat wasting. Compared to the vehicle treated tumor bearers, we observed a reduction in the final tumor mass (Figure 2-7A). Given the significant decrease in tumor size, we expected muscle wasting to be attenuated. In this model, the severity of cachexia generally correlates with the level of tumor burden. However, in all the skeletal muscle tissues analyzed, both Selumetinib and vehicle treated tumor bearers exhibited a similar level of wasting (Figure 2-7A). Further analysis of the muscle cross-sectional area showed the same pattern of wasting as those observed with the muscle weights (Figure 2-7B). These data suggest that Selumetinib does not protect against cancer-induced cachexia.

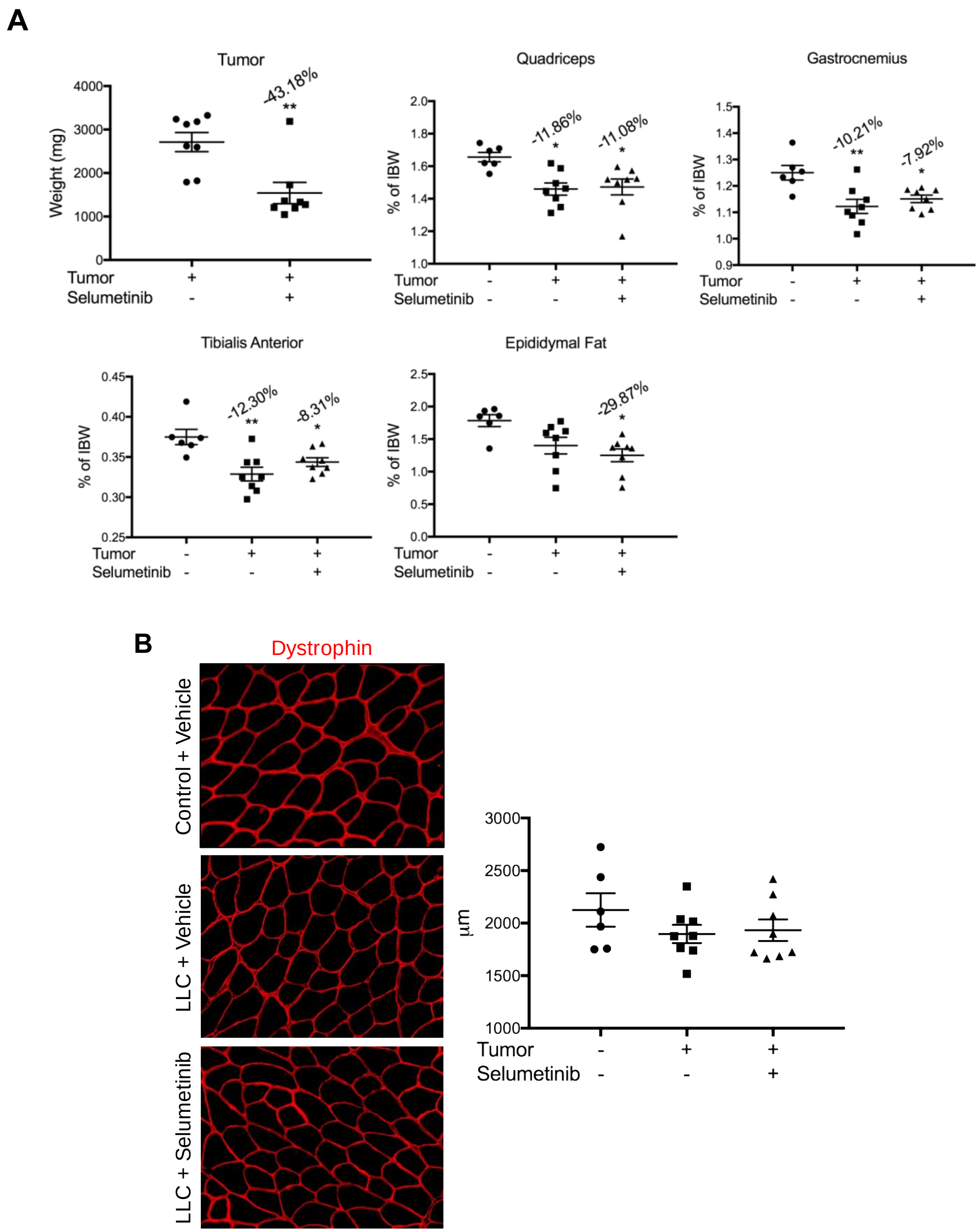

Figure 2-7. Selumetinib does not protect against cancer-induced cachexia. Weights of tumor, various muscles, and adipose tissues were weigh at the time of necropsy. Tissue weights are normalized to the IBW (except tumor). **A:** Tumor mass was significantly reduced with Selumetinib treatment. Similar wasting in the quadriceps, gastrocnemius, and tibialis anterior muscles were observed in both vehicle and Selumetinib treated tumor bearing mice. Loss of epididymal fat mass appears to be greater in the Selumetinib treated group. Data are expressed as the means ± SD. Statistical significance was determined by one-way ANOVA. *p<0.05, **p<0.01 versus Control + Vehicle. **B:** Representative images of muscle fiber cross-sectional area analysis from tibialis anterior muscles. Data are expressed as the means ± SD.

Selumetinib does not protect against LLC plasma-induced myotube atrophy

While we observed a decrease in both tumor mass and circulating levels of IL-6, Selumetinib treatment did not display any protective effects against muscle or fat wasting. This led us to question if there were other cachexia drivers present in the LLC model that could not be modulated by Selumetinib. In order to investigate this question, we went back to an *in vitro* model using C2C12 myotubes. In this experiment, C2C12 myotubes were simultaneously treated with plasma from control or LLC tumor bearing mice, and either vehicle or 10 nM Selumetinib (Figure 2-8).

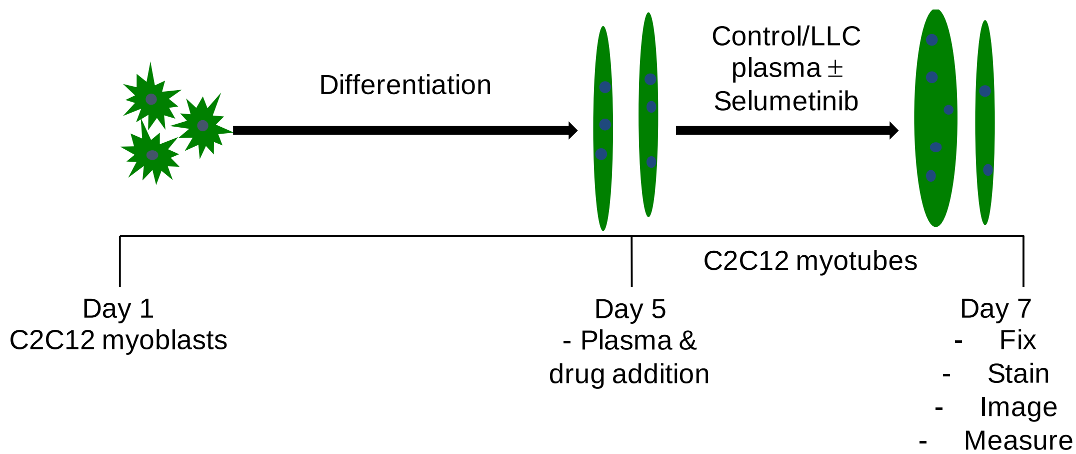

Figure 2-8. LLC plasma and Selumetinib model. Graphical representation of experimental design. C2C12 myoblasts were differentiated into myotube for four days. The myotubes were then incubated for an additional two days with the designated treatments.

As with our prior *in vitro* experiment (Figure 2-2B), 10 nM Selumetinib was able to reproducibly induce myotube hypertrophy. Treatment of myotubes with plasma from LLC tumor bearing mice induced atrophy, which was not prevented with co-treatment of 10 nM Selumetinib (Figure 2-9A). Further analysis showed that ERK1/2 inhibition resulted in a significant increase in the number of nuclei per fiber (Figure 2-9B). Western blotting analysis confirmed the inhibition of ERK1/2 phosphorylation in myotubes treated with Selumetinib (Figure 2-9C). Taken together, these data suggest that there are other factors driving the cachectic phenotype observed in the LLC model. Although Selumetinib was able to reduce levels on IL-6 in the tumor and blood, it does not appear to be able to modulate other potential drivers, resulting in the disconnect between the hypertrophic phenotype observed *in vitro,* and the lack of protection against cancer-induced cachexia *in vivo*.

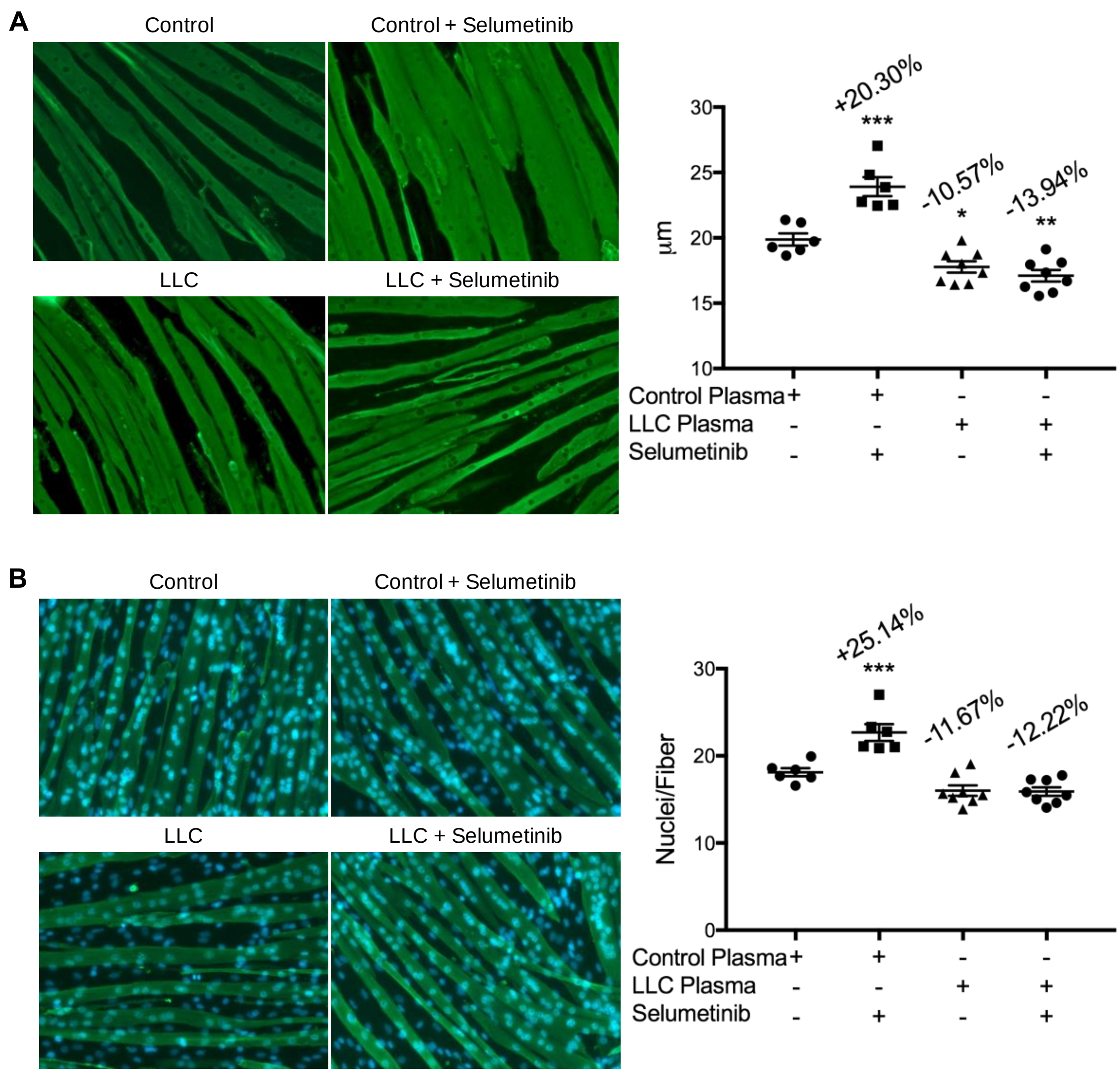

C

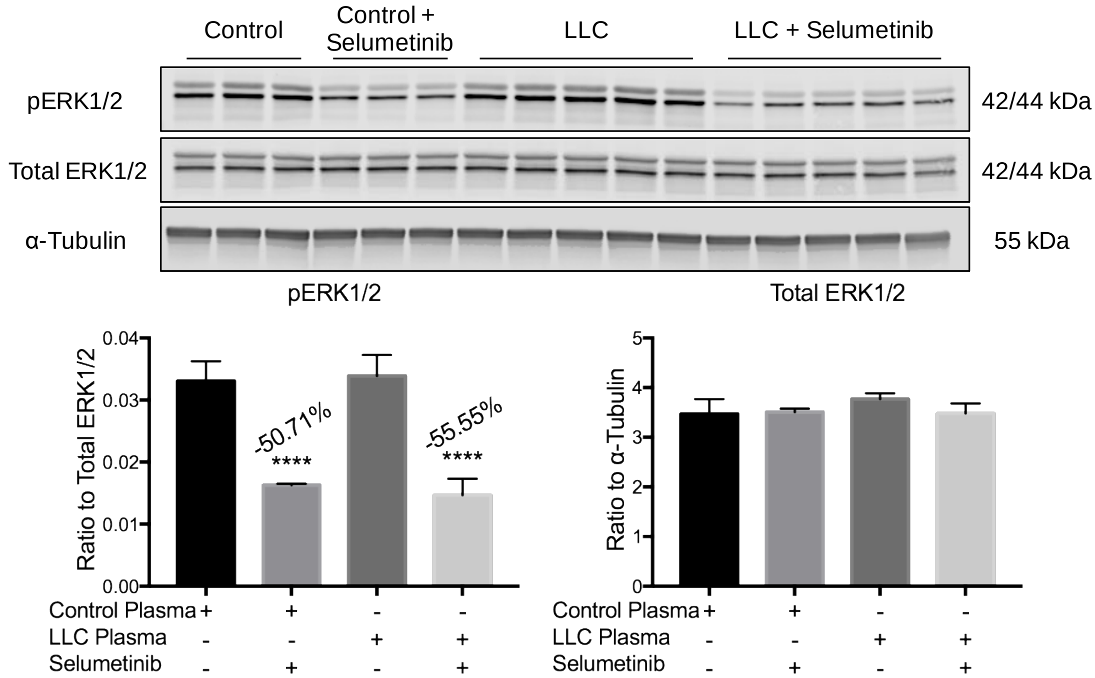

Figure 2-9. Inhibition of ERK1/2 phosphorylation does not prevent LLC plasma-induce atrophy. C2C12 cells were differentiated for four days before being incubated for an additional two days with the indicated treatment. The experimental groups are as follows: Control, Control + 10 nM Selumetinib, LLC Plasma, LLC Plasma + 10 nM Selumetinib. **A:** Representative images and quantification of myotube diameter. Myotubes treated with Selumetinib showed hypertrophy, while those treated with plasma from tumor bearing mice atrophied. Co-treatment of LLC plasma with Selumetinib was unable to block the atrophy. All conditions were performed in triplicate and the data are expressed as the means ± SEM. Statistical significance was determined by one-way ANOVA. *p<0.05, **p<0.01, ***p<0.001 versus Control Plasma only. **B:** Representative images and quantification of nuclei per fiber. Myotubes treated with Selumetinib showed a significant increase in the number of nuclei per fiber, while this was decreased with LLC plasma. Again, Selumetinib was unable to attenuate the reduction in nuclei per fiber induced by plasma from LLC tumor bearing mice. All conditions were performed in triplicate and the data are expressed as the means ± SEM. Statistical significance was determined by one-way ANOVA. ***p<0.001 versus Control Plasma only. **C:** Western blotting analysis of myotubes treated with control or LLC plasma, with or without 10 nM Selumetinib. Phosphorylation of ERK1/2 (normalized to total ERK1/2) was significantly reduced in both groups receiving Selumetinib. Total ERK1/2 protein levels were unchanged amongst the groups. Data are expressed as the means ± SD. Statistical significance was determined by one-way ANOVA. ****p<0.0001 versus Control Plasma only.

Discussion

In this study, we show that unlike the results reported in patients with biliary cancers, mice with lung cancer do not exhibit a preservation of lean muscle mass with Selumetinib treatment, despite a reduction in tumor size. These results were unexpected, as we found that Selumetinib was able to increase C2C12 fiber size *in vitro,* suggestive of a potential pro-anabolic effect on skeletal muscle. Moreover, we observed an increase in the number of nuclei per fiber, suggesting that inhibition of ERK1/2 phosphorylation may have increased the differentiation or fusion potential of myoblasts. However, despite reducing ERK1/2 phosphorylation in the skeletal muscle of LLC tumor bearing mice, Selumetinib did not provide any protective or hypertrophic effects. This was especially surprising due to the substantial inhibition of tumor growth that we observed. In general, tumor mass directly correlates to the extent of wasting, therefore a diminished tumor burden should theoretically reduce the severity of cachexia. The disconnect seen here suggests that Selumetinib, in this context, may actually inadvertently inhibit pro-anabolic pathways or enhance pro-cachectic pathways in the skeletal muscle of LLC tumor bearing mice. Lastly, the pro-cachectic pathways must be independent of IL-6. In this study, both circulating and tumor levels of IL-6 were greatly reduced with Selumetinib treatment. This was further supported due to the inability of Selumetinib to block LLC plasma-induced C2C12 myotube atrophy. The data suggest that another, or multiple other, inflammatory cytokines or circulating factors are the main driver/s of skeletal muscle wasting the in the LLC model, and Selumetinib was unable to attenuate it/them.

It is possible that the effects of Selumetinib on tumor growth and the preservation of muscle mass are disease specific, as Selumetinib treatment is associated with increased lean body mass in patients with biliary cancers [104]. In murine models of experimental cancer cachexia, Selumetinib shows efficacy in the C26 colon adenoma model. Biliary, colon, and lung cancers might all induce muscle wasting through a variety of different effectors. In some studies which utilize the C26 model, ERK inhibition is shown to have no effect on tumor mass, while protecting against cancer-induced cachexia [108,117]. However, another study using the same model reports a preservation of skeletal muscle and total and lean body weight, but the tumor mass is significantly less than the vehicle treated tumor bearers [109]. It should be noted though that these studies all use a different inhibitor and mice from a different genetic background than those used in this study.

The MEK pathway may also play different and context dependent roles in human versus murine cancer cachexia. In the phase II clinical trial of patients with biliary cancers, 52% of the patients that were treated with Selumetinib experienced a decrease in the target lesion size, similar to what we observed in our study. This could offer an explanation as to the gain in total body mass of patients treated with Selumetinib, as opposed to those patients receiving standard therapy. The increase in muscle mass could be a result of a reduced tumor burden, and not a direct effect on the skeletal muscles themselves. The authors hypothesize that the anabolic effects of Selumetinib is likely due to the inhibition of cytokine secretion. However, we observed a significant decrease in both tumor tissue and circulating levels of IL-6, with no preservation of skeletal muscle mass.

Lastly, the lack of muscle preservation we observed could be due to the differential regulation and requirements of the MEK pathway during myogenesis. While skeletal muscle satellite cells were not investigated in this study, it is possible that the constant inhibition of the MEK pathway led to a decrease in proliferation and subsequent depletion of the satellite cell pool. Published literature shows that ERK signaling is both stimulatory and inhibitory in the context of muscle differentiation. It has been shown the ERK1/2 activation is required for the proliferation and self-renewal of satellite cells [118,119]. However, this activation was not shown to be necessary for fusion of the expression of various muscle specific genes [120]. Additionally, ERK2 is necessary for the formation of mature myotubes. In C2C12 myoblasts, siRNA mediated knockdown of ERK2 resulted in an inability to fuse and form multinucleated myotubes [59]. There is also potential crosstalk from other pathways that should be considered. The Akt pathway, which is a positive regulator of muscle mass, is activated during differentiation of myotubes and leads to inhibition of the MEK pathway [105]. Conversely, effectors such as leukemia inhibitory factor, part of the IL-6 family of ligands, inhibit myogenic differentiation through ERK1/2 phosphorylation and activation [121]. Further work in C2C12 cells show that in the first 24 hours post induction of differentiation, ERK1/2 activation represses myogenic inhibition.

Inhibition of MEK1 in the latter stages of differentiation show similar effects of defective myotube formation [122]. These data show that myogenesis is a coordination of low MEK1 activity in the initial stages of differentiation, and high pathway activity thereafter. As such, while administration of Selumetinib inhibited tumor growth in LLC bearing mice, achieving the desired anabolic effects appear to be much more complicated.

Due to the apparent differential activation of ERK1/2 during myogenesis, it would seem that constant inhibition of the pathway may be detrimental to skeletal muscle mass. The prior studies mentioned had the ability to control the myogenic stages at which the pathway was inhibited or activated. This approach would be challenging to accomplish *in vivo*, although a potential alternative would be to administer the Selumetinib treatment intermittently. This method of dosing would allow for times of pathway activation, as opposed to being in a relatively constant state of inhibition. Based upon the published literature, allowing for cycles of activation and inhibition could potentially produce the desired stimulatory effects that are needed for skeletal muscle hypertrophy. Future investigations will be necessary in order to determine a proper dosing regimen required to exploit the therapeutic potential of ERK inhibition as a treatment against cancer-induced cachexia, and the effects of such dosing on tumor growth.

Taken together, this study suggests the need to consider the differential regulation of not only the MEK and IL-6 pathways, but other pathways that have been implicated in the muscle wasting of cancer cachexia. Moreover, the data point to deeply distinct drug-response phenotypes in conventional models of experimental cancer cachexia. This suggests a diversity in the underlying cellular and molecular mechanisms and a need for careful consideration when extrapolating results across different disease states, clinical trials, and model systems.

Chapter 3

Investigating the role of the Hedgehog signaling pathway in adult skeletal muscle homeostasis

Introduction

The loss of skeletal muscle can stem from a variety of causes. These can include severe trauma, volumetric muscle loss [22,123], chronic diseases including AIDS, cardiac failure, and cancer [3], and degenerative diseases like the muscular dystrophies [124,125]. Significant losses of skeletal muscle can reduce quality of life, cause permanent disabilities, decrease response or tolerance to therapies, and contribute directly to morbidity and mortality.

Our lab has found the Hedgehog (Hh) pathway to be dysregulated in the skeletal muscle of cachectic tumor bearing mice. In addition, we have substantial data implicating the pathway as a causal factor in wasting. From a clinical standpoint, GDC-0449 (Vismodegib) and LDE225 (Sonidegib), which inhibit pathway activity through inhibition of Smo, are currently FDA-approved for the treatment of advanced basal cell carcinoma. Given this, it would be advantageous to explore other potential applications and clinical uses for these drugs. Investigating new pathways to target for the treatment or aid in skeletal muscle preservation, growth, or regeneration would benefit patients across several disease states. However, in order to safely and effectively take advantage of any drug, we must first understand the role of the Hh pathway in maintaining skeletal muscle homeostasis, which is currently unclear.

The Hh pathway is of vital importance during the embryonic development of insects, some invertebrates, and vertebrates [126-128]. In vertebrates, three homologs have been identified, Shh, Indian hedgehog, and Desert hedgehog [129]. The core of the Hh signaling pathway revolves around four main components, ligands, the Ptch receptor, the Smo receptor, and the Gli family of transcription factors. During the absence of a ligand, Ptch normally acts to constitutively repress Hh signaling by inhibiting the activity of the Smo receptor. Upon binding of a ligand, Ptch repression of Smo is relieved, allowing for Smo activation of a cytoplasmic signal transduction cascade. This leads to the activation and nuclear translocation of Gli transcription factors and modulation of target gene expression [130-132].

The importance of Shh signaling during embryonic development has been well described. It plays an essential role in patterning of both chick and mouse embryos [133,134]. During the development of skeletal muscle, the Hh pathway plays a role in regulating the expression of myogenic regulatory factors such as Myf5 and MyoD [134-137]. However, in the context of muscle myogenesis, the published data on the role of Shh signaling are conflicting and there is a lack of investigation of the pathways role in adult skeletal muscle. It has been shown that treating primary chick myoblasts and murine C2 cells, with an active N-terminal peptide of Shh, results in the promotion of both proliferation and differentiation [138]. Similar results were observed in another study using primary chick myoblasts, where exogenous Shh increases myotube formation and bromodeoxyuridine incorporation, a marker for cellular proliferation [139].

Conversely, treatment of murine C2C12 and primary satellite cells with Shh retained the cells in a mononucleated and undifferentiated state. Concomitant treatment with cyclopamine, a Smo inhibitor, was able to reverse these effects and allow for formation of multinucleated myotubes [140].

While some investigation on the pathways role in myogenesis has been done, the role of the Hh pathway in the maintenance of skeletal muscle mass has yet to be examined. Given our findings of elevated Hh signaling in atrophic muscle, we hypothesized that the Hh pathway acts as a negative regulator of adult skeletal muscle mass. Therefore, we sought to explore the skeletal muscle phenotype of mice with elevated Hh pathway activity. To approach this question, we utilized several *in vitro* and *in vivo* models. *In vitro*, Hh pathway activity was modulated through pharmacological means, as well as with siRNA mediated knockdown of Hh pathway members. From these experiments, we observed alterations in both myotube diameter and the number of nuclei per fiber, suggesting that the pathway alters the dynamics of differentiation. *In vivo*, systemic administration of a Hh pathway agonist in wild-type (WT) C57BL/6J mice resulted in a muscle wasting phenotype. In addition, we also used a transgenic model of increased Hh pathway activity. These mice were heterozygous for *Ptch1*, which normally functions as the endogenous inhibitor of the pathway [141]. As such, it would be expected that these mice would have elevated Hh pathway activity [142]. We found these mice to have a hypotrophic/atrophic skeletal muscle phenotype, with additional evidence of reduced myogenesis and muscle function.

Materials and methods

Cell cultures

Murine C2C12 cells (ATCC) were grown in DMEM with 10% FBS, 100 U/mL penicillin, and 100 mg/mL streptomycin. The cells were maintained at low confluency at 37°C in a humidified atmosphere of 5% CO_2. To induce differentiation, confluent cells were switched to a low serum medium containing DMEM supplemented with 2% horse serum, 100 U/mL penicillin, and 100 mg/mL streptomycin. The pharmacologic compounds GDC-0449, LDE225, GANT61, or SAG (Selleck Chemicals) were diluted to the indicated concentration in differentiation medium.

For siRNA-mediated knockdown, a commercially available siRNA targeted towards *Ptch1* and a negative control were purchased (Table 1). C2C12 myoblasts were cultured in growth medium as above. Transfection of the designated siRNA was performed using Lipofectamine 3000 as per the manufacturer's instructions (Thermo Fisher Scientific). Knockdown of *Ptch1* was confirmed via qPCR at 24 hours post transfection.

Animals

All experimental animal protocols were approved by and used in compliance with the Indiana University School of Medicine Institutional Animal Care and Use Committee. Purmorphamine (Selleck Chemicals) was administered at a dose of 30 mg/kg in a solution of 30% polyethylene glycol via intraperitoneal injection, to eight week old male C57BL/6J mice (The Jackson Laboratory). Ptch1$^{+/lacZ}$ mice and WT littermates at various ages were obtained from The Jackson Laboratory. All mice were maintained on a regular light-dark cycle and allowed free access to food and water at all times.

Skeletal muscle function was assessed using the four-limb grip strength assay with a digital force gauge (Extech). This assay was performed by allowing the mice to grip a gauge with all four paws before being pulled from the base of the tail until the mouse could no longer hang on, thus generating a measurement of peak force [143].

Body composition analysis was measured using EchoMRI-500 Whole Body Magnetic Resonance Analyzer (EchoMRI) [144]. This equipment allows for live animal analysis without the use of anesthetics. The EchoMRI analyzer can quantify total body lean and fat mass.

At the conclusion of the experiment, euthanasia was performed under isoflurane general anesthesia. Skeletal muscles were identified, dissected free, and weighed. Portions of the muscle tissue were immediately snap frozen in liquid nitrogen before being stored at -80°C. This tissue was later used for protein and RNA extraction. Skeletal muscle designated for histomorphometric analysis was frozen in liquid nitrogen cooled 2-methylbutane before being stored at -80°C for future sectioning. The weights of skeletal muscle tissues are expressed as a percentage of total body weight (TBW) in order to normalize for any variations in body size.

Immunofluorescence

C2C12 myotubes were fixed and permeabilized in an ice cold acetone:methanol (1:1) solution for 20 minutes at -20°C. The cells were then rehydrated with PBS at room temperature for 10 minutes before being blocked in an 8% BSA solution for one hour. Primary antibody against MyHC, at a dilution of 1:200 in PBS, (MF 20, Developmental Studies Hybridoma Bank) was incubated overnight at 4°C with gentle agitation. The following day, cultures were washed with PBS before being incubated with an AlexaFluor 488-labeled anti-mouse IgG secondary antibody (R37120, Life Technologies), at a dilution of 1:1,000 in PBS, for one hour at room temperature and protected from light. Following rounds of PBS washes, nuclei were stained with DAPI and images were captured on an Axio Observer.Z1 (Zeiss). Myotube diameters were measured using ImageJ analysis software (Wayne Rasband, U.S. National Institutes of Health). Only fully formed myotubes with the majority in the field of view were measured.

For analysis of skeletal muscle fiber cross-sectional area, tibialis anterior muscles were mounted on cork discs with Optimal Cutting Temperature compound and frozen as mentioned above. Frozen sections were cut using a Leica CM1860 Cryostat (Leica Microsystems Inc.). The sections were then fixed in 100% acetone for 10 minutes at -20°C, rehydrated with PBS for 10 minutes at room temperature, and blocked for one hour with an 8% BSA solution. Primary antibody against dystrophin (VP-D508, Vector Laboratories), at a dilution of 1:60 in PBS, was incubated on the slides overnight at 4°C. Following washes with PBS, the slides were incubated with an AlexaFluor 594-labeled anti-mouse IgG secondary antibody (R37121, Life technologies), at a dilution of 1:1,000 in PBS, for one hour at room temperature and protected from light. Images were captured using an Axio Observer.Z1 (Zeiss) and muscle fiber cross-sectional area quantified using a macro installed on ImageJ analysis software [115].

Primary myofibers were isolated from the flexor digitorum brevis (FDB) muscle and fixed as previously described [145]. Primary antibody against Pax7 (Pax7, Developmental Studies Hybridoma Bank) was incubated on the cultures overnight at 4°C. Following PBS washes, detection was performed using an AlexaFluor 594-labeled anti-mouse IgG1 secondary antibody (A-21125, Life Technologies) at a dilution of 1:1,000 in PBS. The Nuclei were stained with DAPI and images were captured on an Axio Observer.Z1 (Zeiss).

Western blotting

Frozen quadriceps muscles were homogenized on ice in tissue lysis buffer consisting of 25 nM TrisHCl pH 7.6, 150 mM NaCl, 1% NP-40, 1% sodium deoxycholate, 0.1% SDS, and protease and phosphatase inhibitor cocktail tablets (Roche). Whole tissue homogenates were centrifuged at 14,000 rpm at 4°C for 15 minutes and the supernatant collected and stored at -80°C. The concentration of protein extracts was determined as previously mentioned in Chapter 2, and equal amounts of protein were denatured at 95°C for 5 minutes in loading buffer containing 125 mM Tris pH 6.8, 4% SDS, 20% glycerol, 1% bromphenol blue, and 200 mM dithiothreitol. Protein samples were resolved on Tris-Glycine gels before being transferred to nitrocellulose membranes (Bio-Rad Laboratories). The membranes were then blocked in Odyssey Blocking Buffer (LI-COR) for one hour at room temperature while shaking. The membranes were incubated overnight at 4°C with gentle agitation with primary antibodies directed against: Phospho-Akt Substrate, Phospho-Akt, Akt, Phospho-AMPK Substrate, Phospho-(Ser) Arg-X-Tyr/Phe-X-pSer Motif, Phospho-ATM/ATR Substrate, Phospho-CDK Substrate, eNOS, Phospho-p44/42 MAPK (ERK1/2) , p44/42 MAPK (ERK1/2), Phospho-MAPK Substrate, nNOS, Phospho-PKA Substrate, Phospho-PKC Substrate, Phospho-Stat3, Stat3, and Ubiquitin (9614, 4060, 9272, 5759, 2981, 6966, 9477, 32027, 4370, 4695, 2325, 4231, 9624, 6967, 9145, 4904, 3933, Cell Signaling Technology), and α-Tubulin (12G10, Developmental Studies Hybridoma Bank). All primary antibodies were used at a dilution of 1:1,000 in SEA BLOCK. Anti-mouse IgG DyLight 680 and Anti-rabbit IgG DyLight 800 fluorescent dye secondary antibodies at a dilution of 1:10,000 in SEA BLOCK (5470, 5151, Cell Signaling Technology) were used for detection, and incubated on the membranes for one hour at room temperature while shaking and protected from light. Membranes were imaged and quantified using the ODYSSEY CLx Infrared Imaging System and software (LI-COR).

Gene expression analysis

Total RNA was extracted from cells and whole tissue using the QIAGEN miRNeasy kit (QIAGEN Inc.) and cDNA generated using the Verso cDNA Synthesis kit (Thermo Fisher Scientific) as per the manufacturer's instructions. Relative mRNA expression levels of the genes of interest were measured using TaqMan Assay based probes (Thermo Fisher Scientific) on a LightCycler 96 (Roche). A complete list of the probes used in this study can be found on Table 3-1 below.

For RNA-Sequencing, total RNA was first evaluated for quantity and quality using an Agilent Bioanalyzer (Agilent). For quality purposes, only samples with a RIN number of 7 or higher were used. For library preparation, a starting amount of 1000 ng of total RNA was used. PolyA mRNA capture of total RNA was performed using the Dynabeads mRNA DIRECT Micro Kit (Ambion). Preparation of the cDNA library included enzymatic fragmentation, hybridization and ligation of adaptors, reverse transcription, size-selection, and amplification with barcode primers, following the Ion Total RNA-Seq Kit as per the manufacturer's instructions (Life Technologies). The resulting barcoded libraries were quantified and the qualities assessed using an Agilent Bioanalyzer. Eight microliters of 100 pM pooled libraries were then applied to an Ion Sphere Particles (ISP) template preparation, and amplification done using an Ion OneTouch 2 (Life Technologies), followed by ISP loading onto a PI chip and sequencing performed on an Ion Proton semiconductor (Life Technologies). Each PI chip allowed for approximately 140 million ISP templates, thus generating approximately 80-100 million usable reads, up to 10-15 Gb.

Data analysis

Statistical significance was determined by unpaired t-test for experiments containing two groups. For experiments containing groups of three or more, statistical significance was determined by one-way ANOVA followed by Tukey's multiple comparisons test. For experiments with two independent variables, a two-way ANOVA was used. A p-value less than 0.05 was considered to be statistically significant.

Table 3-1.

siRNA

Target	**Catalog #**	**Manufacturer**
Negative	4390846	Thermo Fisher Scientific
Ptch1	s72339	Thermo Fisher Scientific

Probes

Target	**Catalog #**	**Manufacturer**
Fbxo32	Mm00499523_m1	Thermo Fisher Scientific
Gli1	Mm00494654_m1	Thermo Fisher Scientific
Gli2	Mm01293117_m1	Thermo Fisher Scientific
Gli3	Mm00492337_m1	Thermo Fisher Scientific
Mrln	Mm01175781_m1	Thermo Fisher Scientific
MyHC	Mm01332564_m1	Thermo Fisher Scientific
Myogenin	Mm00446194_m1	Thermo Fisher Scientific
MyoD	Mm00440387_m1	Thermo Fisher Scientific
Pax3	Mm00435491_m1	Thermo Fisher Scientific
Pax7	Mm01354484_m1	Thermo Fisher Scientific
Ptch1	Mm00436026_m1	Thermo Fisher Scientific
Smo	Mm01162710_m1	Thermo Fisher Scientific
Trim63	Mm01185221_m1	Thermo Fisher Scientific

Results

Modulation of the Hedgehog pathway altered myotube diameter and nuclear accretion

We first wanted to look at the regulation of the Hh pathway during myogenesis. To approach this question, we used murine C2C12 cells and collected total RNA at various time points throughout the differentiation process. We began with mononucleated myoblasts and differentiated them into multinucleated myotubes for four days (Figure 3-1A). Total RNA was collected from baseline myoblasts and at every 24 hours of differentiation. Consistent with what is known about the expression of myogenic regulatory factors during myogenesis, we saw a decrease in the expression of the satellite cell markers Pax3 and Pax7, and a robust increase in the expression levels of myogenin and myosin heavy chain. Analysis of mRNA expression levels of *Ptch1* and *Gli1* showed that both were downregulated upon the onset of differentiation, and their expression decreased as it progressed (Figure 3-1B). As *Ptch1* is a target gene for Gli1 transcriptional activity, these data would suggest that Hh pathway activity is decreased during C2C12 myogenesis [146-148].

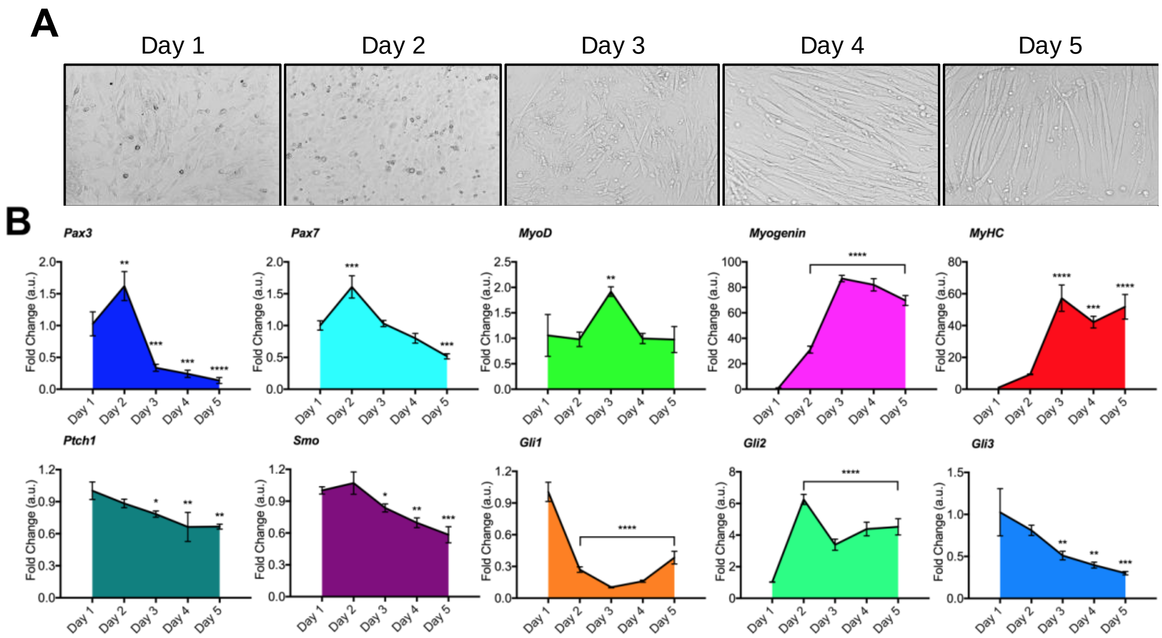

Figure 3-1. Time course analysis of *Ptch1* and *Gli1* during differentiation. Total RNA was collected from myoblasts and differentiating myotubes every 24 hours. **A:** Representative images of C2C12 cells undergoing differentiation. **B:** Analysis of mRNA expression levels of *Ptch1* and *Gli1* shows they decreased as myoblasts began forming mature myotubes. All conditions were performed in triplicate and the data are expressed as the means ± SD. Statistical significance was determined by one-way ANOVA. *p<0.05, **p<0.01, ***p<0.001, ****p<0.0001 versus Day 1.

Next, we sought to investigate the *in vitro* effects of Hh pathway manipulation on C2C12 myotubes (Figure 3-2). For inhibitors of the pathway, we used the Smo inhibitors GDC-0449 and LDE225 and the Gli inhibitor GANT61. Activation of the pathway was done using Smoothened Agonist (SAG) [149]. These inhibitors have been well characterized, with GDC-0449 and LDE225 being FDA-approved [150,151].

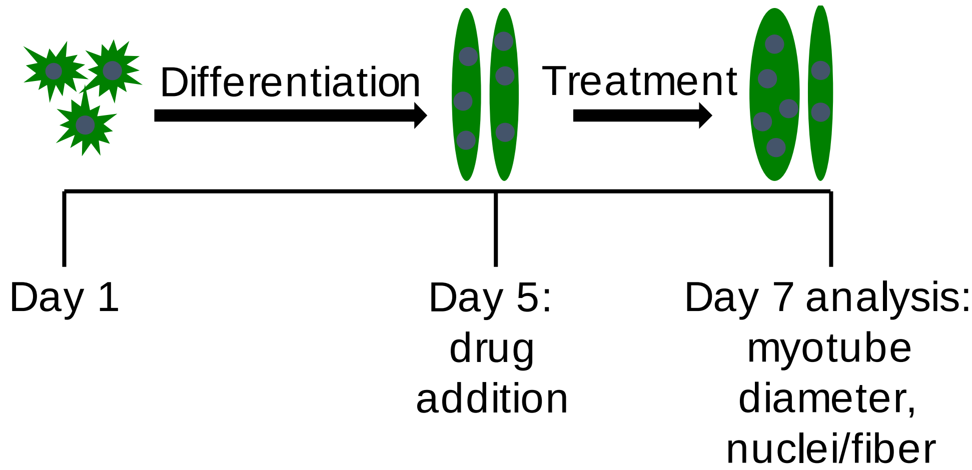

Figure 3-2. C2C12 model of treatment with Hh pathway agents. Graphical representation of the *in vitro* C2C12 model used to assess the phenotypic effects of Hh pathway modulation on myotubes. Myoblasts were differentiated into myotubes for four days before the designated treatment was added and incubated for an additional two.

We found that all the Hh pathway inhibitors used were able to induce significant myotube hypertrophy (Figure 3-3A-B). Conversely, treatment with SAG resulted in myotube atrophy (Figure 3-3C). In addition to the hypertrophic and atrophic effects, we also observed an alteration in nuclear accretion. Treatment with SAG caused a decrease in the number of nuclei per fiber, while use of the pathway antagonist GANT61 led to an increase in nuclei accumulation (Figure 3-3D). Taken together, these data suggest that Hh pathway activity can affect muscle fiber size, potentially through effects on myogenic differentiation.

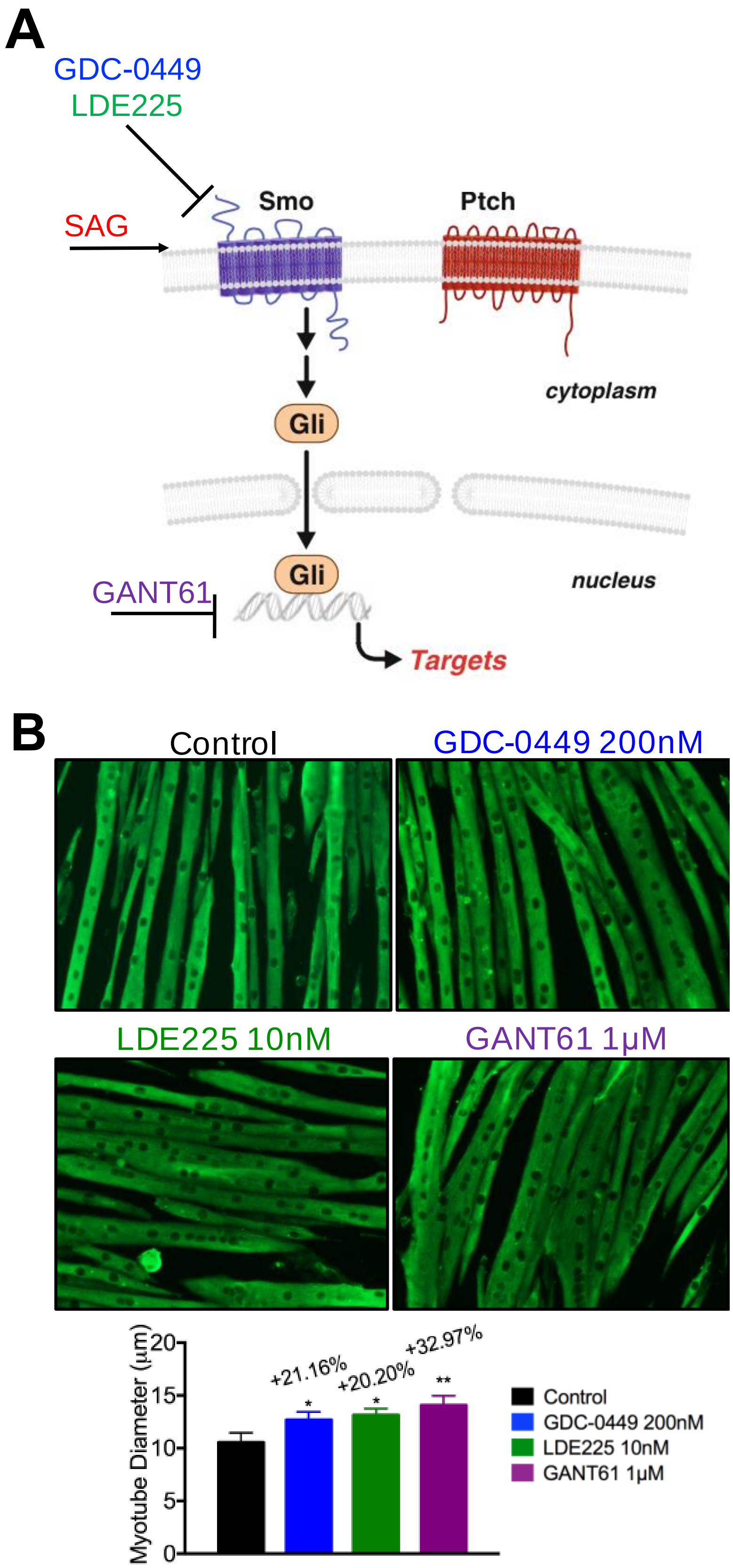
A
GDC-0449
LDE225
SAG
Smo
Ptch
cytoplasm
Gli
Gli
nucleus
GANT61
Targets
B
Control
GDC-0449 200nM
LDE225 10nM
GANT61 1μM
Myotube Diameter (μm)
0
5
10
15
20
+21.16%
*
+20.20%
*
+32.97%
**
Control
GDC-0449 200nM
LDE225 10nM
GANT61 1μM

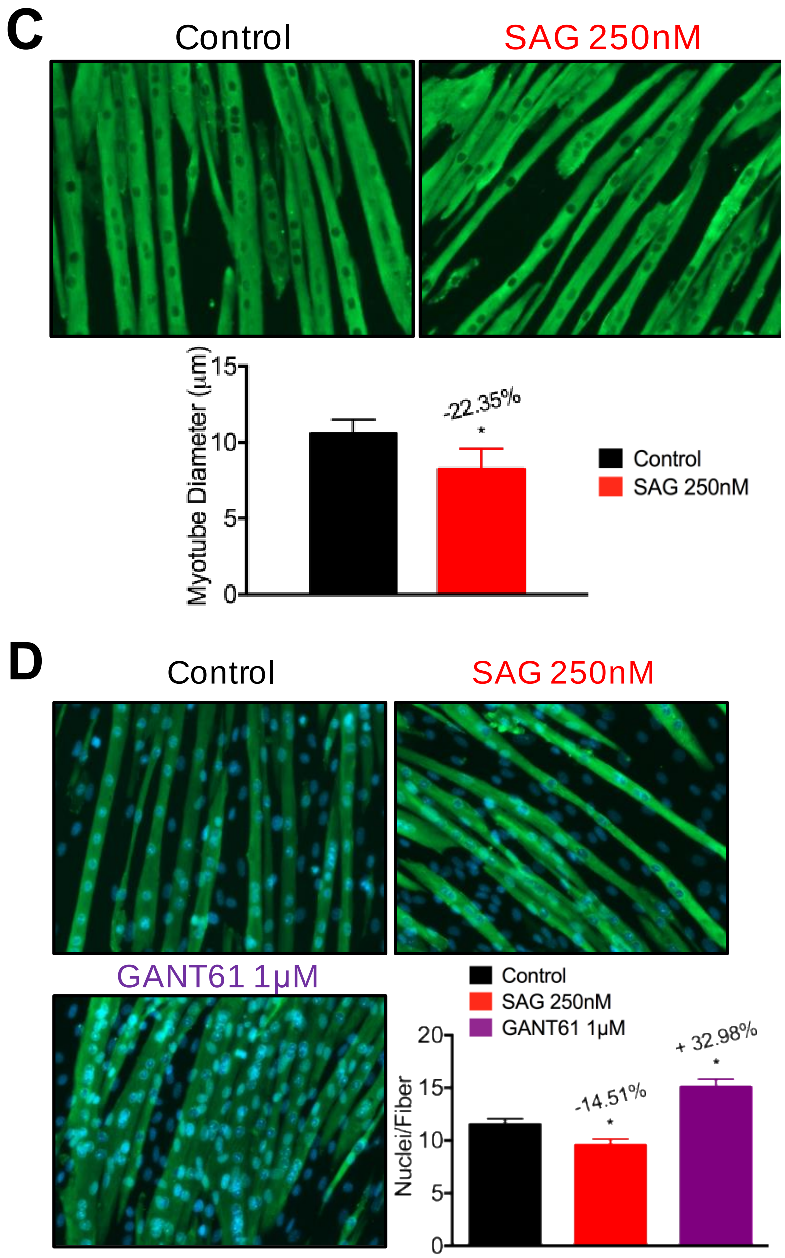

Figure 3-3. Modulation of the Hh pathway altered myogenesis. Myotubes were treated with an activator or inhibitors of the pathway before analysis of the myogenic phenotype. **A:** GDC-0449 and LDE225 are inhibitors of Smo. SAG is a Smo agonist. GANT61 is a Gli inhibitor. **B:** Treatment with Hh pathway inhibitors GDC-0449, LDE225, and GANT61 resulted in larger myotubes. All conditions were performed in triplicate and the data are expressed as the means ± SEM. Statistical significance was determined by one-way ANOVA. *$p<0.05$, **$p<0.01$ versus Control. **C:** The addition of a pathway agonist to the culture media caused a reduction in myotube diameter. All conditions were performed in triplicate and the data are expressed as the means ± SEM. Statistical significance was determined by unpaired t test. *$p<0.05$ versus Control. **D:** The number of nuclei inside of the myotubes were counted for the various treatment conditions. An inhibitor of the Hh pathway increased the number of nuclei per fiber, while an activator decreased it. The same number of fibers were counted for each condition. All conditions were performed in triplicate and the data are expressed as the means ± SEM. Statistical significance was determined by one-way ANOVA. *$p<0.05$ versus Control.

A Hedgehog pathway agonist induced muscle wasting *in vivo*

Given the observed atrophy from treatment with a Hh pathway agonist *in vitro*, we next looked at whether these same effects could be seen *in vivo*. To test this hypothesis, eight week old male C57BL/6J mice were administered the Hh pathway agonist, Purmorphamine, via intraperitoneal injection once daily for seven days [152]. Body weights were measured at baseline prior to the first dose and recorded every 24 hours over the course of the experiment. Mice treated with Purmorphamine lost a significant amount of weight when compared to the vehicle treated control group (Figure 3-4A). Analysis of body composition confirmed this, as Purmorphamine treatment resulted in a substantial loss in both total body lean and fat mass (Figure 3-4B). Mice in the vehicle treatment group showed no changes in total body lean mass and gained a significant amount of fat mass over the seven days. Analysis of individual skeletal muscles revealed a muscle wasting phenotype, similar to what we observed *in vitro,* and was consistent with the loss of total body weight and lean mass (Figure 3-4C). In addition, a drastic reduction in the epididymal fat pad mass was also observed. We do not believe that this atrophic muscle phenotype was a result of systemic organ wasting or toxicity as the heart and liver masses were not statistically different between the Purmorphamine and vehicle treated groups. These data suggest that in a non-disease state, activation of the Hh pathway results in skeletal muscle atrophy.

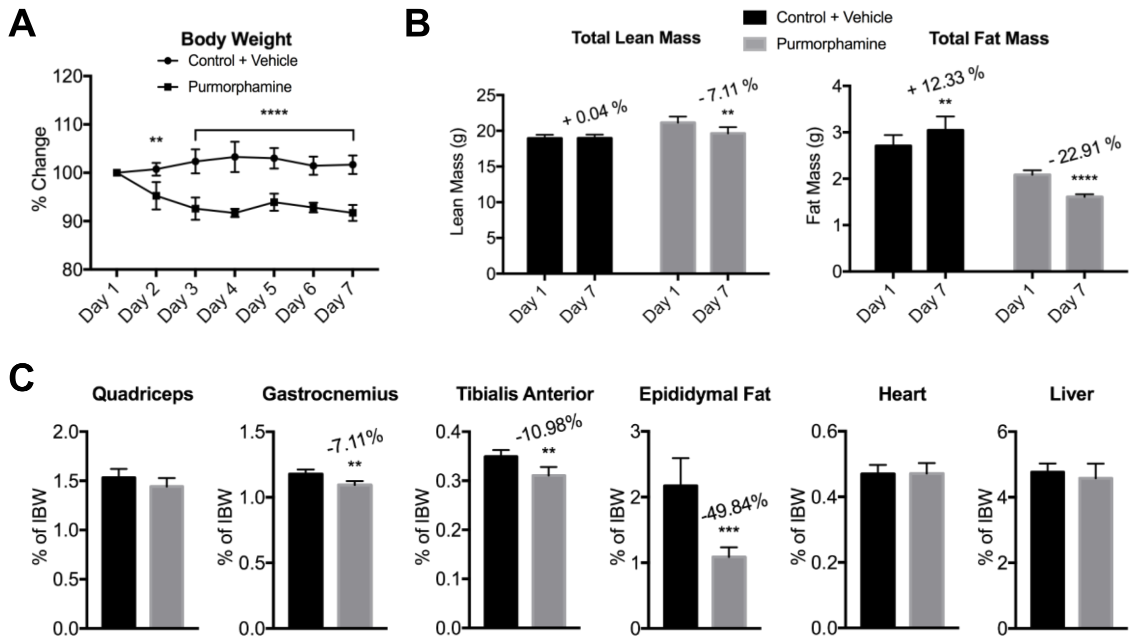

Figure 3-4. Systemic administration of a Hh pathway agonist resulted in skeletal muscle atrophy. Eight week old C57BL/6J mice were given Purmorphamine (n=6) or vehicle (n=6) once a day for seven days via intraperitoneal injection. Body weights were recorded daily and various muscles and organs collected at the time of necropsy. **A:** Purmorphamine treatment caused a significant reduction in body weight when compared to the vehicle control group. Changes are depicted as a percentage of the IBW measured at baseline (100%) prior to receiving the first dose. Data are expressed as the means ± SD. Statistical significance was determined by two-way ANOVA. **p<0.01, ****p<0.0001 versus Control + Vehicle. **B:** Body composition analysis revealed that Purmorphamine treatment caused a significant loss of total body lean and fat mass. Vehicle treated control mice showed no change in total body lean mass and gained fat mass compared to their baseline measurements. Data are expressed as the means ± SD. Statistical significance was determined by paired t test. **p<0.01, ****p<0.0001 versus Day 1. **C:** Various skeletal muscles and organs were compared between the groups. The values are normalized to the IBW of each individual animal in order to account for any difference in body size. Purmorphamine treated mice experienced atrophy in the gastrocnemius and tibialis anterior muscles, with a loss of epididymal fat pad mass as well. No wasting was observed in the heart or the liver. Data are expressed as the means ± SD. Statistical significance was determined by unpaired t test **p<0.01, ***p<0.001 versus Control + Vehicle.

Ptch1 **knockdown resulted in impaired myogenesis**

To further investigate the role of the Hh pathway in the maintenance of skeletal muscle, we next looked at the effects of *Ptch1* knockdown on C2C12 myogenesis (Figure 3-5).

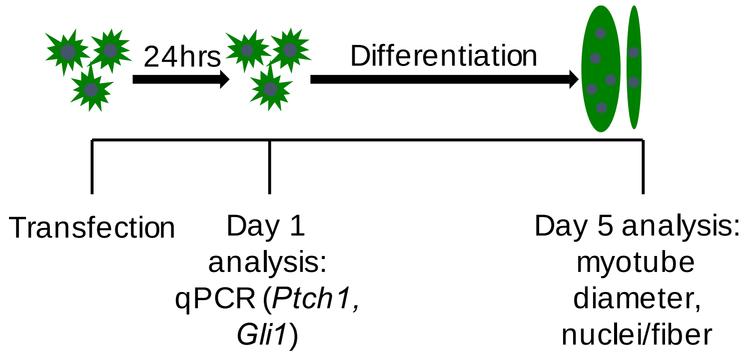

Figure 3-5. *Ptch1* knockdown. Graphical representation of *Ptch1* knockdown in C2C12 myoblasts. Myoblasts were transfected with either a Negative or *Ptch1* siRNA. Knockdown cells were then cultured for 24 hours before qPCR analysis and validation of knockdown. The knockdown cells were then differentiated for four days prior to analysis of myotube diameter and nuclei per fiber.

Ptch1 functions as the endogenous inhibitor of the Hh pathway; thus knockdown of *Ptch1* increased pathway activity, as evidence by the elevated expression of *Gli1* (Figure 3-6A). After the initial 24 hours following transfection, the myoblasts were then differentiated for an additional four days before further analysis. We found that knockdown of *Ptch1* resulted in significant decreases in both myotube diameter and the number of nuclei per myotube when compared to the Negative siRNA transfected controls (Figure 3-6B). Immunofluorescence staining for MyHC depicts the severely impaired differentiation of myoblasts knocked down for *Ptch1* (Figure 3-6C). The myogenic deficiency observed was not due to toxicity from the transfection or cell death. Low magnification imaging shows the cells at full confluency in both experimental groups, indicating that the myoblasts knocked down for *Ptch1* remained in a mononucleate state as opposed to entering terminal differentiation. These results suggest that increased Hh pathway activity, due to *Ptch1* knockdown, significantly reduces the differentiation capacity of myoblasts.

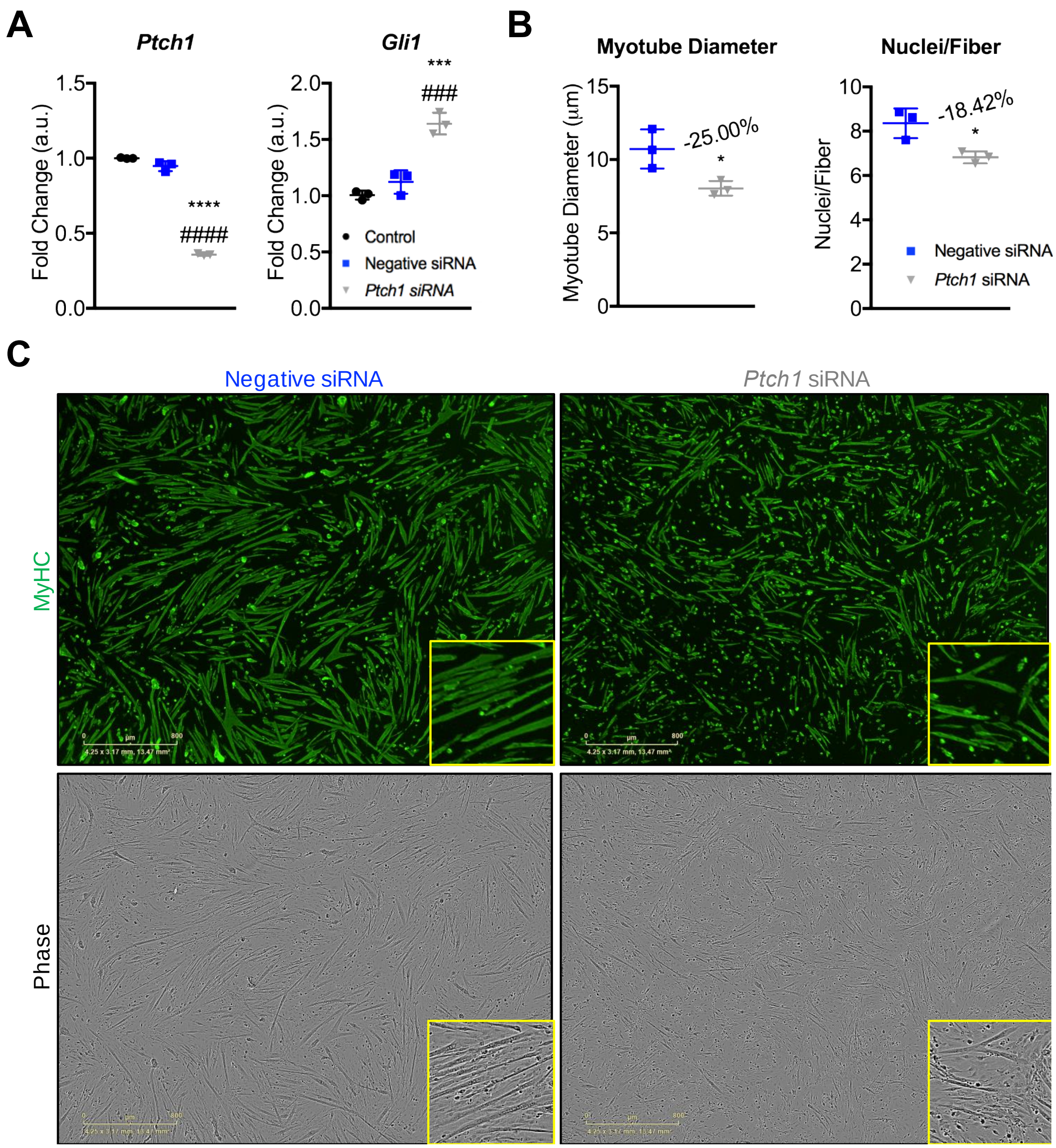

Figure 3-6. Increased Hh pathway activity led to defective differentiation. C2C12 myoblasts were knocked down for *Ptch1* via siRNA. **A:** qPCR analysis confirmed *Ptch1* knockdown and increased Hh pathway activity was confirmed by the upregulation of *Gli1* expression. All conditions were performed in triplicate and the data are expressed as the means ± SD. Statistical significance was determined by one-way ANOVA. ***p<0.001, ****p<0.0001 versus Control, ###p<0.001, ####p<0.0001 versus Negative siRNA. **B:** Myoblasts knocked down for *Ptch1* were differentiated into myotubes. Analysis of myotube diameter and nuclei per fiber shows that both were decreased when compared to the Negative siRNA transfected group. All conditions were performed in triplicate and the data are expressed as the means ± SEM. Statistical significance was determined by unpaired t test. *p<0.05 versus Negative siRNA. **C:** Representative images of myotubes stained for MyHC and phase imagining. *Ptch1* knockdown caused a severe impairment of differentiation. Phase imaging showed that this was not due to transfection toxicity or cell death as a result of the knockdown.

Hedgehog pathway activation results in a hypotrophic/atrophic muscle phenotype in mice

Because *Ptch1* knockdown caused increased Hh pathway activity and impaired myogenesis *in vitro*, we next looked to model this scenario *in vivo*. Here, we assessed the skeletal muscle phenotype of Ptch1$^{+/lacZ}$ mice and WT littermates at various ages. With these transgenic mice, we would expect there to be increased Hh pathway activity due to *Ptch1* haploinsufficiency. To test this, total RNA was extracted from tibialis anterior muscles and qPCR analysis performed. We found that in the Ptch1$^{+/lacZ}$ mice, *Gli1* mRNA expression levels were upregulated when compared to WT littermates, indicating increased activity (Figure 3-7A). Concomitant with this increase in pathway activity, we observed a decrease in muscle mass in both 10 and 12 week old mice (Figure 3-7B). Analysis of muscle fiber cross-sectional area was consistent with the measured weights (Figure 3-7C). These findings are consistent with the prior *in vitro* and *in vivo* data, indicating that the Hh pathway acts as a negative regulator of adult skeletal muscle.

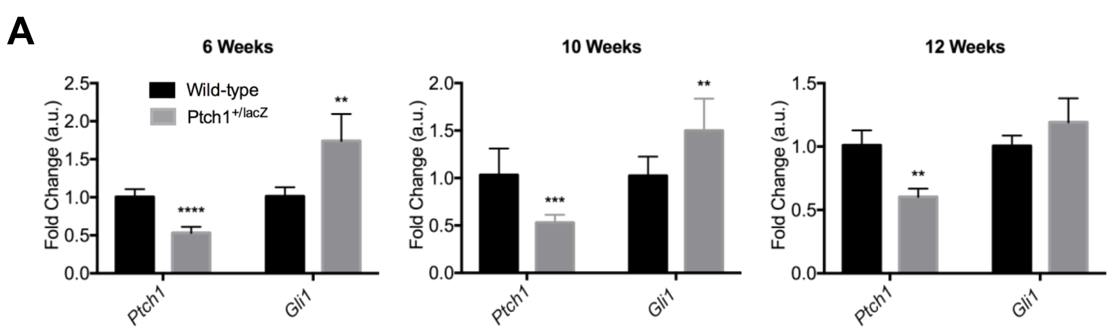

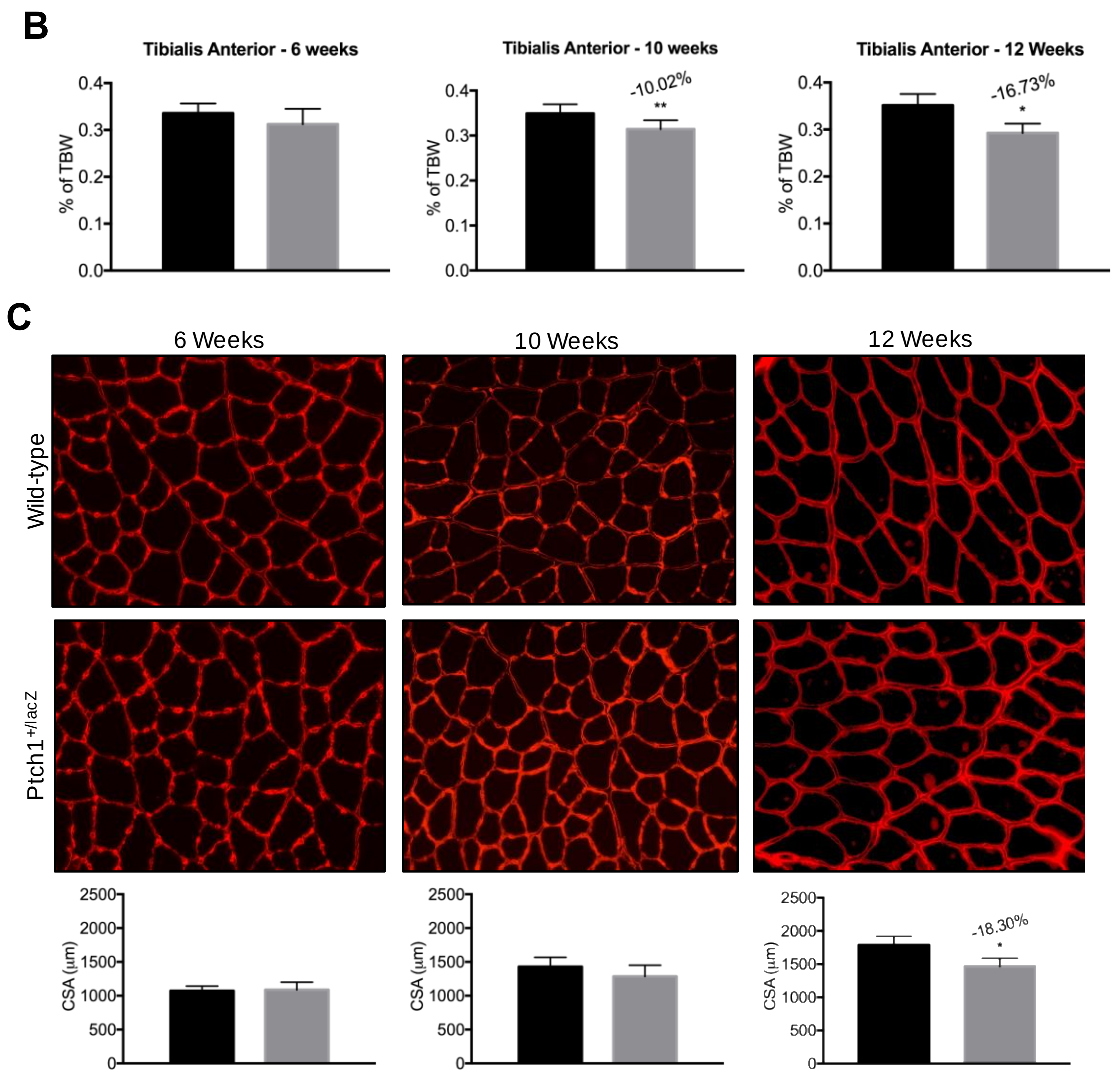

Figure 3-7. *Ptch1* heterozygosity resulted in skeletal muscle atrophy. The skeletal muscle phenotype of *Ptch1* heterozygous mice were compared to WT littermates. Mice were analyzed at 6, 10, and 12 weeks of age. **A:** Functional loss of one *Ptch1* allele resulted in increased Hh pathway activity, as evidenced by qPCR analysis of *Gli1* mRNA expression levels. This was assessed in 6 week old Ptch1$^{+/lacZ}$ mice (n=7) and WT littermates (n=5), 10 week old Ptch1$^{+/lacZ}$ mice (n=9) and WT littermates (n=10), and 12 week old Ptch1$^{+/lacZ}$ mice (n=3) and WT littermates (n=5). Data are expressed as the means ± SD. Statistical significance was determined by unpaired t test. **p<0.01, ***p<0.001, ****p<0.0001 versus WT. **B:** Weights of tibialis anterior muscles, normalized to TBW, were compared to WT littermates. Atrophy was observed at both 10 and 12 weeks of age. Data are expressed as the means ± SD. Statistical significance was determined by unpaired t test. *p<0.05, **p<0.01 versus WT. **C:** Representative images and quantification of tibialis anterior muscle fiber cross-sectional area. Data are expressed as the means ± SD. Statistical significance was determined by unpaired t test. *p<0.05 versus WT.

We next sought to investigate a potential cause of the atrophic phenotype in the Ptch1$^{+/lacZ}$ mice. Western blotting analysis showed a significant decrease in the phosphorylation of substrates in the Akt pathway (Figure 3-8A). The Akt axis is known to be a major pro anabolic pathway, and thus decreased Akt activity is consistent with our findings of smaller skeletal muscles [153]. Conversely, looking at catabolic pathways, we found that the smaller muscle size was not accompanied by increased protein ubiquitylation (Figure 3-8B). Total protein ubiquitination was unchanged between Ptch1$^{+/lacZ}$ mice and WT littermates. In addition, mRNA expression levels of the E3 ubiquitin ligases *Atrogin-1* and *MuRF1* were comparable between the groups (Figure 3-8C). While these are indirect measurements of ubiquitin-mediated proteolytic degradation, they suggest no difference between groups. These data suggest that the skeletal muscle phenotype observed was caused by additional factors beyond Akt-mediated protein synthesis and proteasome-mediated degradation.

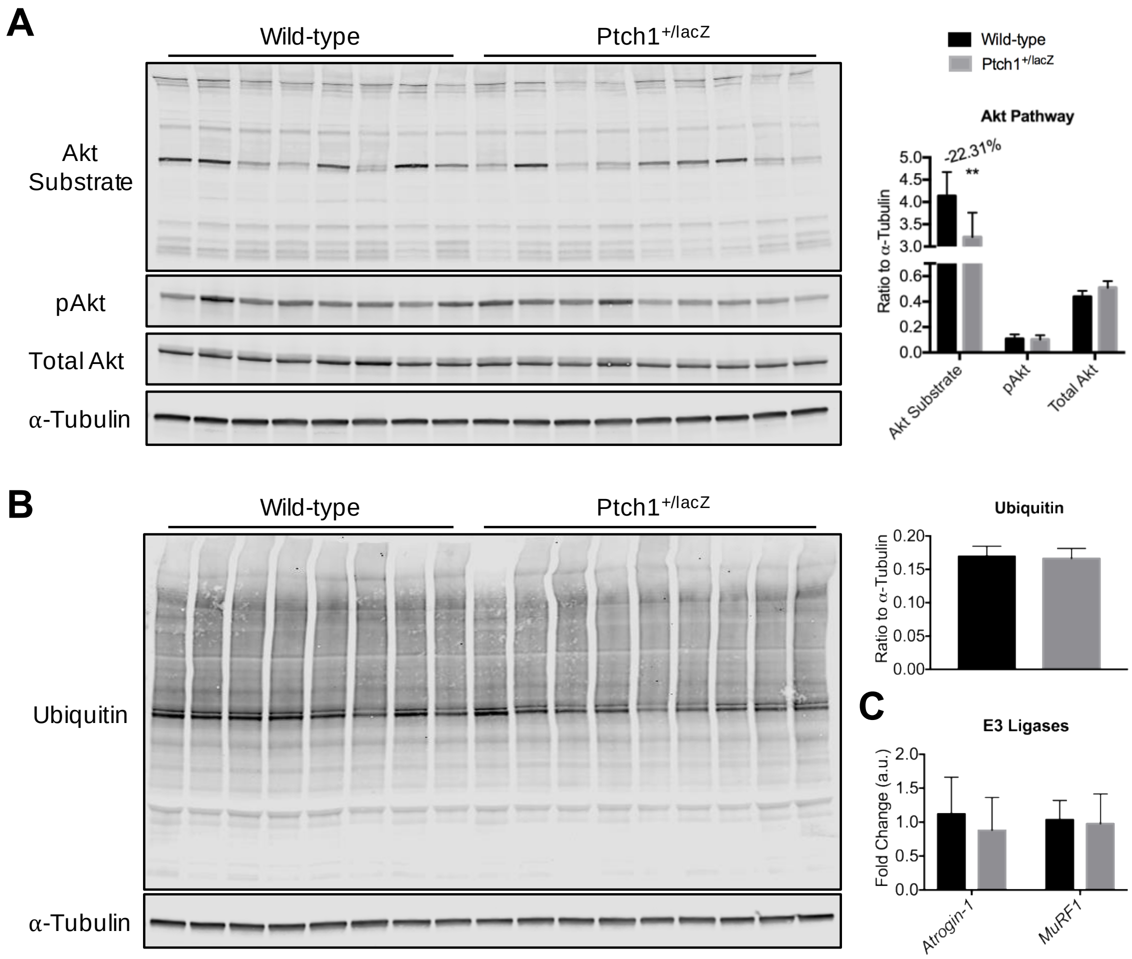

Figure 3-8. Ptch1$^{+/lacZ}$ mice showed decreased activity of a pro anabolic pathway. Western blotting analysis of quadriceps muscle lysates from 10 week old Ptch1$^{+/lacZ}$ mice and WT littermates. **A:** Western blot image and quantification showed that phosphorylation of substrates in the Akt pathway were decreased in *Ptch1* heterozygotes. Phosphorylation of Akt itself and total Akt levels were unchanged. Data are expressed at the means ± SD. Statistical significance was determined by unpaired t test. **p<0.01 versus WT. **B:** Western blot image and quantification showed similar levels of total protein ubiquitination in Ptch1$^{+/lacZ}$ mice compared to WT littermates. Data are expressed as the means ± SD. **C:** Total RNA was extracted from tibialis anterior muscles of 10 week old Ptch1$^{+/lacZ}$ mice and WT littermates. Expression levels of the E3 ubiquitin ligases *Atrogin-1* and *MuRF1* were comparable between the two groups. Data are expressed as the means ± SD.

Given that Hh pathway modulation *in vitro* with pharmacological agents altered nuclear accretion, we next looked to see if those effects were present *in vivo* as well. Analysis of skeletal muscle cross-sections showed a similar number of total nuclei between Ptch1$^{+/lacZ}$ mice and WT littermates. However, we found a significant decrease in the number of nuclei inside of the myofibers of Ptch1$^{+/lacZ}$

mice, consistent with the findings from the *in vitro* SAG treatment (Figure 3-9A). The total number of fibers in the muscle were comparable between the groups. This suggests that the myofibers of Ptch1$^{+/lacZ}$ mice developed normally initially, but subsequently failed to acquire nuclei, rendering them smaller overall versus WT mice. To test the myogenic capacity of satellite cells in Ptch1$^{+/lacZ}$ and WT mice, primary myofibers were isolated from the FDB muscle and cultured in growth media for 24 hours prior to being stained for the satellite cell marker Pax7 [154,155]. This protocol is known to activate proliferation of satellite cells associated with the myofiber. On a per fiber basis, Ptch1$^{+/lacZ}$ mice showed far fewer Pax7 positive cells when compared to WT littermates (Figure 3-9B). Taken together, these data further suggest that the Hh pathway acts as a negative regulator of skeletal muscle mass by reducing myogenesis nuclear accretion.

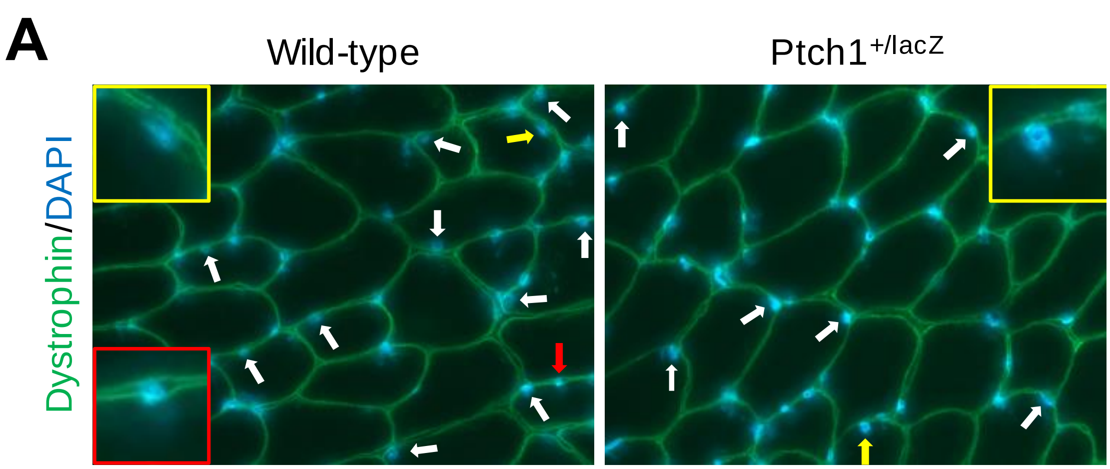

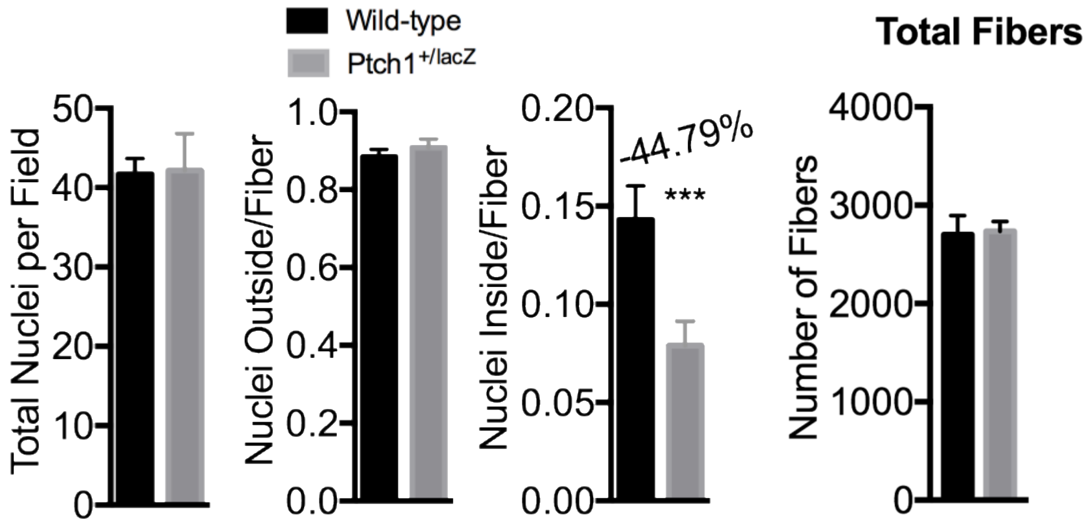
Wild-type
Ptch1+/lacZ
Total Fibers
Total Nuclei per Field
Nuclei Outside/Fiber
Nuclei Inside/Fiber
Number of Fibers
-44.79%
***
50
40
30
20
10
0
1.0
0.8
0.6
0.4
0.2
0.0
0.20
0.15
0.10
0.05
0.00
4000
3000
2000
1000
0

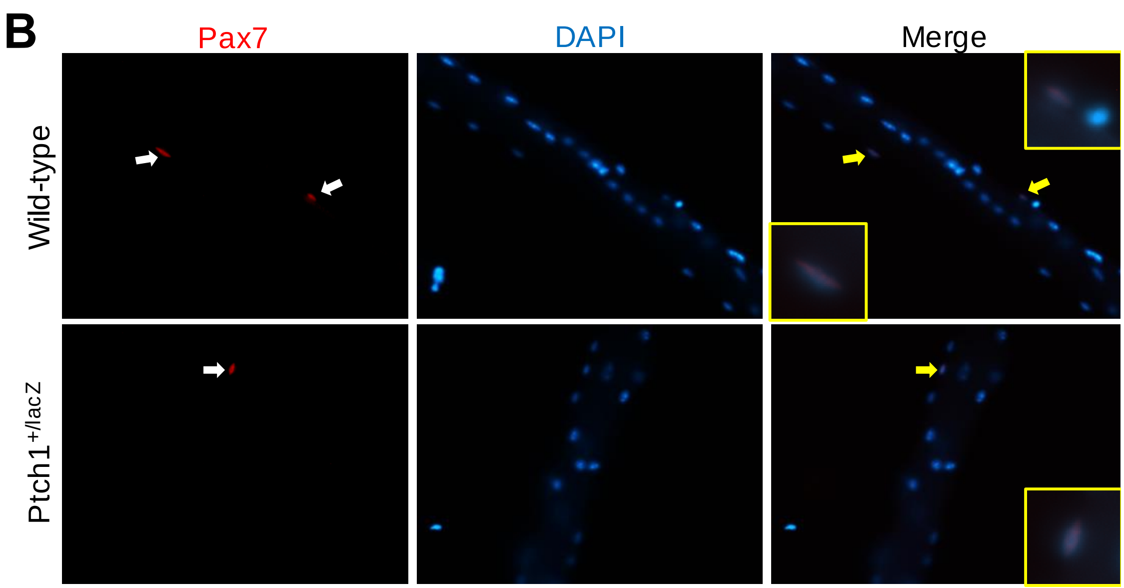
B
Pax7
DAPI
Merge
Wild-type
Ptch1+/lacZ

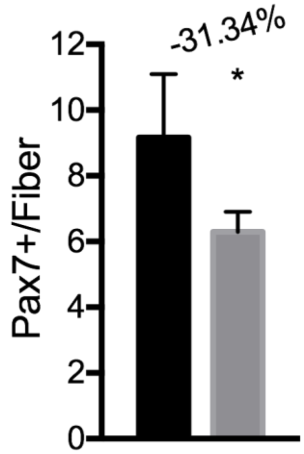

Figure 3-9. Ptch1$^{+/lacZ}$ mice displayed aberrant, reduced myogenesis. Using the 10 week old mice, tibialis anterior cross-sections were assessed for nuclear accretion and FDB primary myofibers were isolated and analyzed for Pax7 expression. **A:** Representative images of cross-sections of tibialis anterior muscles stained for dystrophin (green) and nuclei (blue). Analysis of the nuclei showed that both groups had a comparable number of total nuclei and the number of nuclei outside of myofibers. The red arrow and inset depict an example of a nuclei that was considered to be outside of a myofiber. However, *Ptch1* heterozygotes had significantly less nuclei inside of the myofibers compared to WT littermates (white arrows). The yellow arrows and insets depict specific examples of what was considered to be inside of a myofiber. Data are expressed at the means ± SD. Statistical significance was determined by unpaired t test. ***p<0.001 versus WT. **B:** Primary myofibers were isolated from the FDB muscle and cultured for 24 hours before being stained for Pax7. Representative images show Pax7+ cells (red) indicated by white arrows. Yellow arrows and insets show that the Pax7+ cells colocalized with nuclear staining (blue). Ptch1$^{+/lacZ}$ mice showed a significant decrease in the number of Pax7+ cells per myofiber. Data are expressed at the means ± SD. Statistical significance was determined by unpaired t test. *p<0.05 versus WT.

Ptch1$^{+/lacZ}$ mice showed differential regulation of genes associated with growth

RNA sequencing was performed on the tibialis anterior muscles from Ptch1$^{+/lacZ}$ mice and WT littermates to evaluate differences in the transcriptome. Using Ingenuity Pathway Analysis, we found that a large number of the differentially regulated genes were involved in cell growth (Figure 3-10). In addition, Ptch1$^{+/lacZ}$ mice showed several folds downregulation of genes involved in cell proliferation and cell cycle. Western blotting analysis showed that the phosphorylation of cyclin-dependent kinases was less in Ptch1$^{+/lacZ}$ mice, although this was not statistically significant (Supplemental Data). The downregulation of these genes could potentially explain the phenotype of smaller skeletal muscles. Analysis of muscle cross-sections showed a decrease in the number of nuclei that were inside of the myofibers, and cultured primary myofibers had far fewer Pax7 positive cells. The reduced expression of genes associated with cell cycle and growth could offer an explanation to this phenomenon. A decreased capacity for proliferation would mean a smaller pool of myoblasts and satellite cells. If these cells were less abundant, there would be fewer cells to differentiate and fuse into myofibers.

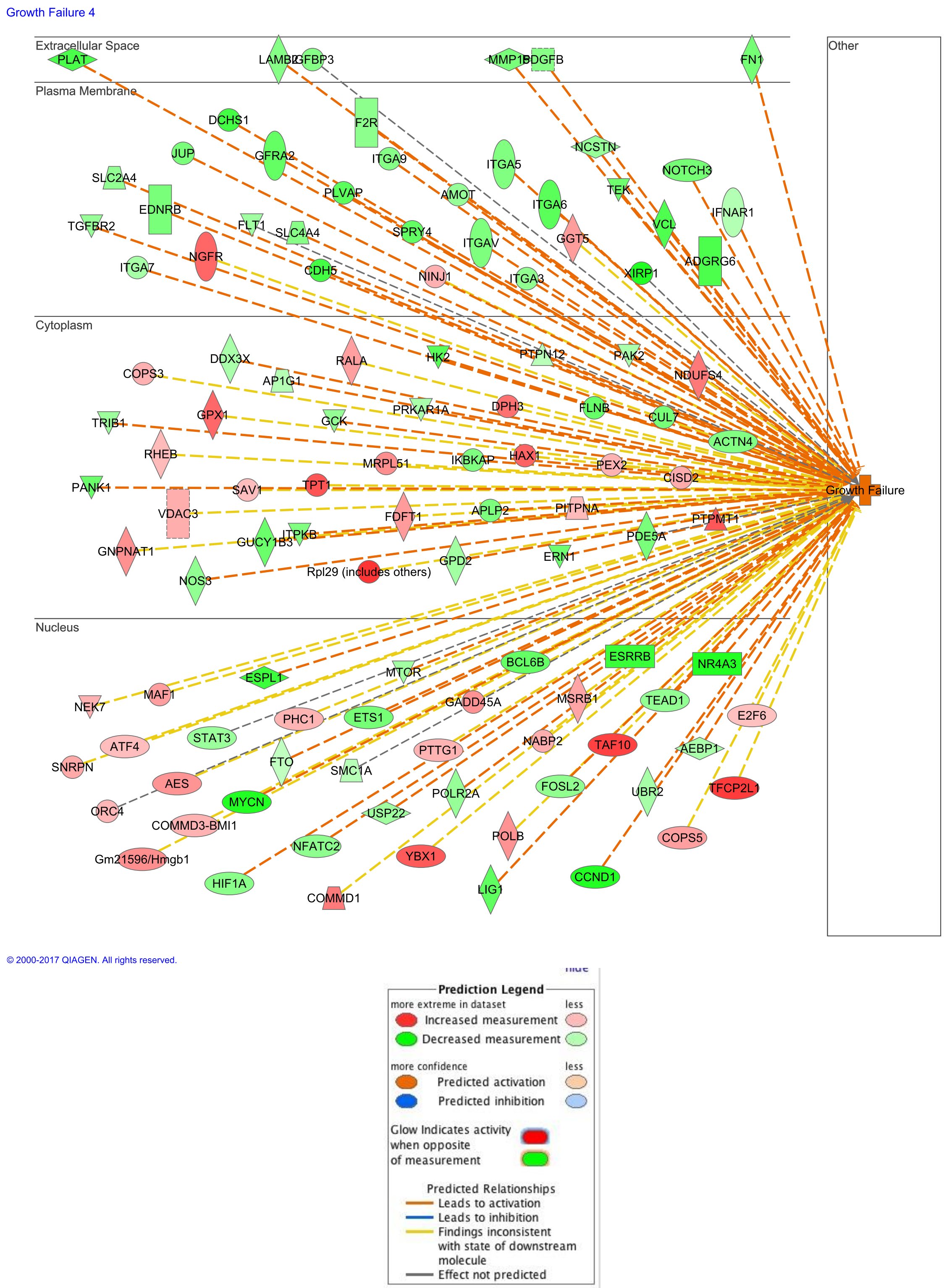

Figure 3-10. Differential regulation of genes associated with growth in Ptch1$^{+/lacZ}$ mice. Total RNA was extracted from the tibialis anterior muscles of 10 week old Ptch1$^{+/lacZ}$ mice (n=3) and WT littermates (n=3) and RNA-Seq analysis performed. RNA-Seq analysis showed decreased expression of several genes associated with cell proliferation and growth. Genes considered statistically significant had a p<0.05 and a false discovery rate (FDR) of less than 5%.

Ptch1$^{+/lacZ}$ mice exhibited a functional impairment of skeletal muscle

The atrophic skeletal muscles were not the only phenotype observed due to *Ptch1* heterozygosity. We also observed a difference in muscle function between Ptch1$^{+/lacZ}$ mice and WT littermates. Four-limb grip strength test determines the peak force with which a mouse can hold on to a grid. The test was repeated three times for each mouse, with an opportunity to rest between each trial, and the recorded values were averaged. We first analyzed the mice at six weeks of age, and while we did observe a slight variation in grip strength, this was not statistically significant. However, when analyzed at 10 and 20 weeks of age, we observed a notable reduction in the strength of Ptch1$^{+/lacZ}$ mice (Figure 3-11A). We then turned our attention to our RNA-Seq data in an attempt to find a possible explanation as to why these mice were so much weaker. These data provided evidence to suggest an alteration in calcium (Ca^{2+}) handling and a decreased expression of genes encoding for myofibrillar structural proteins as a potential cause for the functional deficit. RNA-Seq data, confirmed by qPCR analysis, showed that *Myoregulin* (Mrln) was increased in Ptch1$^{+/lacZ}$ mice (Figure 3-11B). Mrln functions to regulate Ca^{2+} uptake by interacting with the sarcoplasmic reticulum calcium transport ATPase (SERCA), and *Mrln* knockout mice have improved skeletal muscle performance [156,157]. Furthermore, there was a downregulation of genes for several muscle structural proteins (Figure 3-11C). These genes included myomesin-3, α-actinin-2, collagen type XV, and several myosin heavy chain isoforms. Taken together, these data support the observation that Ptch1$^{+/lacZ}$ mice were significantly weaker than WT littermates, as irregular Ca^{2+} handling and a reduced expression of muscle structural proteins could greatly affect the contractility, function, and performance of skeletal muscle.

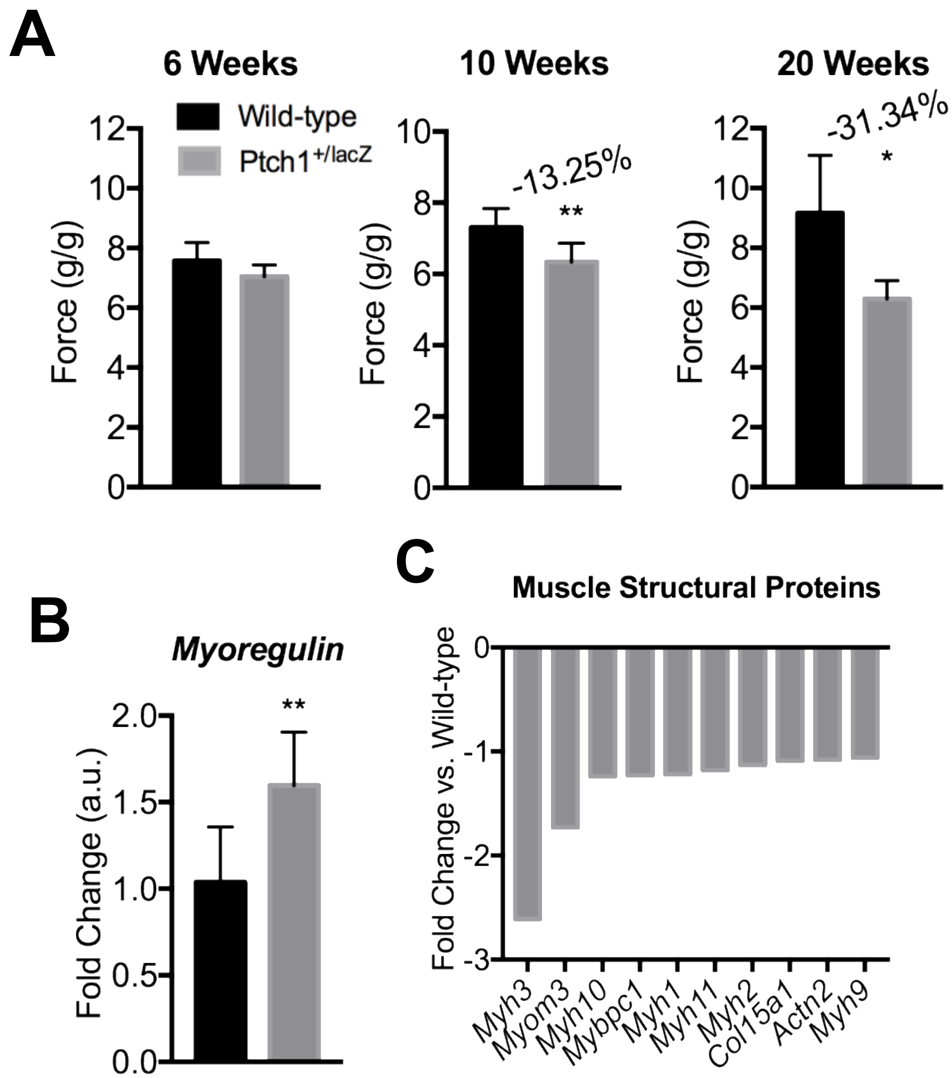

Figure 3-11. *Ptch1* heterozygosity resulted in a functional impairment of skeletal muscle. Four-limb grip strength was assessed in 6, 10, and 20 week old mice (20 week: $Ptch1^{+/lacZ}$ mice n=3, WT littermates n=3). **A:** $Ptch1^{+/lacZ}$ mice were significantly weaker when compared to WT littermates. This phenotype appeared to worsen with age. Data are expressed as the means ± SD. Statistical significance was determined by unpaired t test. *p<0.05, **p<0.01 versus WT. **B:** qPCR validation of *Mrln* expression from RNA extracted from the tibialis anterior muscles of 10 week old $Ptch1^{+/lacZ}$ mice and WT littermates. Data are expressed as the means ± SD. Statistical significance was determined by unpaired t test. **p<0.01 versus WT. **C:** RNA-Seq analysis showed decreased expression of genes encoding for skeletal muscle structural proteins. Genes considered statistically significant had a p<0.05 and an FDR<5%. Data are expressed as the fold change versus WT.

Discussion

Significant losses of skeletal muscle are extremely debilitating. This can occur from severe trauma or in degenerative diseases such as muscular dystrophy. Skeletal muscle atrophy is also a hallmark of many chronic diseases including cancer, AIDS, and organ failure. The Hh pathway plays a crucial role in embryonic skeletal muscle development [63,64,135,137]. Several studies have been done looking at the pathways role in various injury and dystrophic muscle regeneration models [158-162]. In these studies, exogenous overexpression of Shh is shown to be beneficial to the injury response. However, this upregulation of the Hh pathway is transient, and its benefits to regeneration may be explained by reverting the muscle to a more embryonic phenotype, which is known to occur [163,164]. The consequences of a prolonged and sustained elevation of Hh pathway activity, such as in a chronic disease state, have yet to be determined. As it stands, little has been done with regards to Hh in the maintenance of adult skeletal muscle. Here, we characterized the skeletal muscle phenotype of mice with elevated Hh pathway activity due to *Ptch1* heterozygosity. *In vitro*, Hh pathway agonism resulted in myotube atrophy and a decreased number of nuclei per fiber. *In vivo*, systemic administration of Purmorphamine resulted in muscle wasting. A similar phenotype was observed in Ptch1$^{+/lacZ}$ mice, where Hh pathway activity is increased. Compared to WT littermates, Ptch1$^{+/lacZ}$ mice were significantly weaker, had smaller muscles, and showed reduced expression of genes associated with cell proliferation, cycle, and muscle structural proteins.

Together, these data support a role for the Hh pathway in maintaining normal adult skeletal muscle.

Our *in vitro* data suggests that the effects of Hh pathway modulation on myotube diameter is likely due to an alteration in the differentiation capacity of the myoblasts. Similar findings have previously been published by other groups. Lee et al. identified a small molecule inhibitor (SMI) that induces mouse embryonic stem cells to differentiate into muscle cells [165]. The authors show that SMI2 is able to increase mRNA levels of several myogenic regulatory factors such as *MyoD* and *Myogenin*, as well as increasing the percentage of MyHC positive cells. They claim that one of the mechanisms responsible for this is the inhibition of Shh signaling. Moreover, co-treatment of SMI2 with a Smo agonist blunts the increases in myogenic genes induced by SMI2 treatment alone. Koleva et al. demonstrated that treatment of C2C12 myoblasts and primary satellite cells, with recombinant Shh, results in a complete inhibition of myotube formation [140]. Additionally, the authors show that Shh causes a significant increase in BrdU incorporation, in a dose dependent fashion, in C2C12 myoblasts and satellite cells. These data are consistent with our observations from SAG treatment resulting in a decreased number of nuclei per fiber, and *Ptch1* knockdown leading to an impairment of C2C12 myogenesis. This suggests that increased Hh pathway activity inhibits myoblasts from arresting, entering terminal differentiation, and subsequently fusing

In vivo data from Purmorphamine treated and Ptch1$^{+/lacZ}$ mice sheds further light on the effects of increased Hh pathway activity on normal adult skeletal muscle. As with the phenotype of smaller myotubes and impaired myogenesis that others and we have found *in vitro*, a similar observation was made in skeletal muscle tissue. It is well known that the Akt pathway plays a major role in the regulation of skeletal muscle both *in vitro* and *in vivo* [172-175]. *In vivo*, it has been shown that transgenic mice with constitutive activation of Akt in the skeletal muscle exhibit remarkable hypertrophy [176]. Conversely, *Akt1* null mice are significantly smaller than both WT and heterozygous littermates [177]. Though the authors do not specifically compare the skeletal muscles amongst the groups, null mice are 15-20% smaller throughout their lives. In a model of compensatory hypertrophy, Akt phosphorylation increases throughout the hypertrophy process [153]. The study further demonstrates that Akt is also active during muscle hypertrophy in a model of recovery following disuse atrophy. Furthermore, electroporation of a constitutively active Akt plasmid results in significant hypertrophy, which is protective against muscle atrophy when used in a denervation injury model. Further analysis into the atrophic phenotype of $Ptch1^{+/lacZ}$ mice showed a decrease in the phosphorylation of substrates of the Akt pathway. Together those substrates include proteins that are involved in synthesis, proliferation, transcription, and anti-apoptotic proteins [166,167]. Certain substrates of the pathway, such as GSK-3β, have been shown to directly regulate skeletal muscle mass in both human and mouse [168-171]. Reduced Akt activity thus may offer an explanation for the decrease in muscle mass that we observed in the $Ptch1^{+/lacZ}$ mice.

In addition to having smaller muscles, the $Ptch1^{+/lacZ}$ mice also exhibited a functional deficit in skeletal muscle. $Ptch1^{+/lacZ}$ mice mice were much weaker than their WT littermates, and that this disparity was exacerbated with age. In the $Ptch1^{+/lacZ}$ mice, *Mrln* was significantly downregulated. *Mrln* encodes myoregulin, a micropeptide similar to sarcolipin and phospholamban which serve as key regulator of sarcoplasmic reticulum Ca^{2+} ATPases (SERCAs). In C2C12 myoblasts, *Mrln* overexpression decreases Ca^{2+} levels in the sarcoplasmic reticulum, indicating that Mrln functions to inhibit the dynamics of the SERCA pump. When *Mrln* is deleted in the skeletal muscle, mice show a drastic increase in muscle performance. Compared to WT littermates, *Mrln* null mice ran approximately 30% longer when subjected to treadmill running until exhaustion exercise, which translates to a 55% increase in the total distance ran [156]. The decreased expression of *Mrln* observed here could explain why the $Ptch1^{+/lacZ}$ mice were considerably weaker.

Another reason for the decrease in muscle strength in $Ptch1^{+/lacZ}$ mice could be attributed to the reduction in expression of genes encoding muscle structural proteins. In the $Ptch1^{+/lacZ}$ mice, genes encoding for several myosin heavy chain isoforms were downregulated, including both embryonic and adult fast myosins, likely affecting muscle function and myofibril stability [178,179]. Additionally, *Myomesin-3* expression levels were decreased 1.73 fold in the $Ptch1^{+/lacZ}$ mice. This protein is a component of the sarcomeric M-band, and plays a role in the network required for proper contraction of skeletal muscle [180,181]. Furthermore, *α-actinin-2* was downregulated 1.08 fold. This protein is essential to the thin filaments of the muscle Z-disc [182-184]. Our RNA-Seq data also showed a decrease in *collagen type XV* expression, by 1.09 fold. A knockout study of *Col15a1* shows that null mice, while fertile and had normal gross development and lifespan compared to WT littermates, have several abnormalities in their skeletal muscle [185]. At 13 weeks of age, histological analysis of the null mice shows signs of muscle degeneration. Furthermore, the *Col15a1* knockouts were more vulnerable to exercise-induced muscle damage. Following bouts of heavy load treadmill running, *Col15a1* knockout mice showed significantly increased β-glucuronidase activity, a marker of damage, across several muscle groups.

Our data, both *in vitro* and *in vivo*, suggest that increased activation of the Hh pathway results in skeletal muscle atrophy. We believe that this is through a mechanism of impaired myogenesis based on the alterations in nuclear accretion that we observed. In addition, *Ptch1* heterozygosity lead to a functional loss of muscle strength that we did not anticipate. While more work needs to be done to elucidate the exact mechanism for the myogenic deficiency, the data collected here indicate that the Hh pathway may act as a negative regulator of adult skeletal muscle homeostasis. Understanding the mechanism by which the Hh pathway regulates myogenesis will be crucial in determining the pathways therapeutic potential for diseases such as cancer cachexia or chronic illnesses that are known to be associated with skeletal muscle wasting.

Supplemental data

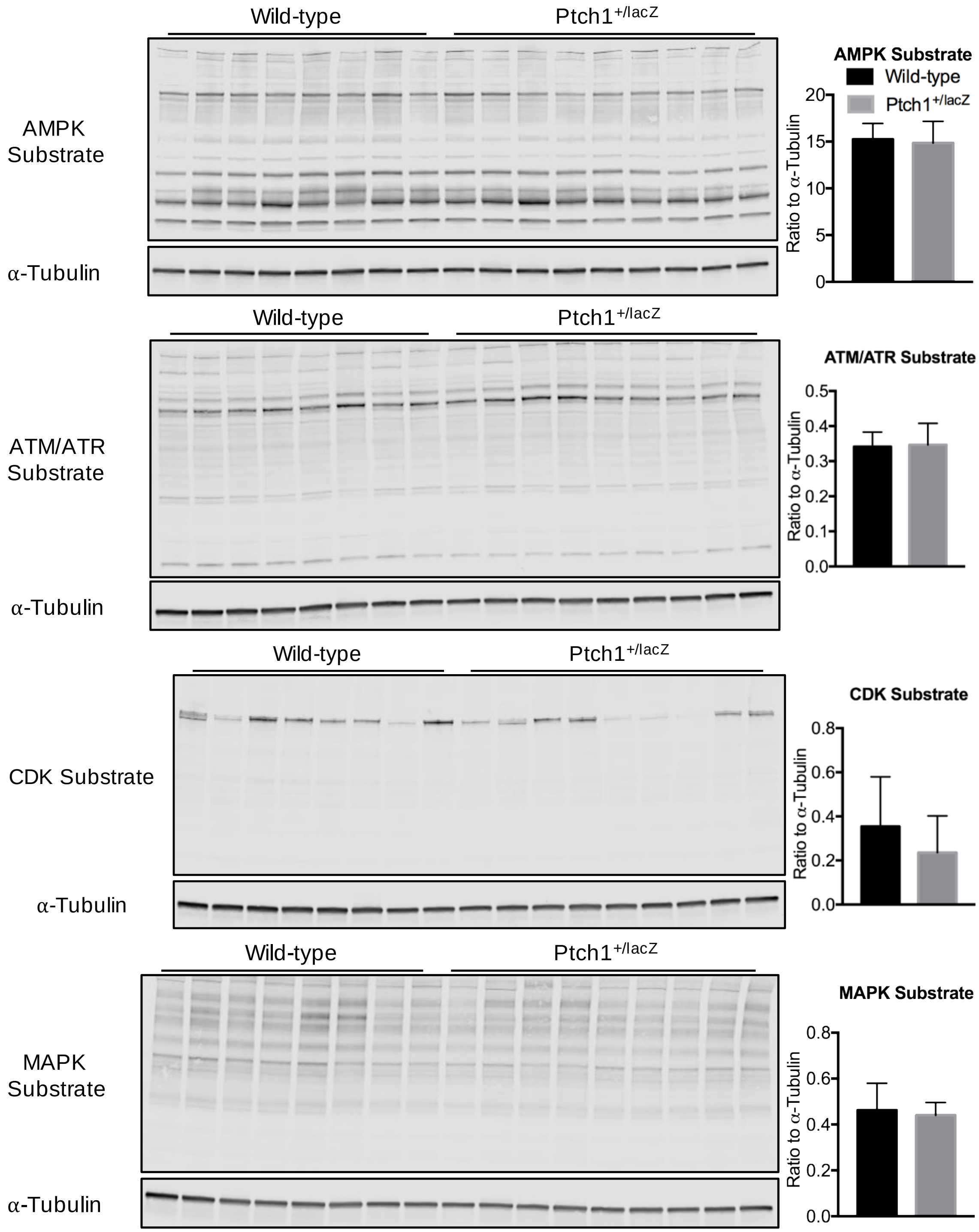

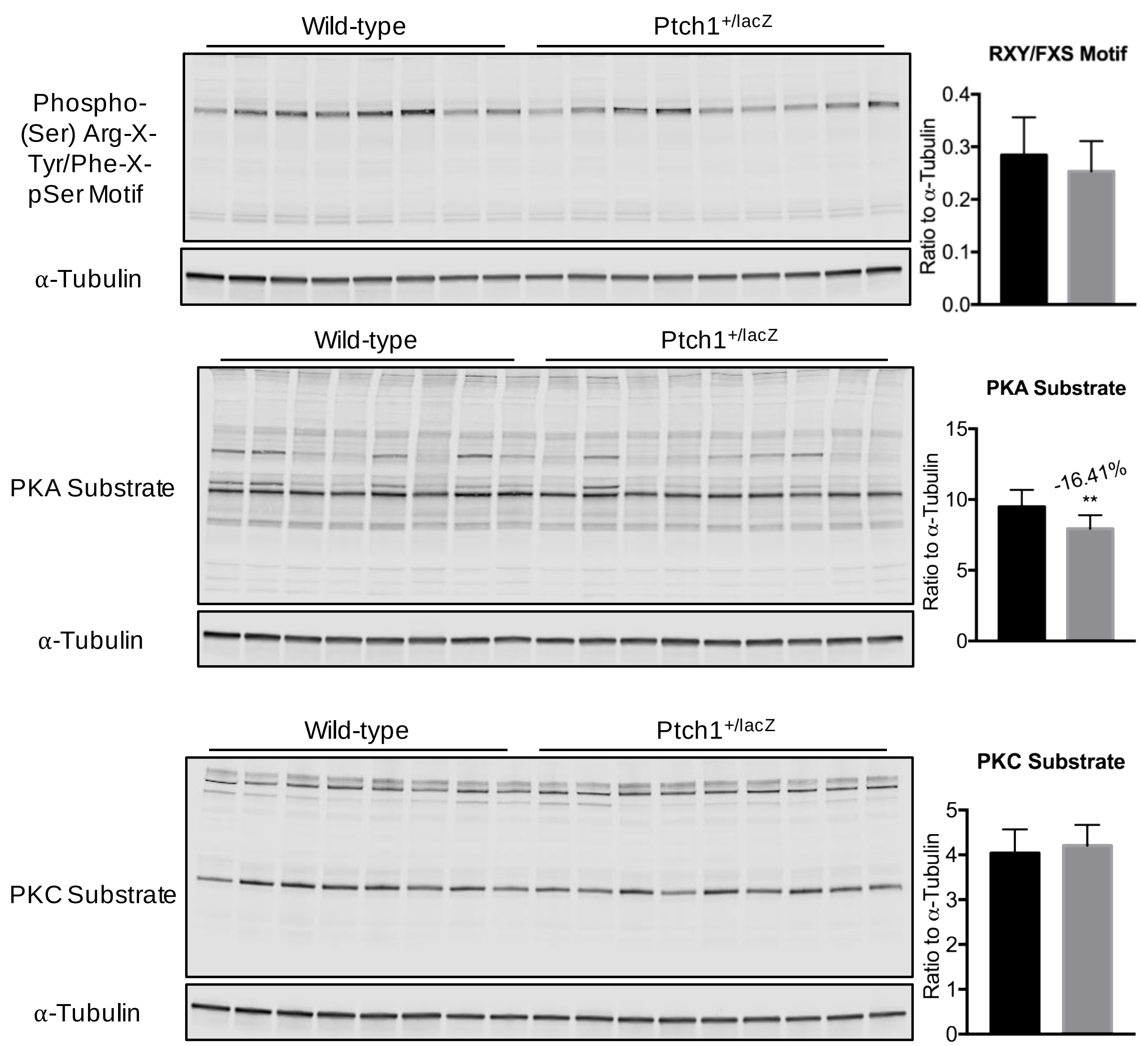

Wild-type
Ptch1$^{+/lacZ}$
Phospho-(Ser) Arg-X-Tyr/Phe-X-pSer Motif
α-Tubulin
RXY/FXS Motif
Ratio to α-Tubulin
0.4
0.3
0.2
0.1
0.0
Wild-type
Ptch1$^{+/lacZ}$
PKA Substrate
α-Tubulin
PKA Substrate
Ratio to α-Tubulin
15
10
5
0
-16.41%
**
Wild-type
Ptch1$^{+/lacZ}$
PKC Substrate
α-Tubulin
PKC Substrate
Ratio to α-Tubulin
5
4
3
2
1
0

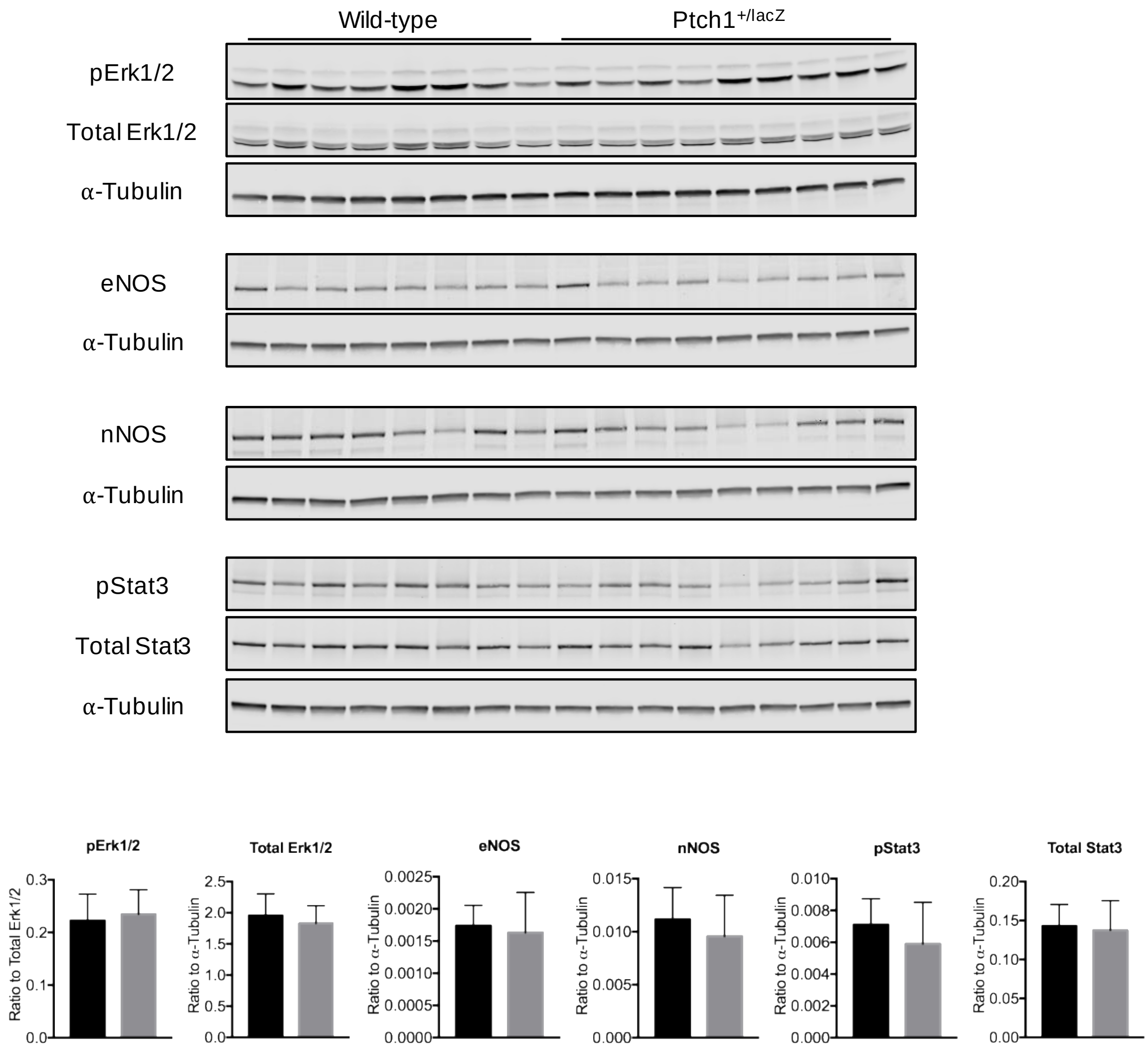

Supplemental figures. Western blotting analysis of quadriceps muscle lysates from 10 week old Ptch1$^{+/lacZ}$ mice and WT littermates. Data are expressed as the means ± SD. Statistical significance was determined by unpaired t test. **p<0.01.

Chapter 4

Distinct roles of Gli1 and Gli2 in the molecular regulation of myogenesis

Introduction

The Gli family of zinc-finger proteins, also known as glioma-associated oncogene, are transcription factors that regulate the downstream signal transduction cascade of the Hh family of ligands [186,187]. In mammals, three members have been identified, Gli1, 2, and 3 [188,189]. While all three members share similarities, their ability to act as a transcriptional activator or repressor varies. All three Gli proteins possess the ability to act as a transcriptional activator [190,191]. Gli1 has not been shown to have any repressor activity, instead functioning solely as a transcriptional activator. Gli2 serves as the primary transcriptional activator, although Gli3 does maintain this ability as well [192,193]. Gli3 serves as the principal transcriptional repressor, with Gli2 also shown to have some repressor activity [194-196]. Together, the Gli family of transcription factors function to mediate the transcriptional output of Hh signaling.

As discussed in the previous chapter, Shh signaling is crucial for the proper formation of skeletal muscle during development. How specific Gli proteins alter myogenesis and muscle development is incompletely understood. Prior studies in zebrafish indicate that the response to Hh signaling in myotomal cells is mediated by Gli1 and Gli2, with the two having partially overlapping functions [197]. During mouse embryogenesis, the Gli proteins have been shown to have variable levels of expression. In epaxial muscle progenitor cells, Gli2 and

Gli3 have both been shown to have activating and repressive functions on *Myf5* transcription [198,199]. However, the role of Gli proteins in the regulation of adult skeletal muscle myogenesis remains unclear.

Our prior *in vitro* and *in vivo* data has suggested that the Hh pathway acts as a negative regulator of adult skeletal muscle homeostasis. The observed effects appear to be through an alteration of myogenesis and differentiation. Here we sought to investigate molecular mechanisms. Gene expression studies during C2C12 myogenesis showed that *Gli1* expression is downregulated upon induction of differentiation. In contrast, we found the opposite for *Gli2*. These proteins also have different functions, because *Gli1* knockdown enhanced myogenic differentiation of C2C12 cells while *Gli2* knockdown impaired differentiation. Taken together, these data suggest that *Gli1* and *Gli2* have distinct and contrasting roles in myogenesis.

Materials and methods

Cell cultures

Murine C2C12 cells (ATCC) were grown in DMEM with 10% FBS, 100 U/mL penicillin, and 100 mg/mL streptomycin, and maintained at low confluency at 37°C in a humidified atmosphere of 5% CO_2. For differentiation of myoblasts, confluent cells were switched to a low serum medium containing DMEM supplemented with 2% horse serum, 100 U/mL penicillin, and 100 mg/mL streptomycin. SAG (Selleck Chemicals) was added to the differentiation media at a concentration of 250nM.

For siRNA-mediated knockdown, commercially available siRNAs for *Gli1, Gli2,* and a negative control (Table 1) were transfected into C2C12 myoblasts using Lipofectamine 3000 as per the manufacturer's instructions (Thermo Fisher Scientific). Knockdown of *Gli1* and *Gli2* in the myoblasts was confirmed via qPCR at 24 hours post transfection.

For overexpression of GLI1, Ad-GLI1/GFP was made by cloning a full-length cDNA of human *GLI1* into a recombinant adenovirus serotype 5 construct co-expressing GFP from a separate promoter (Vector Biolabs). Ad-GLI1/GFP or Ad-GFP was added to the media of fully differentiated myotubes and analysis performed out to 60 hours post-infection. For knockdown of *Gli2* in myotubes, an Ad-Gli2-shRNA was developed by cloning a *Gli2 shRNA* into an adenovirus serotype 5 backbone driven by a U6 promoter, with a separate GFP tag under a CMV promoter (Vector Biolabs). Ad-Gli2-shRNA or Ad-GFP was added to the media of fully differentiated myotubes and incubated for 48 hours before analysis of myotube diameter was performed.

Immunofluorescence

C2C12 myotubes were fixed and permeabilized in an ice cold acetone:methanol (1:1) solution for 20 minutes at -20°C. Cells were rehydrated with PBS at room temperature for 10 minutes, blocked in an 8% BSA solution for one hour, and primary antibody against MyHC (Developmental Studies Hybridoma Bank) incubated overnight at 4°C with gentle agitation. The following day, cultures were washed with PBS before being incubated with an AlexaFluor 488-labeled anti-mouse IgG secondary antibody (Life Technologies) for one hour at room temperature and protected from light. Nuclei were stained with DAPI and images were captured on an Axio Observer.Z1 (Zeiss). Myotube diameters were measured using ImageJ analysis software (Wayne Rasband, U.S. National Institutes of Health). Only fully formed myotubes with the majority in the field of view were measured. MyHC expression was assessed by quantifying the total green fluorescence using the IncuCyte ZOOM platform and analysis software (Essen BioScience).

Gene expression analysis

Total RNA was extracted from myoblasts and myotubes using the QIAGEN miRNeasy kit (QIAGEN Inc.) and cDNA generated using the Verso cDNA Synthesis kit (Thermo Fisher Scientific) as per the manufacturer's instructions. Relative mRNA expression levels were measured using TaqMan Assay based probes (Thermo Fisher Scientific) on a LightCycler 96 (Roche). A complete list of the probes used in these experiments can be found on Table 4-1 below.

Data analysis

Statistical significance was determined by unpaired t-test for experiments containing two groups. For experiments containing groups of three or more, statistical significance was determined by one-way ANOVA and Tukey's multiple comparisons test. A p-value less than 0.05 was considered to be statistically significant.

Table 4-1.

siRNA

Target	**Catalog #**	**Manufacturer**
Negative	4390846	Thermo Fisher Scientific
Gli1 - A	s66723	Thermo Fisher Scientific
Gli1 - B	s66724	Thermo Fisher Scientific
Gli2	s66726	Thermo Fisher Scientific

Probes

Target	**Catalog #**	**Manufacturer**
Gli1	Mm00494654_m1	Thermo Fisher Scientific
Gli2	Mm01293117_m1	Thermo Fisher Scientific
Gli3	Mm00492337_m1	Thermo Fisher Scientific
MyoD	Mm00440387_m1	Thermo Fisher Scientific
Myogenin	Mm00446194_m1	Thermo Fisher Scientific
Pax7	Mm01354484_m1	Thermo Fisher Scientific
Ptch1	Mm00436026_m1	Thermo Fisher Scientific

Results

Gli1 and *Gli2* are inversely regulated during myogenesis

We previously showed that *Gli1* expression was downregulated during C2C12 myogenesis. Upon further analysis of this experiment, *Gli2* was found to be highly upregulated at the onset of differentiation, and remained so throughout the differentiation process (Figure 4-1A-B). This suggested that Gli1 and Gli2 may have specific non-redundant functions in the regulation of myogenesis.

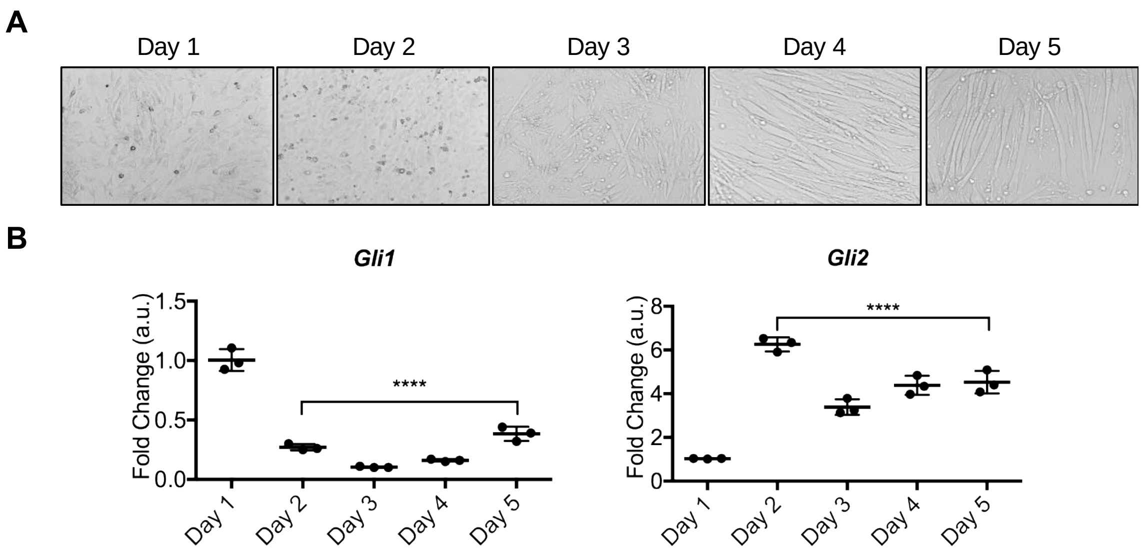

Figure 4-1. *Gli1* was downregulated during differentiation, while *Gli2* was upregulated. Analysis of *Gli1* and *Gli2* mRNA expression levels during C2C12 myogenesis. **A:** Representation images of C2C12 myoblasts differentiating into C2C12 myotubes. **B:** *Gli1* expression became downregulated during differentiation and *Gli1* expression increased. All conditions were performed in triplicate and the data are expressed as the means ± SD. Statistical significance was determined by one-way ANOVA. ****p<0.0001 versus Day 1.

Upregulation of *Gli1* halted differentiation

Given that *Gli1* was downregulated during C2C12 myogenesis, we next sought to determine what the effects of *Gli1* upregulation would be on it. Here, we treated differentiated myotubes with SAG, and assessed the myogenic phenotype. The addition of SAG resulted in a significant upregulation of *Gli1* at both 24 and 48 hours after treatment (Figure 4-2).

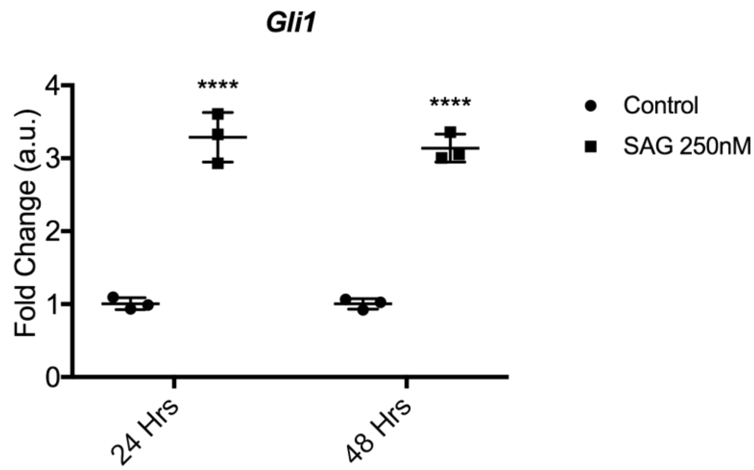

Figure 4-2. SAG induced *Gli1* expression. Differentiating myotubes were incubated with SAG for 48 hours and *Gli1* mRNA levels were analyzed at 24 hour intervals after treatment began. All conditions were performed in triplicate and the data are expressed as the means ± SD. Statistical significance was determined by unpaired t test. ****p<0.0001 versus Control.

We next observed that increased *Gli1* expression appeared to have stopped the progression of differentiation. We assessed the changes in myotube diameter, total nuclei, and the number of nuclei per fiber from differentiating myotubes treated with SAG for 24 and 48 hours (Figure 4-3).

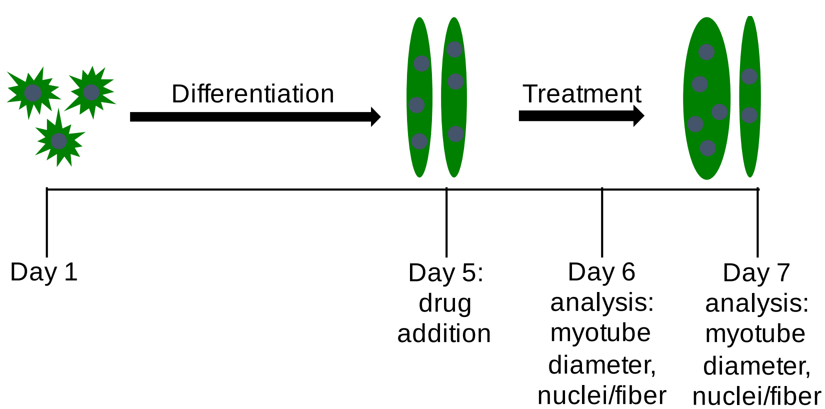

Figure 4-3. SAG treatment of differentiating C2C12 myotubes. C2C12 cells were differentiated for four days before treatment with either vehicle or SAG. Following treatment, myotubes were analyzed for diameter, total nuclei, and nuclei per fiber at 24 (Day 6) and 48 hours (Day 7).

When analyzing the vehicle treated controls from 24 to 48 hours post-treatment, we found that these cells continued to differentiate and fuse, as evidenced by the increase in myotube diameter. However, when looking at the cells treated with

SAG from 24 to 48 hours post-treatment, we found that differentiation had ceased. With SAG treatment, the myotube diameter did not continue to increase as it did in the controls, and no further nuclei were accumulated (Figure 4-4A-C). In addition, the total number of nuclei in the SAG treated group showed an upward trend from 24 to 48 hours after treatment, indicating that there was no toxicity or cell death. Taken together, these data suggest that increased expression of *Gli1* halts differentiation and may maintain myoblasts in a mononucleated state.

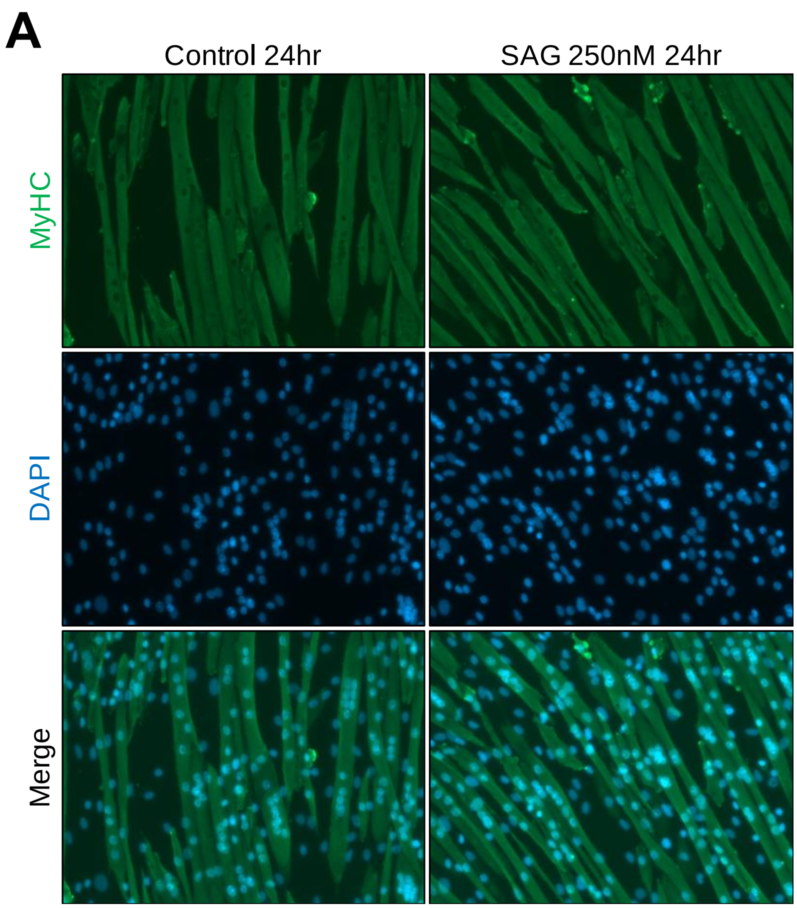

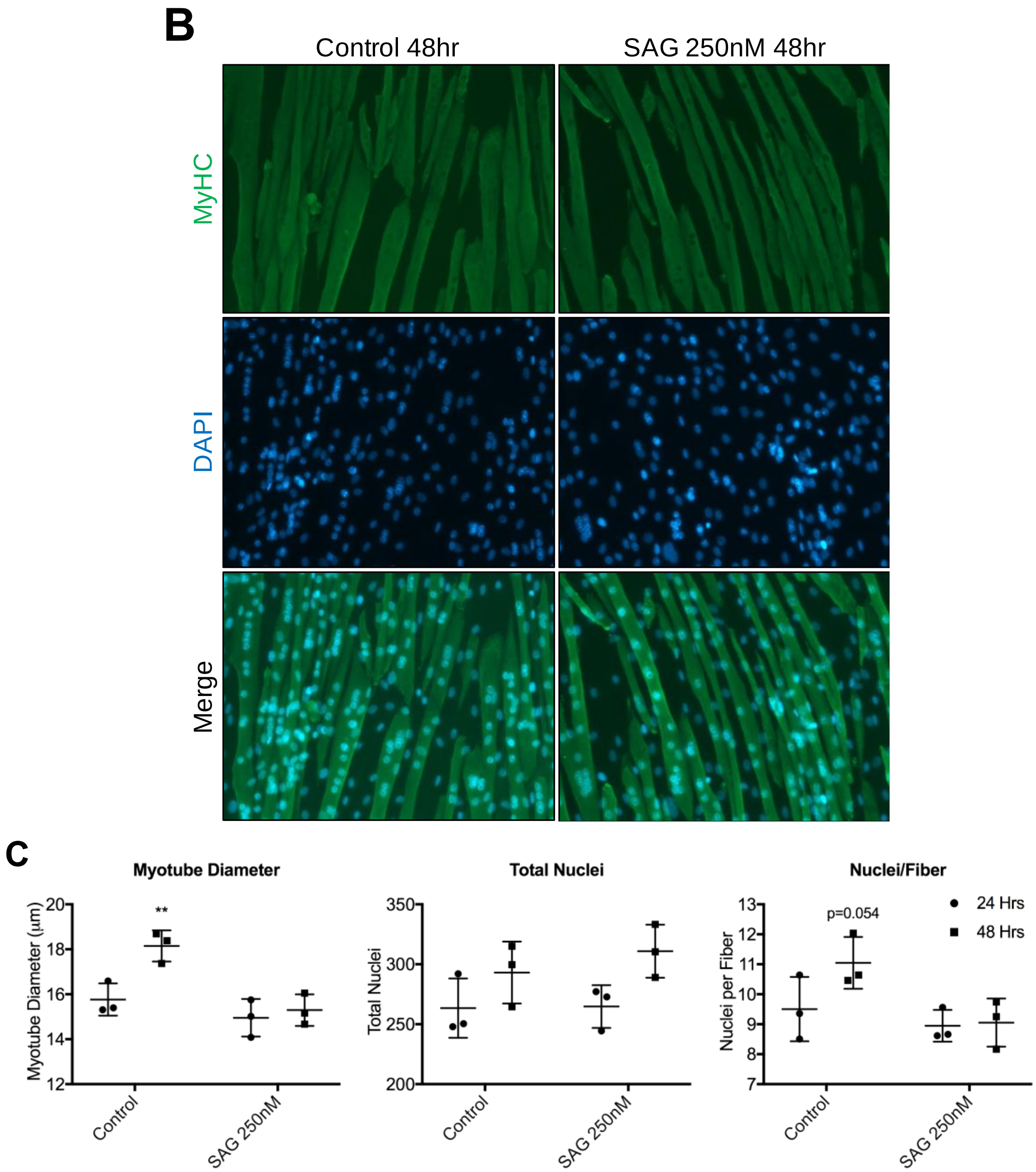

Figure 4-4. Increased *Gli1* expression blocks differentiation. Myotubes with increased *Gli1* expression were unable to continue undergoing differentiation and myoblast fusion. **A:** Representative images of Control and SAG treated myotubes 24 hours after incubation. **B:** Representative images of Control and SAG treated myotubes 48 hours after incubation. **C:** Analysis of myotube diameter, total nuclei, and nuclei per fiber. Control myotubes showed an increase in diameter from 24 to 48 hours following vehicle treatment, and a trend for more nuclei per fiber. SAG treated myotubes did not continue to grow or accrue more nuclei based on the analysis from 24 to 48 hours. All conditions were performed in triplicate and the data are expressed as the means ± SEM. Statistical significance was determined by unpaired t test. **p<0.01 versus 24 hours.

***Gli1* knockdown enhanced myogenesis, *Gli2* knockdown impaired**

We next questioned what the effects on myogenesis would be from knocking down *Gli1* and *Gli2.* Based on our previous data, we hypothesized that knocking down *Gli1* would be beneficial due to the fact that it is downregulated during C2C12 myogenesis, and inducing its expression halted myogenesis. Conversely, since *Gli2* is upregulated during myogenesis, knocking it down would likely be detrimental. To investigate this hypothesis, we transfected C2C12 myoblasts with an siRNA targeting *Gli1, Gli2,* or a negative control (Figure 4-5A). After an initial 24 hours following siRNA knockdown, qPCR analysis was performed to confirm a decreased expression of *Gli1* and *Gli2* (Figure 4-5B)*.* With their downregulation confirmed, these knockdown myoblasts were then differentiated into myotubes and the phenotype assessed. When looking at differentiation as a whole, it was evident that the myoblasts knocked down for *Gli1* formed significantly more myotubes than the Negative siRNA transfected myoblasts. On the other hand, the *Gli2* knockdown myoblasts showed very few myotubes after four days of differentiation (Figure 4-5C). The lack of differentiation observed was not due to toxicity from the transfection or cell death resulting from the knockdown, as phase imaging shows nearly full confluency in all the groups. Upon further analysis, we found that MyHC expression was significantly increased in the myotubes generated from *Gli1* knockdown myoblasts compared to the Negative siRNA, indicating an enhancement of differentiation. In the myotubes generated from *Gli2* knockdown myoblasts, MyHC expression was decreased, consistent with the observation of a severe impairment of differentiation (Figure 4-5D). Additionally, the myotubes generated from *Gli2* knockdown myoblasts showed a decrease in the number of nuclei per fiber and a trend towards smaller myotube diameters, further supporting the phenotype of defective myogenesis.

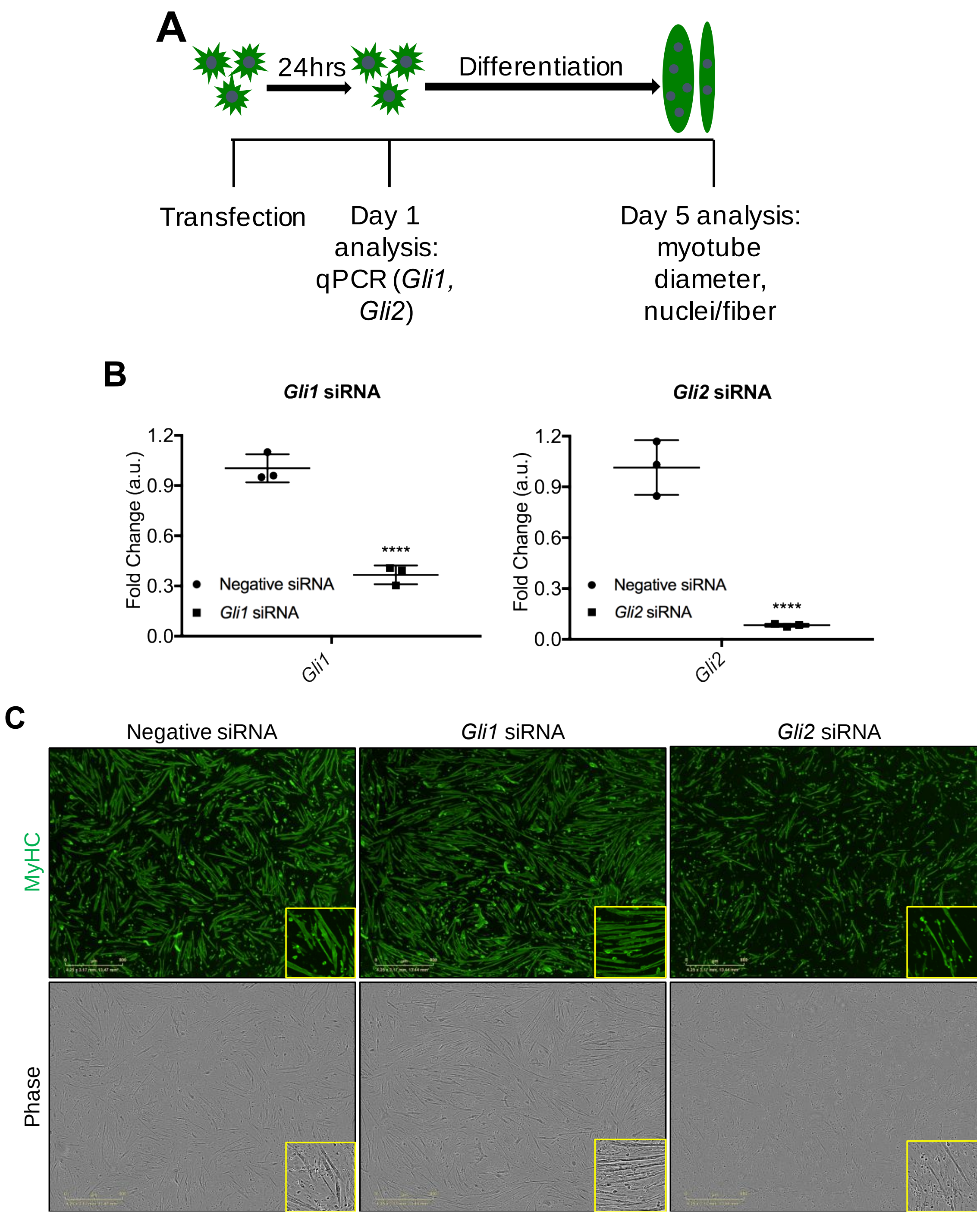

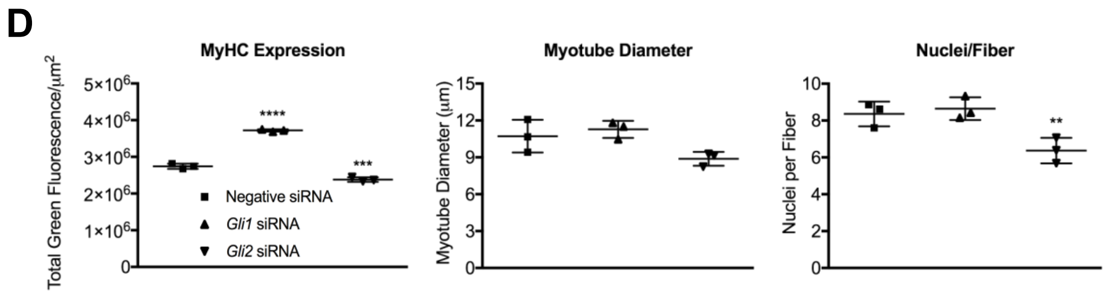

Figure 4-5. *Gli1* and *Gli2* knockdown resulted in enhanced and impaired myogenesis, respectively. The myogenic phenotype of myotubes, differentiated from C2C12 myoblasts knocked down for *Gli1* or *Gli2,* was assessed **A:** C2C12 myoblasts were knocked down for either *Gli1* or *Gli2.* Following 24 hours in culture, the myoblasts were then analyzed to confirm knockdown before being differentiated to myotubes. **B:** qPCR analysis of *Gli1* and *Gli2* mRNA expression levels in myoblasts 24 hours post-transfection. All conditions were performed in triplicate and the data are expressed as the means ± SD. Statistical significance was determined by unpaired t test. ****p<0.0001 versus Negative siRNA. **C:** Representative images of myotubes stained for MyHC and phase imagining. *Gli1* knockdown increased differentiation, while *Gli2* knockdown reduced. **D:** Myoblasts knocked down for *Gli1* or *Gli2* were differentiated into myotubes. *Gli1* knockdown resulted in increased MyHC expression. *Gli2* knockdown resulted in decreased expression of MyHC and a reduced number of nuclei per fiber. All conditions were performed in triplicate and the data are expressed as the means ± SD. Statistical significance was determined by one-way ANOVA. **p<0.01, ***p<0.001, ****p<0.0001 versus Negative siRNA.

Gli2 knockdown resulted in a decreased expression of myogenic genes

Next, we sought to investigate what a potential mechanism for the myogenic deficit of the *Gli2* knockdown myoblasts could be. Total RNA was extracted from *Gli2* knockdown myoblasts cells at baseline (Day 1) and every 24 hours as differentiation progressed. We then analyzed the mRNA expression levels of Gli family members and various myogenic regulatory factors. *Gli2* was found to be decreased at every time point in the experiment, confirming knockdown, while *Gli1* expression was comparable to control levels of the Negative siRNA transfected group. This suggests that *Gli1* and *Gli2* work independently of each other during differentiation. When looking at myogenic regulatory factors, two of the essential genes necessary for myogenesis, *MyoD* and *Myogenin,* were both significantly downregulated at every time point in the *Gli2* knockdown group (Figure 4-6). Furthermore, the satellite cell marker *Pax7* became upregulated while the cells underwent differentiation. Together, these data suggest that the impaired myogenesis observed in the *Gli2* knockdown cells is due to a reduced expression of genes associated with entry and progression through myogenesis, and an increased expression of a progenitor cell marker.

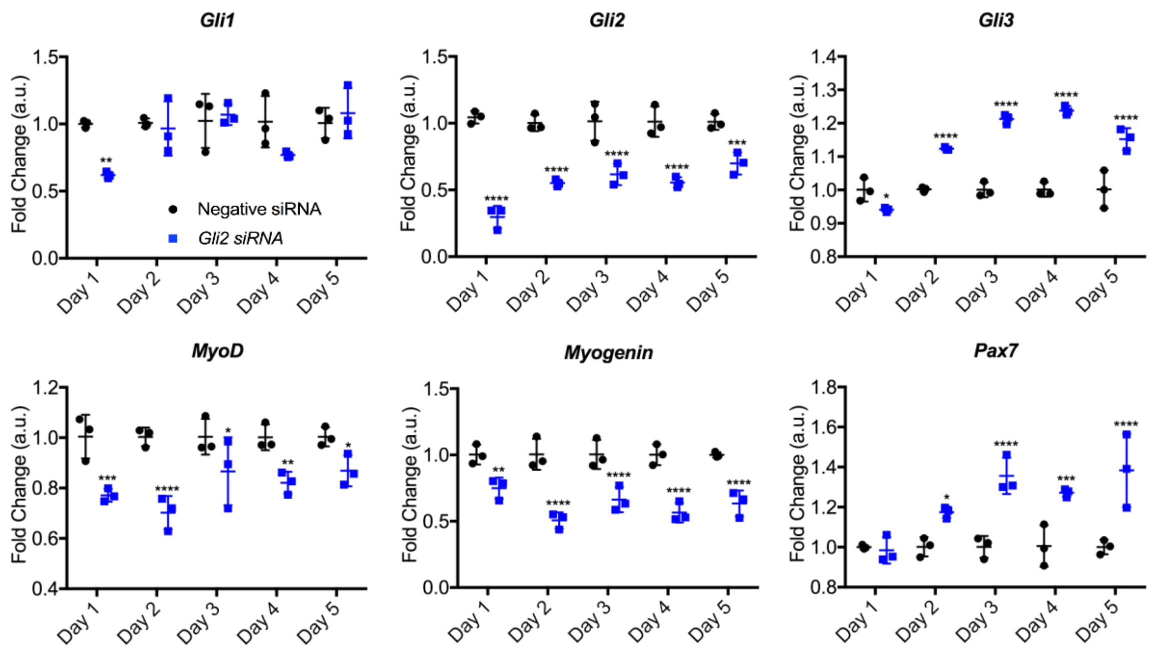

Figure 4-6. *Gli2* knockdown resulted in a reduced expression of myogenic regulatory factors. Time course analysis of gene expression in *Gli2* knockdown cells undergoing differentiation. The muscle specific genes *MyoD* and *Myogenin* were decreased with *Gli2* knockdown and *Pax7* was increased. All conditions were performed in triplicate and the data are expressed as the means ± SD. Statistical significance was determined by one-way ANOVA. *p<0.05, **p<0.01, ***p<0.001, ****p<0.0001 versus Negative siRNA.

GLI1 overexpression caused dedifferentiation of myotubes, *Gli2* knockdown caused atrophy

Thus far, our data looking at the myogenic effects of *Gli1* and *Gli2* manipulation have been performed in myoblasts. We next looked to investigate the effects of these factors being perturbed in fully differentiated myotubes. When GLI1 was overexpressed in myotubes, we observed a phenotype of dedifferentiation. This was accompanied by a loss of MyHC staining that progressed over time and resulted in significantly smaller myotubes (Figure 4-7). Nuclear staining showed that this was not due to toxicity or cell death.

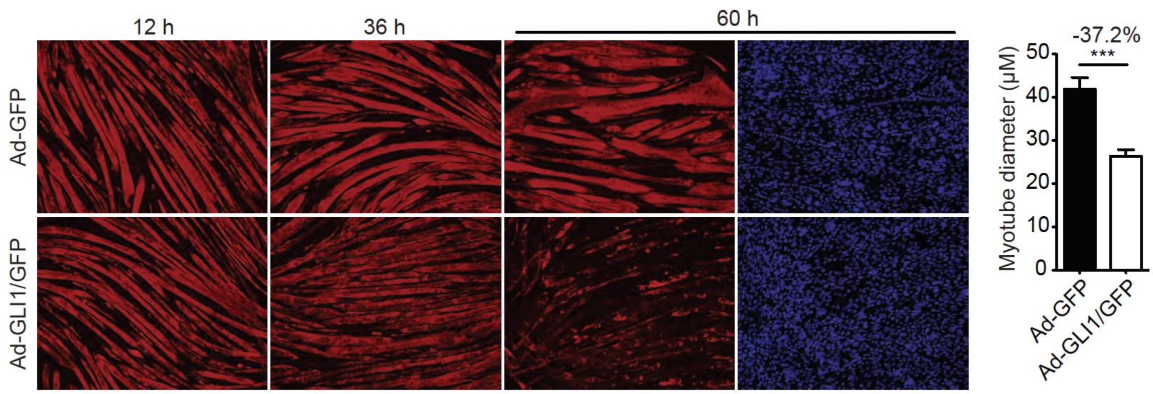

Figure 4-7. Overexpression of GLI1 resulted in myotube dedifferentiation. Differentiated C2C12 myotubes were infected with either Ad-GFP or Ad-GLI/GFP. Staining for MyHC (red) at various time points showed that overexpression of GLI1 resulted in a loss of MyHC in myotubes. Nuclei staining (blue) at the 60 hour time point showed that this was not due to cell death. Analysis of myotube diameters at 60 hours post-infection showed a significant reduction in the myotubes infected with Ad-GLI1/GFP. All conditions were performed in triplicate and the data are expressed as the means ± SD. Statistical significance was determined by unpaired t test. ***$p<0.001$ versus Ad-GFP. These data were collected by a former graduate student, Rui Zhan.

Next, we looked at what the effects of knocking down *Gli2* in differentiated myotubes would be. Infection with a *Gli2* Ad-shRNA resulted in significant myotube atrophy (Figure 4-8A-B). This is consistent with our prior observation that knockdown of *Gli2* in myoblasts impaired differentiation. Analysis of mRNA expression levels showed that *Gli2* was significantly decreased in the myotubes infection with the *Gli2* Ad-shRNA (Figure 4-8B). Taken together, these data further suggest that Gli1 functions to maintain cells in a proliferative state, while Gli2 functions to allow for terminal differentiation and the expression of muscle specific genes.

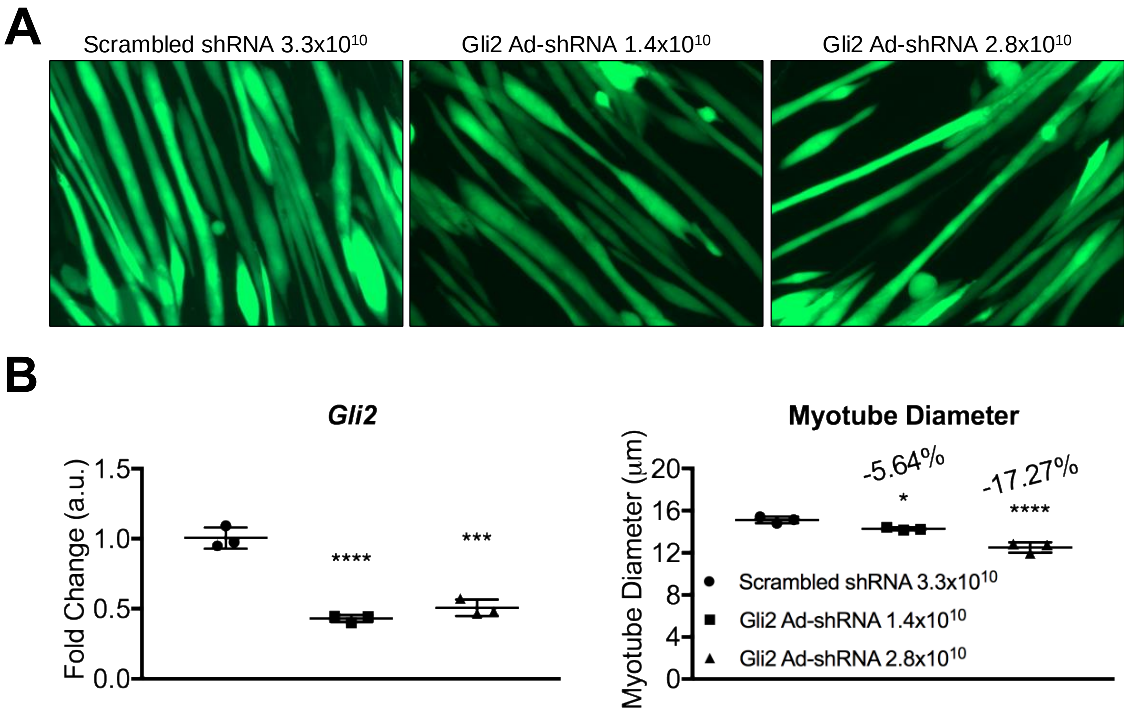

Figure 4-8. Knockdown of *Gli2* in myotubes resulted in fiber atrophy. C2C12 myotubes were infected with an adenovirus expressing either Scrambled shRNA with a GFP tag or a Gli2 shRNA with a GFP tag. **A:** Representative images of myotubes infected with 3.3×10^{10} PFU/mL of Scrambled shRNA, 1.4×10^{10} PFU/mL of *Gli2* Ad-shRNA, or 2.8×10^{10} PFU/mL of *Gli2* Ad-shRNA. **B:** qPCR analysis showed that infection of the myotubes with the adenovirus significantly reduced *Gli2* mRNA expression levels. Measurement of myotube diameters revealed that the reduction of *Gli2* expression caused a decrease in myotube size. All conditions were performed in triplicate and the data are expressed as the means ± SD. Statistical significance was determined by one-way ANOVA. *$p<0.05$, ***$p<0.001$, ****$p<0.0001$ versus Scrambled shRNA.

Discussion

Our previous *in vitro* and *in vivo* data have shown that the Hh pathway acts as a negative regulator of skeletal muscle mass, with further evidence suggesting this to be through a modulation of myogenic potential. In an attempt to further explore the mechanism by which the Hh pathway regulates muscle mass, we looked at *Gli1* and *Gli2* and their role in myogenesis. During C2C12 myogenesis, *Gli1* is downregulated while *Gli2* is upregulated, indicating that these two factors may have distinct roles during this process (Figure 4-9). Looking further into *Gli1,* we found that when its expression was induced, myogenesis was halted. When *Gli1* was knocked down in myoblasts, these cells had a much higher capacity to differentiate, as evidenced by an increase in MyHC expression. Overexpression of Gli1 in myotubes provided further evidence that it functions to keep muscle progenitor cells in an undifferentiated state, as the myotubes dedifferentiated. Conversely, knockdown of *Gli2* resulted in a severely reduced capability of myoblasts to form multinucleated myotubes. This was likely due to a reduced expression of key myogenic regulatory factors, and a sustained and elevated expression of a muscle satellite cell marker. When *Gli2* was knocked down in mature myotubes, they atrophied. These findings suggest that Gli2 is necessary to both initiate and maintain the differentiated state.

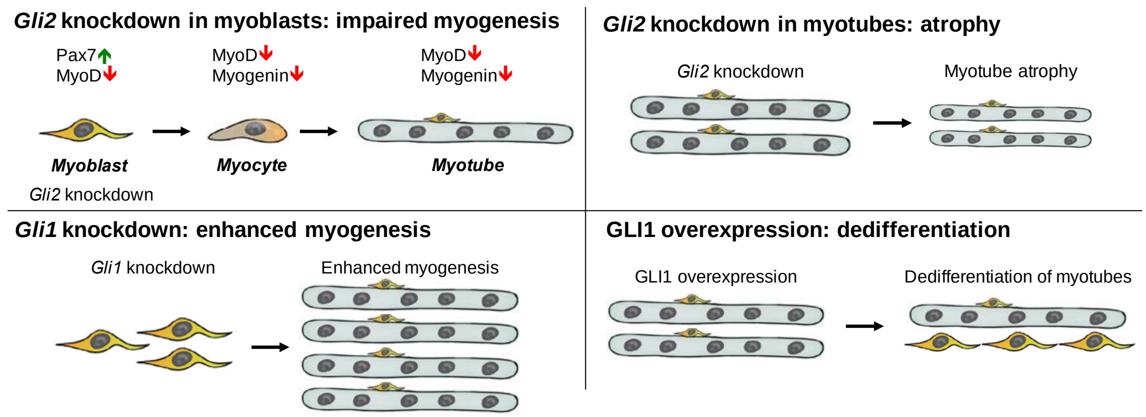

Figure 4-9: Gli1 and Gli2 had non-redundant roles during myogenesis. Our data suggest a model in which Gli1 and Gli1 have unique roles on the molecular regulation of myogenesis. Knockdown of *Gli1* in myoblasts resulted in enhanced myogenesis, while GLI1 overexpression in myotubes caused dedifferentiation. *Gli2* knockdown in myoblasts severely impaired myogenesis, while knockdown in myotubes resulted in atrophy.

The role of Gli1 and Gli2 in myogenesis has been investigated in the literature, although there is no consensus as to whether they are permissive or inhibitory to myogenesis. Several studies performed using pluripotent P19 cells suggest that the Gli proteins are essential to the expression of key myogenic regulatory factors. Arsenic is a toxicant that has been shown to suppress myotube formation in C2C12 cells [200]. When used in P19 cells, exposure to arsenic reduces Gli2 expression both at the mRNA and protein level [201]. Moreover, overexpression of Gli2 is sufficient to induce myogenesis in P19 cells, without the presence of a differentiation inducing agent. This results in expression of MyHC and detection of *Myf5* and *Myogenin* transcripts, which were not observed in control P19 cells. Conversely, when the activation domain of Gli2 was replaced with an engrailed repression domain, P19 cells expressing this form of Gli2 did not differentiate into myocytes or express *Myf5* [202]. A similar study was done that confirmed these findings. Again, Gli2 overexpression was shown to enhance skeletal muscle cell formation in P19 cells, accompanied by an increase in the expression of *MEF2C*, *MyoD*, *Myf5*, and *Myogenin*. This study goes on to show that Gli2 directly interacts with MEF2C and MyoD to form a protein complex, thus enhancing the activity of MyoD [203]. However, it has also been shown that Gli1 and Gli2 are inhibitory to MyoD activity. Using several MyoD-responsive reporters, one study shows that transfection with either a Gli1 or Gli2 expression plasmid severely reduces the expression of the reporters [204]. This would suggest that Gli1 and Gli2 block myogenesis by inhibiting the necessary transcriptional activity of MyoD.

Here, we show that *Gli1* and *Gli2* have unique and non-redundant roles during myogenesis. The published literature showing that Gli1 inhibits MyoD activity would offer a potential explanation as to why we saw an increase in differentiation and myotube formation with *Gli1* knockdown. Although, their finding that Gli2 also blocks MyoD activity is not in agreement with ours or other published data. We found that with *Gli2* knockdown, differentiation was almost completely ablated, and the expression of various myogenic regulatory factors was decreased. This seems to be due to the fact that Gli2 forms a protein complex with MyoD in order to enhance its activity, as shown by Voronova et al.. Taken together, our data suggest the Hh pathway as a potential target for therapeutic intervention of muscle wasting diseases, but *Gli1* and *Gli2* have distinct roles during myogenesis and must be targeted accordingly.

Chapter 5

Conclusions

Skeletal muscle plays an important role in human health and disease. The loss of skeletal muscle can have devastating consequences on a patient's quality of life, response to treatment, or survival. There is an overwhelming need to identify and investigate new targets for therapeutic intervention to treat these patients.

Here, we investigated ERK inhibition as a treatment to prevent cancer-induced cachexia. The effects on lean body mass in the phase II clinical trial using Selumetinib, and the published literature on ERK inhibition in the skeletal muscle, lead us to hypothesize that ERK inhibition with Selumetinib might be effective at blocking cancer-associated muscle wasting. *In vitro*, we found that Selumetinib was able to induce C2C12 myotube hypertrophy and nuclear accretion. In an *in vivo* mouse model of experimental cancer cachexia, however, Selumetinib reduced tumor mass, circulating and tumor levels of IL-6, but did not preserve muscle mass. Similar wasting was seen in limb muscles of Selumetinib and vehicle treated LLC tumor bearing mice, while greater fat loss was observed in the Selumetinib treated group. Additionally, Selumetinib did not block wasting in C2C12 myotubes treated with plasma from LLC tumor mice. Taken together, our results suggest that this inhibitor was not protective in LLC cancer cachexia despite the reduction in IL-6 levels and tumor mass, and may have actually exacerbated tumor-induced wasting.

While positive effects on the tumor were observed, we did not find there to be any reductions in weight loss or muscle wasting with Selumetinib treatment. The data point to the fact that careful consideration must be taken when extrapolating results from clinical trials and applying across different experimental models and disease states. Studies must take into account the potential for differential regulation on pathways in commonly used models of cancer cachexia, and a diversity in the underlying molecular mechanisms. These data do however warrant further investigation into the efficacy of MEK inhibition as a treatment for cancer-induced cachexia. As previously mentioned, ERK1/2 activation is required during different stages of differentiation. Thus, it would seem that constant inhibition of the pathway would actually have a negative effect on muscle mass. While it is not likely that we would be able to modulate a certain stage of differentiation *in vivo* with Selumetinib, an alternative method would be to use a cyclic dosing regimen. This would allow for periods of inhibition, which would be beneficial during the initial stages of differentiation, as well as periods of activation, which is necessary in the later stages. Coupled with the positive effects observed on tumor mass, if future studies can elucidate a more beneficial dose for skeletal muscle hypertrophy, ERK inhibition may be a viable option to combat cancer cachexia.

The data obtained in this study also suggest that there are additional cachectic drivers at play in this model. While a decrease in the tumor and circulating levels of IL-6 were observed *in vivo*, Selumetinib was unable to protect against LLC plasma induced myotube wasting *in vitro*. This result could be due to another, or several other, cachectic mediators that are still present at high levels. Future studies may look to identify what additional factors are elevated such as TNFα, Activins, or members of the TGF-β family. Once identified, a combination therapy approach, targeting the factor(s) in conjunction with Selumetinib, may provide a protective effect against muscle wasting by inhibiting the production of multiple cachectic drivers.

Our lab also has substantial data implicating the Shh pathway as a causal factor in skeletal muscle wasting. Prior work has found the pathway to be activated in the skeletal muscles of LLC tumor bearing mice. Moreover, inhibition of the Shh pathway in LLC tumor bearing mice was able to protect against cancer-induced cachexia, while having no effect on tumor mass. This brought about the question of how the Hh pathway regulates normal adult skeletal muscle mass.

Looking *in vitro,* we found that pharmacological inhibition or activation of the Hh pathway resulted in C2C12 myotube hypertrophy and atrophy, respectively. In addition, we also observed an alteration in the nuclear accretion of these myotubes, with inhibition of the pathway increasing and activation decreasing. Further *in vitro* worked showed that when *Ptch1* was knocked down, resulting in increased Hh pathway activity, C2C12 differentiation was severely impaired. Prior data from the lab showed that *in vivo* inhibition of the Hh pathway resulted in systemic muscle hypertrophy. Here, we showed that the use of a pathway agonist caused systemic skeletal muscle and adipose tissue wasting. Using a transgenic model of increased Hh pathway activity, we found that mice heterozygous for *Ptch1* had smaller muscles and were significantly weaker. Further analysis of the muscle phenotype revealed that this was likely due to a defect in myogenesis, as we observed fewer nuclei inside of the muscle fibers and less Pax7+ cells on isolated primary myofibers. RNA-seq analysis showed a reduction of genes associated with cell cycle and proliferation and muscle structural proteins, offering an explanation to the reduced myogenic phenotype and muscle strength. Together, these data further supported our hypothesis that the Hh pathway acts as a negative regulator of adult skeletal mass.

Lastly, we wanted to look more into the molecular regulation of myogenesis by the Hh pathway, specifically the roles of the Gli1 and Gli2 transcription factors. We found that during normal C2C12 myogenesis, these factors were differentially regulated, as *Gli1* expression decreased as differentiation progressed, and *Gli2* expression increased. When *Gli1* expression was induced, differentiation was arrested, as the myotubes no longer accrued additional nuclei or increased in diameter. In addition, when *Gli1* was knocked down in myoblasts, these cells had an increased capacity to differentiate and form multinucleated myotubes. Furthermore, when GLI1 was overexpressed in fully differentiated myotubes, we observed a dedifferentiation phenotype. Together, these data suggest that Gli1 functions to keep myoblasts in a proliferative state. When *Gli2* was knocked down in myoblasts, we observed a severe impairment of differentiation. This was accompanied by a decreased expression of the muscle specific genes *MyoD* and *Myogenin.* Moreover, when *Gli2* was knocked down in mature myotubes, we observed an atrophic effect, suggesting that Gli2 functions to maintain the differentiated state of myotubes. Our data indicate that Gli1 and Gli2 serve two distinct roles during myogenesis, with Gli1 functioning in myoblasts to maintain their mononucleated state, and Gli2 the differentiated phenotype.

In order to further elucidate the role of Gli1 and Gli2 in myogenesis, future studies will need to be performed both *in vitro* and *in vivo*. *In vitro*, it will be interesting to look at whether the cells that dedifferentiate, due to GLI1 overexpression, can then be induced to differentiate again into myotubes. This may offer clues as to whether the increased expression of GLI1 resulted in a change in the gene profile to a more proliferative state, as our other data would suggest, or if it further transformed the cells into a different lineage or cell type. *In vivo,* future studies would look to confirm the *in vitro* findings with *Gli1* and *Gli2* manipulation. We would look to characterize the skeletal muscle phenotype of mice that were overexpressing or knocked out for Gli1 or Gli2 specifically in the skeletal muscle. This could be accomplished either by the use of transgenic mouse models, or through a targeted local approach of intramuscular injections with plasmids or RNA interference. These studies would help to further validate the results obtained here.

The data shown here present two pathways that warrant further investigation as potential therapeutic targets for the treatment of muscle wasting diseases. ERK inhibition showed positive effects on tumor volume, but not the desired protection of skeletal muscle mass. Future experiments may be able to resolve this with changes to the dosing regimen, either concentration or the frequency of administration. The lab has produced substantial evidence that points to the Hh pathway as a negative regulator of skeletal muscle mass. Inhibition of this pathway was shown to induce hypertrophy, while activation induced wasting. Targeting the pathway may prove to be beneficial in disease where muscle wasting is prevalent. However, the data here suggest that the downstream Gli1 and Gli2 transcription factors have unique and opposing roles during myogenesis. This indicates that caution must be taken as to which factors are inhibited if the pathway is to be targeted. With the overall goal of biomedical research to improve patient outcomes, survival, and quality of life, it is essential to continually investigate pathways and identify new targets for therapeutic intervention.

References

1 Proctor, D. N., O'Brien, P. C., Atkinson, E. J. & Nair, K. S. Comparison of techniques to estimate total body skeletal muscle mass in people of different age groups. *Am J Physiol* **277**, E489-495 (1999).

2 Argiles, J. M., Busquets, S., Stemmler, B. & Lopez-Soriano, F. J. Cachexia and sarcopenia: mechanisms and potential targets for intervention. *Curr Opin Pharmacol* **22**, 100-106, doi:10.1016/j.coph.2015.04.003 (2015).

3 Cohen, S., Nathan, J. A. & Goldberg, A. L. Muscle wasting in disease: molecular mechanisms and promising therapies. *Nat Rev Drug Discov* **14**, 58-74, doi:10.1038/nrd4467 (2015).

4 Fearon, K. *et al.* Definition and classification of cancer cachexia: an international consensus. *Lancet Oncol* **12**, 489-495, doi:10.1016/S1470-2045(10)70218-7 (2011).

5 Tsoli, M., Swarbrick, M. M. & Robertson, G. R. Lipolytic and thermogenic depletion of adipose tissue in cancer cachexia. *Semin Cell Dev Biol* **54**, 68-81, doi:10.1016/j.semcdb.2015.10.039 (2016).

6 Wolfe, R. R. The underappreciated role of muscle in health and disease. *Am J Clin Nutr* **84**, 475-482 (2006).

7 van Venrooij, L. M. *et al.* Postoperative loss of skeletal muscle mass, complications and quality of life in patients undergoing cardiac surgery. *Nutrition* **28**, 40-45, doi:10.1016/j.nut.2011.02.007 (2012).

8 Dos Santos, L., Cyrino, E. S., Antunes, M., Santos, D. A. & Sardinha, L. B. Sarcopenia and physical independence in older adults: the independent and synergic role of muscle mass and muscle function. *J Cachexia Sarcopenia Muscle* **8**, 245-250, doi:10.1002/jcsm.12160 (2017).

9 Giannaki, C. D. *et al.* Evidence of increased muscle atrophy and impaired quality of life parameters in patients with uremic restless legs syndrome. *PLoS One* **6**, e25180, doi:10.1371/journal.pone.0025180 (2011).

10 Metter, E. J., Talbot, L. A., Schrager, M. & Conwit, R. Skeletal muscle strength as a predictor of all-cause mortality in healthy men. *J Gerontol A Biol Sci Med Sci* **57**, B359-365 (2002).

11 Christ, B. & Ordahl, C. P. Early stages of chick somite development. *Anat Embryol (Berl)* **191**, 381-396 (1995).

12 Franz, T., Kothary, R., Surani, M. A., Halata, Z. & Grim, M. The Splotch mutation interferes with muscle development in the limbs. *Anat Embryol (Berl)* **187**, 153-160 (1993).

13 Bober, E., Franz, T., Arnold, H. H., Gruss, P. & Tremblay, P. Pax-3 is required for the development of limb muscles: a possible role for the migration of dermomyotomal muscle progenitor cells. *Development* **120**, 603-612 (1994).

14 Kassar-Duchossoy, L. *et al.* Mrf4 determines skeletal muscle identity in Myf5:Myod double-mutant mice. *Nature* **431**, 466-471, doi:10.1038/nature02876 (2004).
15 Megeney, L. A., Kablar, B., Garrett, K., Anderson, J. E. & Rudnicki, M. A. MyoD is required for myogenic stem cell function in adult skeletal muscle. *Genes Dev* **10**, 1173-1183 (1996).
16 Rudnicki, M. A. *et al.* MyoD or Myf-5 is required for the formation of skeletal muscle. *Cell* **75**, 1351-1359 (1993).
17 Rudnicki, M. A., Braun, T., Hinuma, S. & Jaenisch, R. Inactivation of MyoD in mice leads to up-regulation of the myogenic HLH gene Myf-5 and results in apparently normal muscle development. *Cell* **71**, 383-390 (1992).
18 Black, B. L. & Olson, E. N. Transcriptional control of muscle development by myocyte enhancer factor-2 (MEF2) proteins. *Annu Rev Cell Dev Biol* **14**, 167-196, doi:10.1146/annurev.cellbio.14.1.167 (1998).
19 Wright, W. E., Sassoon, D. A. & Lin, V. K. Myogenin, a factor regulating myogenesis, has a domain homologous to MyoD. *Cell* **56**, 607-617 (1989).
20 Edmondson, D. G. & Olson, E. N. A gene with homology to the myc similarity region of MyoD1 is expressed during myogenesis and is sufficient to activate the muscle differentiation program. *Genes Dev* **3**, 628-640 (1989).
21 Dumont, N. A., Bentzinger, C. F., Sincennes, M. C. & Rudnicki, M. A. Satellite Cells and Skeletal Muscle Regeneration. *Compr Physiol* **5**, 1027-1059, doi:10.1002/cphy.c140068 (2015).
22 Corona, B. T., Rivera, J. C., Owens, J. G., Wenke, J. C. & Rathbone, C. R. Volumetric muscle loss leads to permanent disability following extremity trauma. *J Rehabil Res Dev* **52**, 785-792, doi:10.1682/JRRD.2014.07.0165 (2015).
23 Garg, K. *et al.* Volumetric muscle loss: persistent functional deficits beyond frank loss of tissue. *J Orthop Res* **33**, 40-46, doi:10.1002/jor.22730 (2015).
24 Hatakeyama, S. *et al.* ActRII blockade protects mice from cancer cachexia and prolongs survival in the presence of anti-cancer treatments. *Skelet Muscle* **6**, 26, doi:10.1186/s13395-016-0098-2 (2016).
25 Zhou, X. *et al.* Reversal of cancer cachexia and muscle wasting by ActRIIB antagonism leads to prolonged survival. *Cell* **142**, 531-543, doi:10.1016/j.cell.2010.07.011 (2010).
26 Marquis, K. *et al.* Midthigh muscle cross-sectional area is a better predictor of mortality than body mass index in patients with chronic obstructive pulmonary disease. *Am J Respir Crit Care Med* **166**, 809-813, doi:10.1164/rccm.2107031 (2002).
27 Swallow, E. B. *et al.* Quadriceps strength predicts mortality in patients with moderate to severe chronic obstructive pulmonary disease. *Thorax* **62**, 115-120, doi:10.1136/thx.2006.062026 (2007).
28 Adams, G. R., Haddad, F., Bodell, P. W., Tran, P. D. & Baldwin, K. M. Combined isometric, concentric, and eccentric resistance exercise

prevents unloading-induced muscle atrophy in rats. *J Appl Physiol (1985)* **103**, 1644-1654, doi:10.1152/japplphysiol.00669.2007 (2007).
29 Gielen, S. *et al.* Exercise training attenuates MuRF-1 expression in the skeletal muscle of patients with chronic heart failure independent of age: the randomized Leipzig Exercise Intervention in Chronic Heart Failure and Aging catabolism study. *Circulation* **125**, 2716-2727, doi:10.1161/CIRCULATIONAHA.111.047381 (2012).
30 Greig, C. A. *et al.* Phase I/II trial of formoterol fumarate combined with megestrol acetate in cachectic patients with advanced malignancy. *Support Care Cancer* **22**, 1269-1275, doi:10.1007/s00520-013-2081-3 (2014).
31 Wen, H. S. *et al.* Clinical studies on the treatment of cancer cachexia with megestrol acetate plus thalidomide. *Chemotherapy* **58**, 461-467, doi:10.1159/000346446 (2012).
32 Cuvelier, G. D. *et al.* A randomized, double-blind, placebo-controlled clinical trial of megestrol acetate as an appetite stimulant in children with weight loss due to cancer and/or cancer therapy. *Pediatr Blood Cancer* **61**, 672-679, doi:10.1002/pbc.24828 (2014).
33 Madeddu, C. *et al.* Randomized phase III clinical trial of a combined treatment with carnitine + celecoxib +/- megestrol acetate for patients with cancer-related anorexia/cachexia syndrome. *Clin Nutr* **31**, 176-182, doi:10.1016/j.clnu.2011.10.005 (2012).
34 Hamrick, M. W. *et al.* Recombinant myostatin (GDF-8) propeptide enhances the repair and regeneration of both muscle and bone in a model of deep penetrant musculoskeletal injury. *J Trauma* **69**, 579-583, doi:10.1097/TA.0b013e3181c451f4 (2010).
35 Zhang, L. *et al.* Pharmacological inhibition of myostatin suppresses systemic inflammation and muscle atrophy in mice with chronic kidney disease. *FASEB J* **25**, 1653-1663, doi:10.1096/fj.10-176917 (2011).
36 Heineke, J. *et al.* Genetic deletion of myostatin from the heart prevents skeletal muscle atrophy in heart failure. *Circulation* **121**, 419-425, doi:10.1161/CIRCULATIONAHA.109.882068 (2010).
37 Nagaya, N. *et al.* Effects of ghrelin administration on left ventricular function, exercise capacity, and muscle wasting in patients with chronic heart failure. *Circulation* **110**, 3674-3679, doi:10.1161/01.CIR.0000149746.62908.BB (2004).
38 Nagaya, N. *et al.* Treatment of cachexia with ghrelin in patients with COPD. *Chest* **128**, 1187-1193, doi:10.1378/chest.128.3.1187 (2005).
39 Strasser, F. *et al.* Safety, tolerability and pharmacokinetics of intravenous ghrelin for cancer-related anorexia/cachexia: a randomised, placebo-controlled, double-blind, double-crossover study. *Br J Cancer* **98**, 300-308, doi:10.1038/sj.bjc.6604148 (2008).
40 Ashby, D. R. *et al.* Sustained appetite improvement in malnourished dialysis patients by daily ghrelin treatment. *Kidney Int* **76**, 199-206, doi:10.1038/ki.2009.114 (2009).

41 Temel, J. S. *et al.* Anamorelin in patients with non-small-cell lung cancer and cachexia (ROMANA 1 and ROMANA 2): results from two randomised, double-blind, phase 3 trials. *Lancet Oncol* **17**, 519-531, doi:10.1016/S1470-2045(15)00558-6 (2016).
42 Garcia, J. M., Friend, J. & Allen, S. Therapeutic potential of anamorelin, a novel, oral ghrelin mimetic, in patients with cancer-related cachexia: a multicenter, randomized, double-blind, crossover, pilot study. *Support Care Cancer* **21**, 129-137, doi:10.1007/s00520-012-1500-1 (2013).
43 Garcia, J. M. & Polvino, W. J. Pharmacodynamic hormonal effects of anamorelin, a novel oral ghrelin mimetic and growth hormone secretagogue in healthy volunteers. *Growth Horm IGF Res* **19**, 267-273, doi:10.1016/j.ghir.2008.12.003 (2009).
44 Jarkovska, Z., Krsek, M., Rosicka, M. & Marek, J. Endocrine and metabolic activities of a recently isolated peptide hormone ghrelin, an endogenous ligand of the growth hormone secretagogue receptor. *Endocr Regul* **38**, 80-86 (2004).
45 Boulton, T. G. *et al.* An insulin-stimulated protein kinase similar to yeast kinases involved in cell cycle control. *Science* **249**, 64-67 (1990).
46 Ray, L. B. & Sturgill, T. W. Rapid stimulation by insulin of a serine/threonine kinase in 3T3-L1 adipocytes that phosphorylates microtubule-associated protein 2 in vitro. *Proc Natl Acad Sci U S A* **84**, 1502-1506 (1987).
47 Gibney, G. T., Messina, J. L., Fedorenko, I. V., Sondak, V. K. & Smalley, K. S. Paradoxical oncogenesis--the long-term effects of BRAF inhibition in melanoma. *Nat Rev Clin Oncol* **10**, 390-399, doi:10.1038/nrclinonc.2013.83 (2013).
48 Kook, S. H. *et al.* Cyclic mechanical stress suppresses myogenic differentiation of adult bovine satellite cells through activation of extracellular signal-regulated kinase. *Mol Cell Biochem* **309**, 133-141, doi:10.1007/s11010-007-9651-y (2008).
49 Volonte, D., Liu, Y. & Galbiati, F. The modulation of caveolin-1 expression controls satellite cell activation during muscle repair. *FASEB J* **19**, 237-239, doi:10.1096/fj.04-2215fje (2005).
50 Heller, H., Gredinger, E. & Bengal, E. Rac1 inhibits myogenic differentiation by preventing the complete withdrawal of myoblasts from the cell cycle. *J Biol Chem* **276**, 37307-37316, doi:10.1074/jbc.M103195200 (2001).
51 Clegg, C. H., Linkhart, T. A., Olwin, B. B. & Hauschka, S. D. Growth factor control of skeletal muscle differentiation: commitment to terminal differentiation occurs in G1 phase and is repressed by fibroblast growth factor. *J Cell Biol* **105**, 949-956 (1987).
52 Chakravarthy, M. V., Abraha, T. W., Schwartz, R. J., Fiorotto, M. L. & Booth, F. W. Insulin-like growth factor-I extends in vitro replicative life span of skeletal muscle satellite cells by enhancing G1/S cell cycle progression via the activation of phosphatidylinositol 3'-kinase/Akt

signaling pathway. *J Biol Chem* **275**, 35942-35952, doi:10.1074/jbc.M005832200 (2000).
53 Milasincic, D. J., Calera, M. R., Farmer, S. R. & Pilch, P. F. Stimulation of C2C12 myoblast growth by basic fibroblast growth factor and insulin-like growth factor 1 can occur via mitogen-activated protein kinase-dependent and -independent pathways. *Mol Cell Biol* **16**, 5964-5973 (1996).
54 Nagata, Y., Honda, Y. & Matsuda, R. FGF2 induces ERK phosphorylation through Grb2 and PKC during quiescent myogenic cell activation. *Cell Struct Funct* **35**, 63-71 (2010).
55 Tortorella, L. L., Milasincic, D. J. & Pilch, P. F. Critical proliferation-independent window for basic fibroblast growth factor repression of myogenesis via the p42/p44 MAPK signaling pathway. *J Biol Chem* **276**, 13709-13717, doi:10.1074/jbc.M100091200 (2001).
56 Bennett, A. M. & Tonks, N. K. Regulation of distinct stages of skeletal muscle differentiation by mitogen-activated protein kinases. *Science* **278**, 1288-1291 (1997).
57 Gredinger, E., Gerber, A. N., Tamir, Y., Tapscott, S. J. & Bengal, E. Mitogen-activated protein kinase pathway is involved in the differentiation of muscle cells. *J Biol Chem* **273**, 10436-10444 (1998).
58 Khurana, A. & Dey, C. S. Subtype specific roles of mitogen activated protein kinases in L6E9 skeletal muscle cell differentiation. *Mol Cell Biochem* **238**, 27-39 (2002).
59 Li, J. & Johnson, S. E. ERK2 is required for efficient terminal differentiation of skeletal myoblasts. *Biochem Biophys Res Commun* **345**, 1425-1433, doi:10.1016/j.bbrc.2006.05.051 (2006).
60 Sarbassov, D. D., Jones, L. G. & Peterson, C. A. Extracellular signal-regulated kinase-1 and -2 respond differently to mitogenic and differentiative signaling pathways in myoblasts. *Mol Endocrinol* **11**, 2038-2047, doi:10.1210/mend.11.13.0036 (1997).
61 Michailovici, I. *et al.* Nuclear to cytoplasmic shuttling of ERK promotes differentiation of muscle stem/progenitor cells. *Development* **141**, 2611-2620, doi:10.1242/dev.107078 (2014).
62 Duprez, D., Lapointe, F., Edom-Vovard, F., Kostakopoulou, K. & Robson, L. Sonic hedgehog (SHH) specifies muscle pattern at tissue and cellular chick level, in the chick limb bud. *Mechanisms of development* **82**, 151-163 (1999).
63 Anderson, C. *et al.* Sonic hedgehog acts cell-autonomously on muscle precursor cells to generate limb muscle diversity. *Genes Dev* **26**, 2103-2117, doi:10.1101/gad.187807.112 (2012).
64 Hu, J. K., McGlinn, E., Harfe, B. D., Kardon, G. & Tabin, C. J. Autonomous and nonautonomous roles of Hedgehog signaling in regulating limb muscle formation. *Genes Dev* **26**, 2088-2102, doi:10.1101/gad.187385.112 (2012).
65 Martin, J., Donnelly, J. M., Houghton, J. & Zavros, Y. The role of sonic hedgehog reemergence during gastric cancer. *Dig Dis Sci* **55**, 1516-1524, doi:10.1007/s10620-010-1252-z (2010).

66 Evans, W. J. *et al.* Cachexia: a new definition. *Clin Nutr* **27**, 793-799, doi:10.1016/j.clnu.2008.06.013 (2008).

67 Anker, S. D. *et al.* Wasting as independent risk factor for mortality in chronic heart failure. *Lancet* **349**, 1050-1053, doi:10.1016/S0140-6736(96)07015-8 (1997).

68 McGregor, R. A., Cameron-Smith, D. & Poppitt, S. D. It is not just muscle mass: a review of muscle quality, composition and metabolism during ageing as determinants of muscle function and mobility in later life. *Longev Healthspan* **3**, 9, doi:10.1186/2046-2395-3-9 (2014).

69 von Haehling, S. & Anker, S. D. Cachexia as a major underestimated and unmet medical need: facts and numbers. *J Cachexia Sarcopenia Muscle* **1**, 1-5, doi:10.1007/s13539-010-0002-6 (2010).

70 Johns, N., Stephens, N. A. & Fearon, K. C. Muscle wasting in cancer. *The international journal of biochemistry & cell biology* **45**, 2215-2229, doi:10.1016/j.biocel.2013.05.032 (2013).

71 Barreto, R. *et al.* Chemotherapy-related cachexia is associated with mitochondrial depletion and the activation of ERK1/2 and p38 MAPKs. *Oncotarget*, doi:10.18632/oncotarget.9779 (2016).

72 Chen, J. A. *et al.* Ghrelin prevents tumour- and cisplatin-induced muscle wasting: characterization of multiple mechanisms involved. *J Cachexia Sarcopenia Muscle* **6**, 132-143, doi:10.1002/jcsm.12023 (2015).

73 Toledo, M. *et al.* A multifactorial anti-cachectic approach for cancer cachexia in a rat model undergoing chemotherapy. *J Cachexia Sarcopenia Muscle* **7**, 48-59, doi:10.1002/jcsm.12035 (2016).

74 de Lima Junior, E. A. *et al.* Doxorubicin caused severe hyperglycaemia and insulin resistance, mediated by inhibition in AMPk signalling in skeletal muscle. *J Cachexia Sarcopenia Muscle*, doi:10.1002/jcsm.12104 (2016).

75 Fearon, K., Arends, J. & Baracos, V. Understanding the mechanisms and treatment options in cancer cachexia. *Nat Rev Clin Oncol* **10**, 90-99, doi:10.1038/nrclinonc.2012.209 (2013).

76 Laviano, A., Meguid, M. M., Inui, A., Muscaritoli, M. & Rossi-Fanelli, F. Therapy insight: Cancer anorexia-cachexia syndrome--when all you can eat is yourself. *Nat Clin Pract Oncol* **2**, 158-165, doi:10.1038/ncponc0112 (2005).

77 Evans, W. K. *et al.* Limited impact of total parenteral nutrition on nutritional status during treatment for small cell lung cancer. *Cancer Res* **45**, 3347-3353 (1985).

78 Acharyya, S. & Guttridge, D. C. Cancer cachexia signaling pathways continue to emerge yet much still points to the proteasome. *Clin Cancer Res* **13**, 1356-1361, doi:10.1158/1078-0432.CCR-06-2307 (2007).

79 Mammucari, C. *et al.* FoxO3 controls autophagy in skeletal muscle in vivo. *Cell Metab* **6**, 458-471, doi:10.1016/j.cmet.2007.11.001 (2007).

80 Narsale, A. A. & Carson, J. A. Role of interleukin-6 in cachexia: therapeutic implications. *Curr Opin Support Palliat Care* **8**, 321-327, doi:10.1097/SPC.0000000000000091 (2014).

81 Tsoli, M. & Robertson, G. Cancer cachexia: malignant inflammation, tumorkines, and metabolic mayhem. *Trends Endocrinol Metab* **24**, 174-183, doi:10.1016/j.tem.2012.10.006 (2013).
82 Jackman, R. W. & Kandarian, S. C. The molecular basis of skeletal muscle atrophy. *Am J Physiol Cell Physiol* **287**, C834-843, doi:10.1152/ajpcell.00579.2003 (2004).
83 Londhe, P. & Guttridge, D. C. Inflammation induced loss of skeletal muscle. *Bone* **80**, 131-142, doi:10.1016/j.bone.2015.03.015 (2015).
84 Fearon, K. C., Glass, D. J. & Guttridge, D. C. Cancer cachexia: mediators, signaling, and metabolic pathways. *Cell Metab* **16**, 153-166, doi:10.1016/j.cmet.2012.06.011 (2012).
85 Belizario, J. E., Fontes-Oliveira, C. C., Borges, J. P., Kashiabara, J. A. & Vannier, E. Skeletal muscle wasting and renewal: a pivotal role of myokine IL-6. *Springerplus* **5**, 619, doi:10.1186/s40064-016-2197-2 (2016).
86 Bonetto, A. *et al.* JAK/STAT3 pathway inhibition blocks skeletal muscle wasting downstream of IL-6 and in experimental cancer cachexia. *Am J Physiol Endocrinol Metab* **303**, E410-421, doi:10.1152/ajpendo.00039.2012 (2012).
87 Bonetto, A. *et al.* STAT3 activation in skeletal muscle links muscle wasting and the acute phase response in cancer cachexia. *PLoS One* **6**, e22538, doi:10.1371/journal.pone.0022538 (2011).
88 Zimmers, T. A., Fishel, M. L. & Bonetto, A. STAT3 in the systemic inflammation of cancer cachexia. *Semin Cell Dev Biol*, doi:10.1016/j.semcdb.2016.02.009 (2016).
89 White, J. *et al.* The regulation of skeletal muscle protein turnover during the progression of cancer cachexia in the Apc(Min/+) mouse. *PLoS ONE* **6**, e24650 (2011).
90 Oldenburg, H. S. *et al.* in *Eur J Immunol* Vol. 23 1889-1894 (1993).
91 Silva, K. A. *et al.* Inhibition of Stat3 activation suppresses caspase-3 and the ubiquitin-proteasome system, leading to preservation of muscle mass in cancer cachexia. *J Biol Chem* **290**, 11177-11187, doi:10.1074/jbc.M115.641514 (2015).
92 Strassmann, G., Fong, M., Kenney, J. S. & Jacob, C. O. in *The Journal of clinical investigation* Vol. 89 1681-1684 (1992).
93 Bayliss, T. J., Smith, J. T., Schuster, M., Dragnev, K. H. & Rigas, J. R. in *Expert Opin Biol Ther* Vol. 11 1663-1668 (2011).
94 Guan, K. L. The mitogen activated protein kinase signal transduction pathway: from the cell surface to the nucleus. *Cellular signalling* **6**, 581-589 (1994).
95 Zheng, C. F. & Guan, K. L. Cloning and characterization of two distinct human extracellular signal-regulated kinase activator kinases, MEK1 and MEK2. *J Biol Chem* **268**, 11435-11439 (1993).
96 Hommes, D. W., Peppelenbosch, M. P. & van Deventer, S. J. Mitogen activated protein (MAP) kinase signal transduction pathways and novel anti-inflammatory targets. *Gut* **52**, 144-151 (2003).

97 Neuzillet, C. *et al.* MEK in cancer and cancer therapy. *Pharmacology & therapeutics* **141**, 160-171, doi:10.1016/j.pharmthera.2013.10.001 (2014).
98 Yeh, T. C. *et al.* Biological characterization of ARRY-142886 (AZD6244), a potent, highly selective mitogen-activated protein kinase kinase 1/2 inhibitor. *Clin Cancer Res* **13**, 1576-1583, doi:10.1158/1078-0432.CCR-06-1150 (2007).
99 Facciorusso, A., Licinio, R., Carr, B. I., Di Leo, A. & Barone, M. MEK 1/2 inhibitors in the treatment of hepatocellular carcinoma. *Expert Rev Gastroenterol Hepatol* **9**, 993-1003, doi:10.1586/17474124.2015.1040763 (2015).
100 Shoushtari, A. N. & Carvajal, R. D. Treatment of Uveal Melanoma. *Cancer Treat Res* **167**, 281-293, doi:10.1007/978-3-319-22539-5_12 (2016).
101 Heigener, D. F., Gandara, D. R. & Reck, M. Targeting of MEK in lung cancer therapeutics. *Lancet Respir Med* **3**, 319-327, doi:10.1016/S2213-2600(15)00026-0 (2015).
102 Miller, C. R., Oliver, K. E. & Farley, J. H. MEK1/2 inhibitors in the treatment of gynecologic malignancies. *Gynecol Oncol* **133**, 128-137, doi:10.1016/j.ygyno.2014.01.008 (2014).
103 Bekaii-Saab, T. *et al.* Multi-institutional phase II study of selumetinib in patients with metastatic biliary cancers. *Journal of clinical oncology : official journal of the American Society of Clinical Oncology* **29**, 2357-2363, doi:10.1200/JCO.2010.33.9473 (2011).
104 Prado, C. M. *et al.* Skeletal muscle anabolism is a side effect of therapy with the MEK inhibitor: selumetinib in patients with cholangiocarcinoma. *Br J Cancer* **106**, 1583-1586, doi:10.1038/bjc.2012.144 (2012).
105 Rommel, C. *et al.* Differentiation stage-specific inhibition of the Raf-MEK-ERK pathway by Akt. *Science* **286**, 1738-1741 (1999).
106 Miyake, T. *et al.* Cardiotrophin-1 maintains the undifferentiated state in skeletal myoblasts. *J Biol Chem* **284**, 19679-19693, doi:10.1074/jbc.M109.017319 (2009).
107 Adi, S., Bin-Abbas, B., Wu, N. Y. & Rosenthal, S. M. Early stimulation and late inhibition of extracellular signal-regulated kinase 1/2 phosphorylation by IGF-I: a potential mechanism mediating the switch in IGF-I action on skeletal muscle cell differentiation. *Endocrinology* **143**, 511-516, doi:10.1210/endo.143.2.8648 (2002).
108 Penna, F. *et al.* Muscle wasting and impaired myogenesis in tumor bearing mice are prevented by ERK inhibition. *PLoS One* **5**, e13604, doi:10.1371/journal.pone.0013604 (2010).
109 Quan-Jun, Y. *et al.* Selumetinib attenuate skeletal muscle wasting in murine cachexia model through ERK inhibition and AKT activation. *Mol Cancer Ther*, doi:10.1158/1535-7163.MCT-16-0324 (2016).
110 Bennani-Baiti, N. & Walsh, D. Animal models of the cancer anorexia-cachexia syndrome. *Support Care Cancer* **19**, 1451-1463, doi:10.1007/s00520-010-0972-0 (2011).
111 Au, E. D., Desai, A. P., Koniaris, L. G. & Zimmers, T. A. The MEK-Inhibitor Selumetinib Attenuates Tumor Growth and Reduces IL-6 Expression but

Does Not Protect against Muscle Wasting in Lewis Lung Cancer Cachexia. *Front Physiol* **7**, 682, doi:10.3389/fphys.2016.00682 (2016).
112 Huang, M. H. *et al.* MEK inhibitors reverse resistance in epidermal growth factor receptor mutation lung cancer cells with acquired resistance to gefitinib. *Molecular oncology* **7**, 112-120, doi:10.1016/j.molonc.2012.09.002 (2013).
113 Shannon, A. M. *et al.* The mitogen-activated protein/extracellular signal-regulated kinase kinase 1/2 inhibitor AZD6244 (ARRY-142886) enhances the radiation responsiveness of lung and colorectal tumor xenografts. *Clin Cancer Res* **15**, 6619-6629, doi:10.1158/1078-0432.CCR-08-2958 (2009).
114 Troiani, T. *et al.* Intrinsic resistance to selumetinib, a selective inhibitor of MEK1/2, by cAMP-dependent protein kinase A activation in human lung and colorectal cancer cells. *Br J Cancer* **106**, 1648-1659, doi:10.1038/bjc.2012.129 (2012).
115 Minamoto, V. B. *et al.* Increased efficacy and decreased systemic-effects of botulinum toxin A injection after active or passive muscle manipulation. *Dev Med Child Neurol* **49**, 907-914, doi:10.1111/j.1469-8749.2007.00907.x (2007).
116 Tai, Y. T. *et al.* Targeting MEK induces myeloma-cell cytotoxicity and inhibits osteoclastogenesis. *Blood* **110**, 1656-1663, doi:10.1182/blood-2007-03-081240 (2007).
117 Talbert, E. E. *et al.* Dual Inhibition of MEK and PI3K/Akt Rescues Cancer Cachexia through both Tumor-Extrinsic and -Intrinsic Activities. *Mol Cancer Ther* **16**, 344-356, doi:10.1158/1535-7163.MCT-16-0337 (2017).
118 Hindi, S. M. & Kumar, A. TRAF6 regulates satellite stem cell self-renewal and function during regenerative myogenesis. *J Clin Invest* **126**, 151-168, doi:10.1172/JCI81655 (2016).
119 Ogura, Y. *et al.* TAK1 modulates satellite stem cell homeostasis and skeletal muscle repair. *Nat Commun* **6**, 10123, doi:10.1038/ncomms10123 (2015).
120 Jones, N. C., Fedorov, Y. V., Rosenthal, R. S. & Olwin, B. B. ERK1/2 is required for myoblast proliferation but is dispensable for muscle gene expression and cell fusion. *Journal of cellular physiology* **186**, 104-115, doi:10.1002/1097-4652(200101)186:1<104::AID-JCP1015>3.0.CO;2-0 (2001).
121 Jo, C. *et al.* Leukemia inhibitory factor blocks early differentiation of skeletal muscle cells by activating ERK. *Biochimica et biophysica acta* **1743**, 187-197, doi:10.1016/j.bbamcr.2004.11.002 (2005).
122 Jo, C., Jang, B. G. & Jo, S. A. MEK1 plays contrary stage-specific roles in skeletal myogenic differentiation. *Cellular signalling* **21**, 1910-1917, doi:10.1016/j.cellsig.2009.08.008 (2009).
123 Grogan, B. F., Hsu, J. R. & Skeletal Trauma Research, C. Volumetric muscle loss. *J Am Acad Orthop Surg* **19 Suppl 1**, S35-37 (2011).
124 McNally, E. M. & Pytel, P. Muscle diseases: the muscular dystrophies. *Annu Rev Pathol* **2**, 87-109, doi:10.1146/annurev.pathol.2.010506.091936 (2007).

125 Mercuri, E. & Muntoni, F. Muscular dystrophies. *Lancet* **381**, 845-860, doi:10.1016/S0140-6736(12)61897-2 (2013).
126 Ingham, P. W. & McMahon, A. P. Hedgehog signaling in animal development: paradigms and principles. *Genes Dev* **15**, 3059-3087, doi:10.1101/gad.938601 (2001).
127 Farzan, S. F., Singh, S., Schilling, N. S. & Robbins, D. J. The adventures of sonic hedgehog in development and repair. III. Hedgehog processing and biological activity. *American journal of physiology. Gastrointestinal and liver physiology* **294**, G844-849, doi:10.1152/ajpgi.00564.2007 (2008).
128 Walterhouse, D. O., Yoon, J. W. & Iannaccone, P. M. Developmental pathways: Sonic hedgehog-Patched-GLI. *Environmental health perspectives* **107**, 167-171 (1999).
129 Echelard, Y. *et al.* Sonic hedgehog, a member of a family of putative signaling molecules, is implicated in the regulation of CNS polarity. *Cell* **75**, 1417-1430 (1993).
130 Briscoe, J. & Therond, P. P. The mechanisms of Hedgehog signalling and its roles in development and disease. *Nature reviews. Molecular cell biology* **14**, 416-429, doi:10.1038/nrm3598 (2013).
131 Simpson, F., Kerr, M. C. & Wicking, C. Trafficking, development and hedgehog. *Mechanisms of development* **126**, 279-288, doi:10.1016/j.mod.2009.01.007 (2009).
132 Robbins, D. J., Fei, D. L. & Riobo, N. A. The Hedgehog signal transduction network. *Science signaling* **5**, re6, doi:10.1126/scisignal.2002906 (2012).
133 Chiang, C. *et al.* Cyclopia and defective axial patterning in mice lacking Sonic hedgehog gene function. *Nature* **383**, 407-413, doi:10.1038/383407a0 (1996).
134 Johnson, R. L., Laufer, E., Riddle, R. D. & Tabin, C. Ectopic expression of Sonic hedgehog alters dorsal-ventral patterning of somites. *Cell* **79**, 1165-1173 (1994).
135 Borycki, A. G. *et al.* Sonic hedgehog controls epaxial muscle determination through Myf5 activation. *Development* **126**, 4053-4063 (1999).
136 Borycki, A. G., Mendham, L. & Emerson, C. P., Jr. Control of somite patterning by Sonic hedgehog and its downstream signal response genes. *Development* **125**, 777-790 (1998).
137 Gustafsson, M. K. *et al.* Myf5 is a direct target of long-range Shh signaling and Gli regulation for muscle specification. *Genes Dev* **16**, 114-126, doi:10.1101/gad.940702 (2002).
138 Elia, D., Madhala, D., Ardon, E., Reshef, R. & Halevy, O. Sonic hedgehog promotes proliferation and differentiation of adult muscle cells: Involvement of MAPK/ERK and PI3K/Akt pathways. *Biochimica et biophysica acta* **1773**, 1438-1446, doi:10.1016/j.bbamcr.2007.06.006 (2007).

139 Duprez, D., Fournier-Thibault, C. & Le Douarin, N. Sonic Hedgehog induces proliferation of committed skeletal muscle cells in the chick limb. *Development* **125**, 495-505 (1998).
140 Koleva, M. *et al.* Pleiotropic effects of sonic hedgehog on muscle satellite cells. *Cell Mol Life Sci* **62**, 1863-1870, doi:10.1007/s00018-005-5072-9 (2005).
141 Goodrich, L. V., Milenkovic, L., Higgins, K. M. & Scott, M. P. Altered neural cell fates and medulloblastoma in mouse patched mutants. *Science* **277**, 1109-1113 (1997).
142 Oliver, T. G. *et al.* Loss of patched and disruption of granule cell development in a pre-neoplastic stage of medulloblastoma. *Development* **132**, 2425-2439, doi:10.1242/dev.01793 (2005).
143 Aartsma-Rus, A. & van Putten, M. Assessing functional performance in the mdx mouse model. *J Vis Exp*, doi:10.3791/51303 (2014).
144 Nixon, J. P. *et al.* Evaluation of a quantitative magnetic resonance imaging system for whole body composition analysis in rodents. *Obesity (Silver Spring)* **18**, 1652-1659, doi:10.1038/oby.2009.471 (2010).
145 Pasut, A., Jones, A. E. & Rudnicki, M. A. Isolation and culture of individual myofibers and their satellite cells from adult skeletal muscle. *J Vis Exp*, e50074, doi:10.3791/50074 (2013).
146 Mullor, J. L., Dahmane, N., Sun, T. & Ruiz i Altaba, A. Wnt signals are targets and mediators of Gli function. *Curr Biol* **11**, 769-773 (2001).
147 Yoon, J. W. *et al.* Gene expression profiling leads to identification of GLI1-binding elements in target genes and a role for multiple downstream pathways in GLI1-induced cell transformation. *J Biol Chem* **277**, 5548-5555, doi:10.1074/jbc.M105708200 (2002).
148 Agren, M., Kogerman, P., Kleman, M. I., Wessling, M. & Toftgard, R. Expression of the PTCH1 tumor suppressor gene is regulated by alternative promoters and a single functional Gli-binding site. *Gene* **330**, 101-114, doi:10.1016/j.gene.2004.01.010 (2004).
149 Frank-Kamenetsky, M. *et al.* Small-molecule modulators of Hedgehog signaling: identification and characterization of Smoothened agonists and antagonists. *J Biol* **1**, 10 (2002).
150 Rudin, C. M. Vismodegib. *Clin Cancer Res* **18**, 3218-3222, doi:10.1158/1078-0432.CCR-12-0568 (2012).
151 Casey, D. *et al.* FDA Approval Summary: Sonidegib for Locally Advanced Basal Cell Carcinoma. *Clin Cancer Res* **23**, 2377-2381, doi:10.1158/1078-0432.CCR-16-2051 (2017).
152 Sinha, S. & Chen, J. K. Purmorphamine activates the Hedgehog pathway by targeting Smoothened. *Nat Chem Biol* **2**, 29-30, doi:10.1038/nchembio753 (2006).
153 Bodine, S. C. *et al.* Akt/mTOR pathway is a crucial regulator of skeletal muscle hypertrophy and can prevent muscle atrophy in vivo. *Nat Cell Biol* **3**, 1014-1019, doi:10.1038/ncb1101-1014 (2001).
154 Keire, P., Shearer, A., Shefer, G. & Yablonka-Reuveni, Z. Isolation and culture of skeletal muscle myofibers as a means to analyze satellite cells.

Methods Mol Biol **946**, 431-468, doi:10.1007/978-1-62703-128-8_28 (2013).
155 Shefer, G. & Yablonka-Reuveni, Z. Isolation and culture of skeletal muscle myofibers as a means to analyze satellite cells. *Methods Mol Biol* **290**, 281-304 (2005).
156 Anderson, D. M. *et al.* A micropeptide encoded by a putative long noncoding RNA regulates muscle performance. *Cell* **160**, 595-606, doi:10.1016/j.cell.2015.01.009 (2015).
157 Anderson, D. M. *et al.* Widespread control of calcium signaling by a family of SERCA-inhibiting micropeptides. *Science signaling* **9**, ra119, doi:10.1126/scisignal.aaj1460 (2016).
158 Kusano, K. F. *et al.* Sonic hedgehog myocardial gene therapy: tissue repair through transient reconstitution of embryonic signaling. *Nat Med* **11**, 1197-1204, doi:10.1038/nm1313 (2005).
159 Palladino, M. *et al.* Pleiotropic beneficial effects of sonic hedgehog gene therapy in an experimental model of peripheral limb ischemia. *Mol Ther* **19**, 658-666, doi:10.1038/mt.2010.292 (2011).
160 Pola, R. *et al.* Postnatal recapitulation of embryonic hedgehog pathway in response to skeletal muscle ischemia. *Circulation* **108**, 479-485, doi:10.1161/01.CIR.0000080338.60981.FA (2003).
161 Straface, G. *et al.* Sonic hedgehog regulates angiogenesis and myogenesis during post-natal skeletal muscle regeneration. *J Cell Mol Med* **13**, 2424-2435, doi:10.1111/j.1582-4934.2008.00440.x (2009).
162 Piccioni, A. *et al.* Sonic hedgehog gene therapy increases the ability of the dystrophic skeletal muscle to regenerate after injury. *Gene Ther* **21**, 413-421, doi:10.1038/gt.2014.13 (2014).
163 Sartore, S., Gorza, L. & Schiaffino, S. Fetal myosin heavy chains in regenerating muscle. *Nature* **298**, 294-296 (1982).
164 Schiaffino, S., Gorza, L., Dones, I., Cornelio, F. & Sartore, S. Fetal myosin immunoreactivity in human dystrophic muscle. *Muscle Nerve* **9**, 51-58, doi:10.1002/mus.880090108 (1986).
165 Lee, H. *et al.* Identification of Small Molecules Which Induce Skeletal Muscle Differentiation in Embryonic Stem Cells via Activation of the Wnt and Inhibition of Smad2/3 and Sonic Hedgehog Pathways. *Stem Cells* **34**, 299-310, doi:10.1002/stem.2228 (2016).
166 Pallafacchina, G., Calabria, E., Serrano, A. L., Kalhovde, J. M. & Schiaffino, S. A protein kinase B-dependent and rapamycin-sensitive pathway controls skeletal muscle growth but not fiber type specification. *Proc Natl Acad Sci U S A* **99**, 9213-9218, doi:10.1073/pnas.142166599 (2002).
167 Sandri, M. *et al.* Foxo transcription factors induce the atrophy-related ubiquitin ligase atrogin-1 and cause skeletal muscle atrophy. *Cell* **117**, 399-412 (2004).
168 Cross, D. A., Alessi, D. R., Cohen, P., Andjelkovich, M. & Hemmings, B. A. Inhibition of glycogen synthase kinase-3 by insulin mediated by protein kinase B. *Nature* **378**, 785-789, doi:10.1038/378785a0 (1995).

169 Csibi, A. *et al.* The translation regulatory subunit eIF3f controls the kinase-dependent mTOR signaling required for muscle differentiation and hypertrophy in mouse. *PLoS One* **5**, e8994, doi:10.1371/journal.pone.0008994 (2010).

170 Jefferson, L. S., Fabian, J. R. & Kimball, S. R. Glycogen synthase kinase-3 is the predominant insulin-regulated eukaryotic initiation factor 2B kinase in skeletal muscle. *The international journal of biochemistry & cell biology* **31**, 191-200 (1999).

171 Leger, B. *et al.* Akt signalling through GSK-3beta, mTOR and Foxo1 is involved in human skeletal muscle hypertrophy and atrophy. *J Physiol* **576**, 923-933, doi:10.1113/jphysiol.2006.116715 (2006).

172 Egerman, M. A. & Glass, D. J. Signaling pathways controlling skeletal muscle mass. *Crit Rev Biochem Mol Biol* **49**, 59-68, doi:10.3109/10409238.2013.857291 (2014).

173 Schiaffino, S. & Mammucari, C. Regulation of skeletal muscle growth by the IGF1-Akt/PKB pathway: insights from genetic models. *Skelet Muscle* **1**, 4, doi:10.1186/2044-5040-1-4 (2011).

174 Park, I. H. & Chen, J. Mammalian target of rapamycin (mTOR) signaling is required for a late-stage fusion process during skeletal myotube maturation. *J Biol Chem* **280**, 32009-32017, doi:10.1074/jbc.M506120200 (2005).

175 Rommel, C. *et al.* Mediation of IGF-1-induced skeletal myotube hypertrophy by PI(3)K/Akt/mTOR and PI(3)K/Akt/GSK3 pathways. *Nat Cell Biol* **3**, 1009-1013, doi:10.1038/ncb1101-1009 (2001).

176 Lai, K. M. *et al.* Conditional activation of akt in adult skeletal muscle induces rapid hypertrophy. *Mol Cell Biol* **24**, 9295-9304, doi:10.1128/MCB.24.21.9295-9304.2004 (2004).

177 Chen, W. S. *et al.* Growth retardation and increased apoptosis in mice with homozygous disruption of the Akt1 gene. *Genes Dev* **15**, 2203-2208, doi:10.1101/gad.913901 (2001).

178 Wells, L., Edwards, K. A. & Bernstein, S. I. Myosin heavy chain isoforms regulate muscle function but not myofibril assembly. *EMBO J* **15**, 4454-4459 (1996).

179 Schiaffino, S., Rossi, A. C., Smerdu, V., Leinwand, L. A. & Reggiani, C. Developmental myosins: expression patterns and functional significance. *Skelet Muscle* **5**, 22, doi:10.1186/s13395-015-0046-6 (2015).

180 Agarkova, I. & Perriard, J. C. The M-band: an elastic web that crosslinks thick filaments in the center of the sarcomere. *Trends Cell Biol* **15**, 477-485, doi:10.1016/j.tcb.2005.07.001 (2005).

181 Schoenauer, R. *et al.* Myomesin 3, a novel structural component of the M-band in striated muscle. *J Mol Biol* **376**, 338-351, doi:10.1016/j.jmb.2007.11.048 (2008).

182 Blanchard, A., Ohanian, V. & Critchley, D. The structure and function of alpha-actinin. *J Muscle Res Cell Motil* **10**, 280-289 (1989).

183 Franzini-Armstrong, C. & Porter, K. R. The Z Disc of Skeletal Muscle Fibrils. *Z Zellforsch Mikrosk Anat* **61**, 661-672 (1964).

184 Sorimachi, H. *et al.* Tissue-specific expression and alpha-actinin binding properties of the Z-disc titin: implications for the nature of vertebrate Z-discs. *J Mol Biol* **270**, 688-695, doi:10.1006/jmbi.1997.1145 (1997).
185 Eklund, L. *et al.* Lack of type XV collagen causes a skeletal myopathy and cardiovascular defects in mice. *Proc Natl Acad Sci U S A* **98**, 1194-1199, doi:10.1073/pnas.031444798 (2001).
186 Kinzler, K. W. & Vogelstein, B. The GLI gene encodes a nuclear protein which binds specific sequences in the human genome. *Mol Cell Biol* **10**, 634-642 (1990).
187 Pavletich, N. P. & Pabo, C. O. Crystal structure of a five-finger GLI-DNA complex: new perspectives on zinc fingers. *Science* **261**, 1701-1707 (1993).
188 Ruppert, J. M. *et al.* The GLI-Kruppel family of human genes. *Mol Cell Biol* **8**, 3104-3113 (1988).
189 Kinzler, K. W., Ruppert, J. M., Bigner, S. H. & Vogelstein, B. The GLI gene is a member of the Kruppel family of zinc finger proteins. *Nature* **332**, 371-374, doi:10.1038/332371a0 (1988).
190 Bai, C. B., Stephen, D. & Joyner, A. L. All mouse ventral spinal cord patterning by hedgehog is Gli dependent and involves an activator function of Gli3. *Dev Cell* **6**, 103-115 (2004).
191 Buttitta, L., Mo, R., Hui, C. C. & Fan, C. M. Interplays of Gli2 and Gli3 and their requirement in mediating Shh-dependent sclerotome induction. *Development* **130**, 6233-6243, doi:10.1242/dev.00851 (2003).
192 Sasaki, H., Nishizaki, Y., Hui, C., Nakafuku, M. & Kondoh, H. Regulation of Gli2 and Gli3 activities by an amino-terminal repression domain: implication of Gli2 and Gli3 as primary mediators of Shh signaling. *Development* **126**, 3915-3924 (1999).
193 Shin, S. H., Kogerman, P., Lindstrom, E., Toftgard, R. & Biesecker, L. G. GLI3 mutations in human disorders mimic Drosophila cubitus interruptus protein functions and localization. *Proc Natl Acad Sci U S A* **96**, 2880-2884 (1999).
194 Dai, P. *et al.* Sonic Hedgehog-induced activation of the Gli1 promoter is mediated by GLI3. *J Biol Chem* **274**, 8143-8152 (1999).
195 Ruiz i Altaba, A. Gli proteins encode context-dependent positive and negative functions: implications for development and disease. *Development* **126**, 3205-3216 (1999).
196 Pan, Y., Bai, C. B., Joyner, A. L. & Wang, B. Sonic hedgehog signaling regulates Gli2 transcriptional activity by suppressing its processing and degradation. *Mol Cell Biol* **26**, 3365-3377, doi:10.1128/MCB.26.9.3365-3377.2006 (2006).
197 Wolff, C., Roy, S. & Ingham, P. W. Multiple muscle cell identities induced by distinct levels and timing of hedgehog activity in the zebrafish embryo. *Curr Biol* **13**, 1169-1181 (2003).
198 McDermott, A. *et al.* Gli2 and Gli3 have redundant and context-dependent function in skeletal muscle formation. *Development* **132**, 345-357, doi:10.1242/dev.01537 (2005).

199 Himeda, C. L., Barro, M. V. & Emerson, C. P., Jr. Pax3 synergizes with Gli2 and Zic1 in transactivating the Myf5 epaxial somite enhancer. *Dev Biol* **383**, 7-14, doi:10.1016/j.ydbio.2013.09.006 (2013).
200 Steffens, A. A., Hong, G. M. & Bain, L. J. Sodium arsenite delays the differentiation of C2C12 mouse myoblast cells and alters methylation patterns on the transcription factor myogenin. *Toxicol Appl Pharmacol* **250**, 154-161, doi:10.1016/j.taap.2010.10.006 (2011).
201 Liu, J. T. & Bain, L. J. Arsenic inhibits hedgehog signaling during P19 cell differentiation. *Toxicol Appl Pharmacol* **281**, 243-253, doi:10.1016/j.taap.2014.10.007 (2014).
202 Petropoulos, H., Gianakopoulos, P. J., Ridgeway, A. G. & Skerjanc, I. S. Disruption of Meox or Gli activity ablates skeletal myogenesis in P19 cells. *J Biol Chem* **279**, 23874-23881, doi:10.1074/jbc.M312612200 (2004).
203 Voronova, A. *et al.* Hedgehog signaling regulates MyoD expression and activity. *J Biol Chem* **288**, 4389-4404, doi:10.1074/jbc.M112.400184 (2013).
204 Gerber, A. N., Wilson, C. W., Li, Y. J. & Chuang, P. T. The hedgehog regulated oncogenes Gli1 and Gli2 block myoblast differentiation by inhibiting MyoD-mediated transcriptional activation. *Oncogene* **26**, 1122-1136, doi:10.1038/sj.onc.1209891 (2007).

Curriculum Vitae
Ernie Dennis Au

Education

Indiana University Indianapolis, IN
PhD August 2013 – May 2018
Biochemistry & Molecular Biology
GPA: 3.93

Thomas Jefferson University Philadelphia, PA
Graduate Student June 2012 – August 2013
Biochemistry & Molecular Pharmacology
GPA: 3.34

Pace University New York, NY
B.S. Biology August 2011
GPA: 3.25, Deans First Honors

GRANTS AND AWARDS

Poster Competition – Honorable Mention Indianapolis, IN
2017 Biochemistry Research Day October 2017

Science Signaling Poster Award Washington, DC
3rd Cancer Cachexia Conference September 2016

RESEARCH EXPERIENCE

PhD Candidate, Biochemistry & Molecular Biology Indianapolis, IN
Indiana University School of Medicine August 2013 – present
Studying cancer cachexia and myogenesis using the following techniques:

- Sterile cell culture
- Transfection
- CRISPR
- Western blotting
- ELISA
- RNA and DNA isolation
- Real-time PCR
- Mouse breeding
- Orthotopic tumor implantation
- Immunofluorescence

Trainee, Nationwide Children's Hospital Myology Course Columbus, OH
Nationwide Children's Hospital, The Ohio State University August 2014
Dedicated myology training course, with lectures given by expert faculty on the pathology, mechanisms of pathogenesis, diagnosis, and current therapies for various neuromuscular disorders and dystrophies. Basic science laboratory training included:

- Primary myoblast isolation
- Single myofiber isolation
- Electroporation
- Flow cytommetry to isolate muscle progenitor cells

Trainee, Eukaryotic Gene Expression Course Cold Spring Harbor, NY
Cold Spring Harbor Laboratory July 2013 – August 2013
Intensive three-week training course focused on state of the art strategies and techniques in the field of gene regulation. Laboratory techniques covered in this course included:
- Northern blot
- Gene silencing
- Chromatin dynamics assay
- Histone acetylation assay
- Nucleosome mapping
- Chromatin remodeling
- Chromatin immunoprecipitation
- Real-time PCR
- Dual luciferase reporter assay
- Genomic data analysis
- *In vitro* transcription and primer extension analysis

Research Assistant, Department of Pathology Brooklyn, NY
SUNY Downstate Medical Center November 2011 – May 2012
Studied the anti-cancer peptide PNC-27 using the following techniques:
- Sterile cell culture
- Mouse tumor models
- Osmotic pump implantation
- Confocal microscopy

Undergraduate Research Assistant, Department of Biology New York, NY
Pace University January 2011 – August 2011
Investigated the role of vasodilator-stimulated phosphoprotein in tumor progression and metastasis in cancer cells using the following techniques:
- Sterile cell culture
- Retroviral transfection
- Western blotting

Undergraduate Research Assistant, Department of Biology New York, NY
Pace University September 2009 – May 2011
Analyzed conformational changes involved in bacterial topoisomerase 1A closing motion using the following technique:
- Molecular analysis with Visual Molecular Dynamics software

Summer Research Student, Metabolism Laboratory Mineola, NY
Winthrop University Hospital July 2009 – August 2009
Studied effects of calcium and vitamin D supplementation on bone resorption in postmenopausal women diagnosed with osteoporosis using the following techniques:

- ELISA
- Bone density scan

CONFERENCE PRESENTATIONS

Au, E.D., Zhan, R., Zimmers, T.A. 2017. **Gli1 and Gli2 act mutually exclusive to promote proliferation of myoblasts and differentiation of myocytes**. Musculoskeletal Regenerative Medicine and Biology, St. Louis, MO.

Au, E.D. and Zimmers, T.A. 2016. **Distinct, non-overlapping roles of Gli1 and Gli2 in the molecular regulation of myogenesis.** 3rd Cancer Cachexia Conference, Washington, DC.

Au, E.D. and Zimmers, T.A. 2016. **Distinct, non-overlapping roles of Gli1 and Gli2 in the molecular regulation of myogenesis.** Cell Therapy and Regenerative Medicine, Indianapolis, IN.

Au, E.D. and Zimmers, T.A. 2016. **Investigating the role of the Shh pathway in myogenesis and regulation of adult skeletal muscle homeostasis.** Advances in Skeletal Muscle Biology in Health and Disease, Gainesville, FL.

Au, E.D. and Zimmers, T.A. 2015. **Selumetinib attenuated tumor growth and exacerbated muscle wasting in LLC cancer cachexia**. 5th Annual Conference Indiana Physiological Society, Marian College of Osteopathic Medicine, Indianapolis, IN.

Au, E.D. and Zimmers, T.A. 2014. **Selumetinib attenuated tumor growth and exacerbated muscle wasting in LLC cancer cachexia**. Indiana University School of Medicine, Department of Biochemistry & Molecular Biology Research Day, Indianapolis, IN.

Au, E.D. and Zimmers, T.A. 2014. **Selumetinib attenuated tumor growth and exacerbated muscle wasting in LLC cancer cachexia**. 2nd Cancer Cachexia Conference, Montreal, QC.

Au, E.D. and Zimmers, T.A. 2014. **Sonic hedgehog pathway inhibition induces hypertrophy in C2C12 myotubes**. The Muscle Microenvironment, Columbus, OH.

Au, E.D., Strahs, D. 2011. **Structural Changes During the Closing Motion of Topoisomerase IA**. Eastern Colleges Science Conference, Pleasantville, NY.

Au, E.D., Strahs, D. 2011. **Structural Changes During the Closing Motion of Topoisomerase IA**. Pace University, Department of Biology and Health Sciences Poster Session, New York, NY.

PEER-REVIEWED PUBLICATIONS

Au, E. D., Desai, A. P., Koniaris, L. G., and Zimmers, T. A. (2016). The MEK-Inhibitor Selumetinib Attenuates Tumor Growth and Reduces IL-6 Expression but Does Not Protect against Muscle Wasting in Lewis Lung Cancer Cachexia. Front Physiol 7, 682.

Zimmers, T. A., Jiang, Y., Wang, M., Liang, T. W., Rupert, J. E., **Au, E. D.**, Marino, F. E., Couch, M. E., and Koniaris, L. G. (2017). Exogenous GDF11 induces cardiac and skeletal muscle dysfunction and wasting. Basic Res Cardiol 112, 48.

Sato, A. Y., Richardson, D., Cregor, M., Davis, H. M., **Au, E. D.**, McAndrews, K., Zimmers, T. A., Organ, J. M., Peacock, M., Plotkin, L. I., and Bellido, T. (2017). Glucocorticoids Induce Bone and Muscle Atrophy by Tissue-Specific Mechanisms Upstream of E3 Ubiquitin Ligases. Endocrinology 158, 664-677.

WRITING EXPERIENCE

- In collaboration with mentor, researched and wrote grant for an Indiana School of Medicine Graduate Student Travel Grant: **Ptch1 haploinsufficiency results in a hypotrophic skeletal muscle phenotype**
- In collaboration with mentor, researched and wrote grant for an individual Ruth L. Kirschstein National Research Service Awards for Individual Predoctoral Fellowship (F31): **Roles of Ptch1 in Regulating Muscle Size in Health and Cancer Cachexia**
- In collaboration with mentor, researched and wrote grant for an Indiana Clinical and Translational Sciences Institute Pre-Doctoral Training in Translational Research: **Roles of Smoothened in Regulating Muscle Size in Health and Cancer Cachexia**
- Attended a workshop presented by Grant Writers' Seminars and Workshops in association with the Indiana University School of Medicine: **Write Winning Grant Proposals**

COMPUTER SKILLS

- Microsoft Office
- ImageJ
- GraphPad Prism